NATIONAL ENERGY TECHNOLOGY LABORATORY

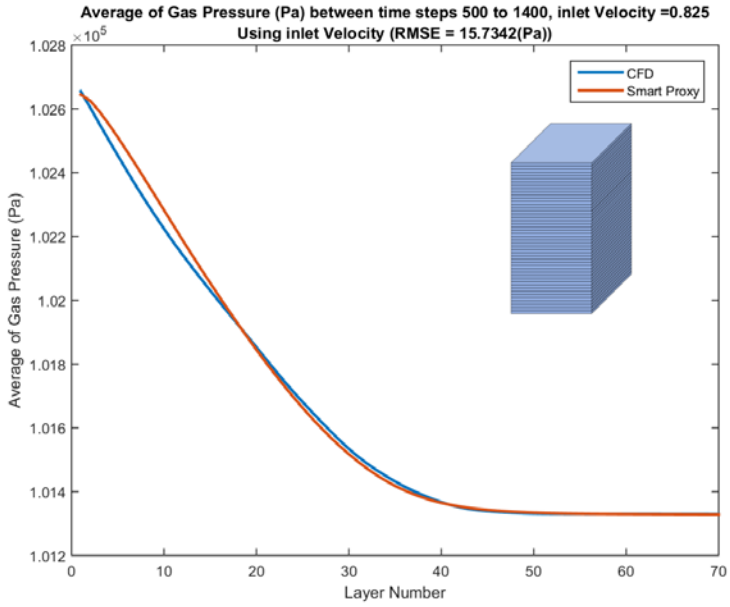

Data Driven Smart Proxy for CFD

Application of Big Data Analytics & Machine Learning in Computational Fluid Dynamics

Report Three: Model Building at the Layer Level

May 2018

U.S. DEPARTMENT OF ENERGY | NATIONAL ENERGY TECHNOLOGY LABORATORY

Office of Fossil Energy

NETL-PUB-21860

Disclaimer

Cover Illustration: Comparing the pressure drop at different layers of a fluidized bed generated by the Smart Proxy (red) with CFD results (blue) at the Layer Level.

Suggested Citation: Ansari, A., Mohaghegh, S., Shahnam, M., Dietiker, J. F., Li, T., Gel, A., *Data Driven Smart Proxy for CFD Application of Big Data Analytics & Machine Learning in Computational Fluid Dynamics, Part Three: Model Building at the Layer Level*; NETL-PUB-21860; NETL Technical Report Series; U.S. Department of Energy, National Energy Technology Laboratory: Morgantown, WV, 2018.

Data Driven Smart Proxy for CFD

Application of Big Data Analytics & Machine Learning in Computational Fluid Dynamics

Part Three: Model Building at the Layer Level

Ansari, A.[1], Mohaghegh, S.[1,2], Shahnam, M.[3], Dietiker, J. F.[3,4], Li, T.[3,5], Gel, A.[3,6]

[1] **Petroleum & Natural Gas Engineering Department, West Virginia University**
[2] **ORISE Faculty Program**
[3] **Energy Conversion Engineering Directorate, Research and Innovation Center, U.S. Department of Energy, National Energy Technology Laboratory**
[4] **West Virginia University Research Corporation, Morgantown, WV**
[5] **AECOM, Morgantown, WV**
[6] **ALPEMI Consulting, LLC, Phoenix, AZ**

NETL-PUB-21860

May 2018

NETL Contacts:

Mehrdad Shahnam, Principal Investigator

Jonathan Lekse, Technical Portfolio Lead

David Alman, Executive Director, Research and Innovation Center

This page intentionally left blank

Table of Contents

List of Figures

List of Tables

Acronyms, Abbreviations, and Symbols

Term	Description
AI	Artificial Intelligence
ANN	Artificial Neural Network
CFD	Computational Fluid Dynamics
CSV	Comma Separated Value
CMG	Computer Modeling Group
DM	Data Mining
KTGF	Kinetic Theory of Granular Flow
MFIX	Multiphase Flow with Interphase eXchanges
NETL	National Energy Technology Laboratory
PDE	Partial Differential Equation
RMSE	Root Square of Mean Square Error
UQ	Uncertainty Quantification

Acknowledgments

Professor Mohaghegh acknowledges the support provided by an appointment to the National Energy Technology Laboratory (NETL) Faculty Research Participation Program, sponsored by the U.S. Department of Energy and administered by the Oak Ridge Institute for Science and Education. This work is performed as part of NETL research for the U.S. Department of Energy's Cross Cutting Program.

EXECUTIVE SUMMARY

To ensure the usefulness of simulation technologies in practice, their credibility needs to be established with Uncertainty Quantification (UQ) methods. In this project smart proxy is introduced to significantly reduce the computational cost of conducting large number of multiphase CFD simulations. Smart proxy for CFD models are developed using pattern recognition capabilities of Artificial Intelligence (AI), Machine Learning (LM) and Data Mining (DM) technologies.

Several CFD simulation runs with different inlet air velocities for a rectangular fluidized bed are used to create a smart CFD proxy that is capable of replicating the CFD results for a wide variety of inlet velocities. The smart CFD proxy is validated with blind CFD runs (CFD runs that have not played any role during the development [training, calibration and validation] of the smart CFD proxy). In our earlier work [1], CFD data was used to train ANN at the cell level. That is an ANN was trained for each computational cell used in the CFD simulations. In the present work, the ANN is constructed and trained based on cross sectional area average of each variable, such as pressure, velocities and volume fraction (*Layer Level*). This leads to improvements in the training time at the expense of less spatial resolution. The resulting trained ANN provides spatially average value of parameters of interest, along the length of the fluidized bed. Upon completion of this project, UQ studies that rely on hundreds or thousands of smart CFD proxy runs can be accomplished in minutes. Following figure demonstrates a validation example (blind CFD run) showing the results from the MFiX and the smart CFD proxy for pressure drop across a fluidized bed at time-step of 1400 (the layer number corresponds to the vertical location in the bed).

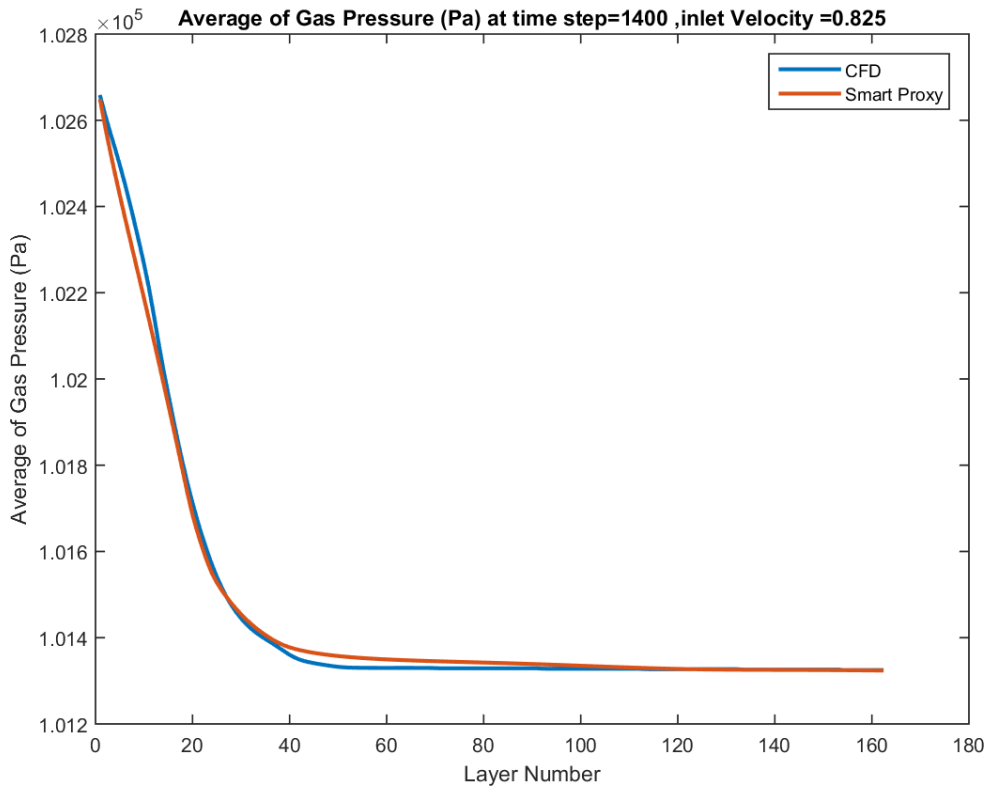

1. INTRODUCTION

Fossil fuel continues to be a reliable source of energy for power generation in the United States and worldwide. Technologies, such as chemical looping and gasification, aim to reduce the carbon emission of fossil fuel based power plants. Simulation technologies can reduce the time and cost of the development and deployment of such advanced technologies and allow rapid scale-up of these technologies. Simulation can be used to test new designs to ensure reliable operation under a variety of operating conditions. However, to ensure their usefulness in practice, the credibility of the simulations needs to be established with Uncertainty Quantification (UQ) methods. To this end, National Energy Technology Laboratory (NETL) has been applying non-intrusive UQ methodologies to identify, characterize, and quantify uncertainties in CFD simulations of gas-solid multiphase flows, which are encountered in fossil fuel based energy systems [2, 3, 4, 5]. Gas-solid flows are inherently highly unsteady and chaotic flows, where sharp discontinuity can exist at the interface between the phases. The challenge in CFD simulation of gas-solid flows is to adequately resolve the structures that exist at different spatial and temporal scales in an inherently transient flow. Additionally, in reacting gas-solid flow simulations, small time steps are needed in order to not only resolve the temporal scales of the flow, but also ensure numerical stability of the solution. A rule of thumb for adequate spatial resolution is for the grid spacing to be about 10 times the particle diameter [6]. The grid requirement for maintaining such a ratio of grid size to particle diameter for smaller size particles makes such simulations computationally costly and impractical [5]. Recent work at NETL [5] has shown the number of simulations, which is required for uncertainty quantification can easily exceed many tens of simulations. The spatial and temporal resolution requirements for multiphase flows make CFD simulations computationally expensive and potentially beyond the reach of many design analysts.

It is clear that a paradigm shift in simulation technology is needed in order to make reacting gas-solid flow CFD simulations with appropriate grid resolution more practical for design and optimization purposes during design scale up. To accelerate the design and analysis process, high fidelity surrogate models that can capture the flow behavior of the design under consideration can be utilized. Surrogate models are increasingly used in design exploration, optimization and sensitivity analysis. Advances in big data analytic and machine learning allow for creation of data-fitted metamodels, which can faithfully duplicate the behavior of the data (CFD model results) that was used for their construction. This new technology has been successfully applied in the upstream petroleum industry [7] [8] [9] [10]. Smart Proxy modeling takes advantage of pattern recognition capabilities of artificial intelligence and machine learning to build powerful tools to predict the behavior of a system with far less computational cost compared to traditional CFD simulators.

The goal of this research project is to build a smart proxy model at the cell level, which is constructed from simulation data generated by high fidelity CFD models to, in effect, replace the use of computationally expensive CFD simulations for the design space under study for further analysis and optimization. When compared to traditional proxy modeling technologies such as Reduced Order Models (ROM), the advantage of smart proxy is associated with its unique characteristics of *(a)* not simplifying the physics of the original CFD model, and *(b)* not reducing the resolution (in time and space) of the original CFD model. Hence, the smart proxy can be used instead of CFD simulations, when performing uncertainty quantification analysis in order to quantify errors and uncertainties that are inherent in any simulation and also perform

computationally inexpensive evaluations when propagating the uncertainties in the input variables. The uniqueness of this approach is in:

1. Developing a unique engineering-based data preparation technology that optimizes the training of the neural networks. This innovative technique incorporates supervised fuzzy cluster analysis to:
    a. Identify the most influential parameters for the training process, and
    b. Identify the optimum partitioning of the data for training, calibration and validation.
2. Unique, innovative, and optimum preparation of the raw data extracted from the CFD for the training, calibration and validation of a series of neural networks that together will form the final CFD smart proxy.
3. Using an "ensemble-based" approach to building the smart proxy, taking advantage of multiple, inner-connected neural networks and intelligent agents to accomplish the objectives of the project.

Proof of concept for the application of this technology to Computational Fluid Dynamics has been established in our first report [11]. Our second report [1] documents the various techniques, which were used for constructing a smart proxy model at the cell level. The goal of the present report is to outline steps employed in constructing a smart proxy at the *Layer Level*[1], (the term *Layer Level* compared to *Cell Level* [1], refers to how CFD data is used for the training. A detailed explanation is provided in section 3.3.2).

1.1 STRUCTURE OF THE WORK

The research and development concentrating on the CFD smart proxy modeling have been presented in multiple reports. Each report concentrates on a major portion of the research work and accomplishments that are useful to the general research community. First report established the background to prove the concept of using smart proxy as a replicate for CFD [11]. In the second report [1], CFD simulations were replicated by smart proxies at the *Cell Level*. This report summarizes the building of the data driven predictive models at the *Layer Level* for replicating the CFD simulation model. The report consists of five chapters. In chapter one (this chapter), the problem is defined, and the final objective of the research is articulated. In chapter two, a brief definition of multiphase flow and its governing equations are provided to lay the groundwork for understanding the engineering and scientific details associate with the CFD model being studied. Also, a literature review about the use of AI and Machine Learning related to fluid dynamics problems is provided.

Chapter three discusses the methodology and the machine learning method which is used in this research, specifically for the *Layer Level* smart proxy modeling (section 3.3.2). Results and discussions are presented in chapter four, and finally, the conclusions and recommendations for the next phase of the research are presented in chapter five.

[1] The CFD data are averaged in each layer (XZ plane) and the ANN is trained using the layer averaged data.

2. BACKGROUND

This section of the report is dedicated to providing some basic, but necessary background on three major components of this research work.

2.1 MFIX

Multiphase flows, both reacting and non-reacting, are part of many processes in power generation and chemical processing industries. As expressed earlier, CFD is a valuable tool in design and optimization of processes and reactors used in these industries. NETL has been in the forefront of developing CFD modeling tools that can help engineers and designers in improving the performance of processes such as gasification, chemical looping. The MFiX (Multiphase Flow with Interphase eXchanges) suite of CFD software [12] is an open-source, general purpose multiphase CFD software suitable for modeling the hydrodynamics, along with heat transfer and chemical reaction for a wide spectrum of flow conditions (dilute to dense). Multiphase flows can be modeled either in a continuum (Eulerian) framework or a discrete (Lagrangian) framework. The two frameworks can be summarized as follow:

- Continuum (Eulerian): Both solid phase and gas phase are treated as interpenetrating continuum (Two-Fluid Model, TFM). Multiple solid phases can be used to describe multiple solid particles of different sizes and properties (Multi Fluid Model, MFM). Continuum approach is computationally less intensive but it cannot capture all the flow complexities, especially in multiphase flow where interaction between particles plays a major role [13].
- Discrete Particle (Lagrangian): Track each particle in the fluid individually by using Newton's Law of motion. This method is more straightforward to apply, even in multiphase flow, but the computational cost is high [13].

There are several approaches to modeling multiphase gas-solid flows. Depending on the application, either the gas phase or the solid phase or both phases can be modeled in Eulerian or Lagrangian framework [13] [14] [15]. Table 2-1 shows the different modeling approaches to gas-solid multiphase flow modeling.

In the present work, the MFiX-TFM is used to model a rectangular 3D fluidized bed. MFIX-TFM, which is based on kinetic theory of granular flow (KTGF) models both the gas phase and particulate phase as interpenetrating continuous phases. The governing equations employed for the conservation of mass and momentum for each phase (m, n = g for gas phase and m, n = s for solid phase) are

$$\frac{\partial}{\partial t}(\varepsilon_m \rho_m) + \nabla.(\varepsilon_m \rho_m \vec{v}_m) = \sum_{\substack{n=1 \\ n \neq m}}^{N_m} R_{mn} \qquad \text{2-1}$$

$$\frac{\partial}{\partial t}(\varepsilon_m \rho_m \vec{v}_m) + \nabla.(\varepsilon_m \rho_m \vec{v}_m \vec{v}_m) = \nabla.(\bar{\bar{S}}_m) + \varepsilon_m \rho_m \vec{g} - \sum_{\substack{n=1 \\ n \neq m}}^{M} I_{mn} \qquad \textbf{2-2}$$

Where

ε_m is the phase volume fraction

ρ_m is the phase density

$\vec{v}_m$ is the phase velocity vector

R_{mn} is mass transfer between phases

$\bar{\bar{S}}_g$ is the phase stress tensor

I_{mn} is the interaction force representing the momentum transfer between the phases

The closure terms for the solid phases are obtained through kinetic theory of granular flow. Detailed information on the constitutive relationships used to model momentum exchange between the phases along with the solid stress model incorporated in MFiX-TFM can be obtained from MFiX online documentations [16] [17].

Equations 2-1 and 2-2 form a system of nonlinear partial differential equations. An iterative algorithm is used in MFiX to solve this system of PDEs. Figure 2-1 illustrates the solution sequences used in MFiX for solving the equations 2-1 and 2-2. As it is discussed in the next section, it is crucial to follow the same sequence in constructing the smart proxy.

Table 2-1 Multiphase Flow Modeling Approaches [13]

	Name	***Gas Phase***	***Solid Phase***	***Coupling***	***Scale***
1	*Discrete bubble model*	*Lagrangian*	*Eulerian*	*Drag Closure for bubbles*	*10 m*
2	*Two Fluid Model*	*Eulerian*	*Eulerian*	*Gas-Solid drag closure*	*1 m*
3	*Unresolved Discrete particle model*	*Eulerian*	*Lagrangian*	*Gas-particle drag closure*	*0.1 m*
4	*Resolved Discrete particle model*	*Eulerian*	*Lagrangian*	*Boundary condition at particle surface*	*0.01 m*
5	*Molecular Dynamics*	*Lagrangian*	*Lagrangian*	*Elastic collisions at particle surface*	*<0.001 m*

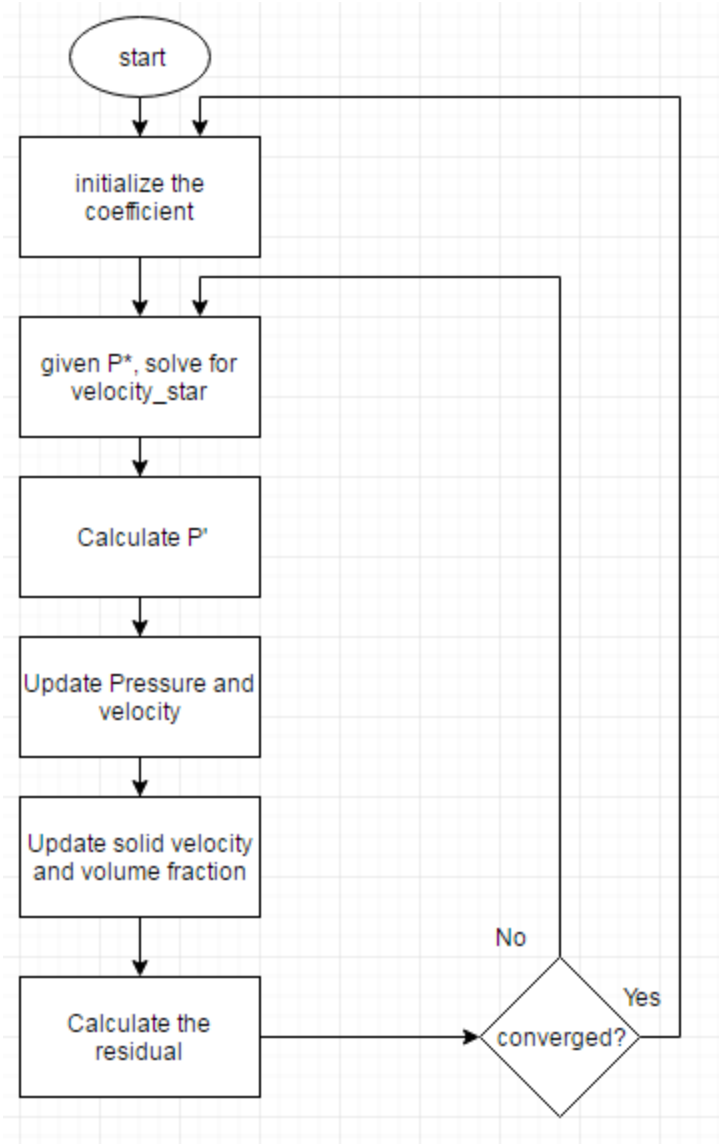

Figure 2-1 MFiX solution algorithm.

2.2 MACHINE LEARNING

Based on the definition presented by Arthur Samuel [18], *"Machine learning is a field of study that gives computers the ability to learn without being explicitly programmed."*

Machine learning is a process through which computer will learn from data to find a possible pattern in the data set. This process encompasses three main components:

- Learning algorithm
- Data
- Patterns in the data

If these three components are present, a successful learning process can be achieved based on the capability of the learning algorithm. There are two major type of Machine Learning: supervised learning and unsupervised learning [19].

2.2.1 Artificial Neural Network

One of the popular machine learning processes is Artificial Neural Network (ANN). The idea of ANN came from the neurons of the brain and the way they are communicating with each other to solve a problem. Each artificial neural network consists of an input layer, one or more hidden layers, and an output layer. The number of neurons (processing elements) in the output and the input layers are chosen based on the nature of the problem being solved and the properties which are going to be predicted. Figure 2-2 shows a typical ANN with three input neurons and two output neurons. ANN has one or more hidden layers and each layer has a specific number of neurons [20]. In order to have a well-trained network, proper parameters should be introduced to the network. If improper data are used to train the network there is no guarantee to have a well-trained network that lead to accurate predictions, in other words, *"Garbage in, Garbage out."* In the upcoming sections of this report, a smart way of selecting parameters will be introduced.

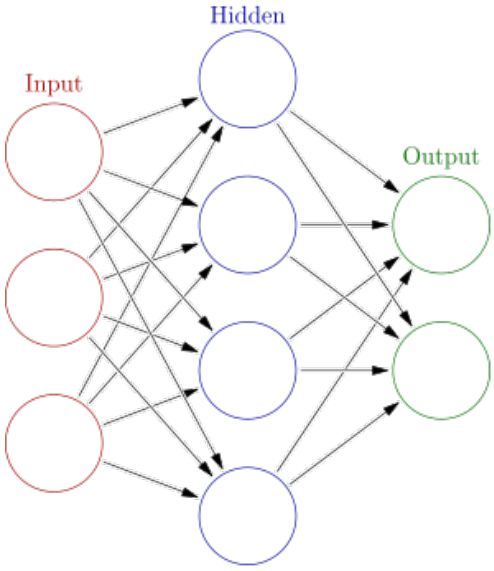

Figure 2-2 Artificial Neural Network schematic

The number of hidden layers and the neurons in each hidden layer depends on the complexity of the problem, number of parameters, and number of records. Experience also plays an important role in this decision making. But generally, there is no solid rule for them. As a rule of thumb, the number of neurons in the first hidden layer shouldn't be less than the number of input parameters.

2.2.1.1 Objective function

Regardless of the learning method, each machine learning process needs an optimization procedure that helps the process reduce the prediction error as much as possible. The very common and simple objective function in supervised learning is the summation of all the differences between predicted values by the learning method and the actual values of the output. Since summation of positive and negative errors can reduce the size of the overall error, the objective function is defined as the square of the difference between actual and predicted values [20], as shown by equation 2-3.

$$J(w_j) = \frac{1}{2m}\sum_{i=1}^{m}\left(y_{actual} - y_{predicted}\right)^2 \qquad \textbf{2-3}$$

Where w_j is the weighting vector. During the learning process, the learning algorithm tries to assign different weights to each of the connection between neurons in Figure 2-2, in a way that the global error of the objective function becomes minimum. Also, a blind calibration is done simultaneously to stop the learning process. We will discuss the validation and test in more depth in the next sections of this report.

In machine learning, the dataset used for training of ANN has to be normalized, before the data is introduced for training. Therefore, the quality of ANN is characterized by error (discrepancy) distribution between mean normalized CFD data (used for training) and mean normalized ANN output as shown by equation 2-4.

$$\%\ Error\ = \frac{(CFD_{value} - CFD_{mean\ value})}{(MAX(CFD_{value}) - MIN(CFD_{value})} - \frac{(Smart\ Proxy_{value} - CFD_{mean\ value})}{(MAX(CFD_{value}) - MIN(CFD_{value})} \qquad \textbf{2-4}$$

2.3 PREVIOUS WORK

The idea of using Artificial Intelligence in petroleum engineering was first introduced by Mohaghegh and Ameri [21]. They took advantage of ANN for predicting the permeability of the formation based on geological well logs. Mohaghegh and Ameri [21] showed that neural network is capable of making the task of permeability determination automated rather than doing it over and over by log analyst. They also stated that neural network can handle far more complex tasks. Mohaghegh et al. [22] used ANN for predicting gas storage well performance after hydraulic fracture in later investigations.

Alizadehdakhel et al. [23] successfully used ANN to predict the pressure loss of a two-phase flow in a 2 cm diameter tube. Gas and liquid velocities and the pressure drop along the pipe were the three input parameters to ANN, with average pressure drop being the output. They utilized 8 different networks with different number of neurons to find out the optimum number neurons. Mean Squared Error and R-square were used as a criterion to pick the best network design. They also obtained the most efficient transfer function between Log-Sigmoid, Hyperbolic-Tangent Sigmoid, and linear.

Shahkarami et al. [10] used ANN to model the pressure and saturation distribution in a reservoir which was used for CO_2 sequestration. This problem required a large number of time steps for simulation of CO_2 injection and storage using a commercial software. They ran 10 different cases in CMG (commercial reservoir simulator) and then the results were used as input for ANN. The output of the ANN was pressure distribution, water saturation, and CO_2 mole fraction. 80% of the data coming from the CMG simulation runs were used to train the network while 10% were used for the calibration. The remaining 10% of data was used for validation process. They have shown that ANN can be used as a powerful tool for multiphase flow simulation in oil and gas industry.

Esmaili et al. [24] incorporated a newly developed AI-based reservoir modeling technology known as Data-Driven Reservoir Modeling [25] in order to model fluid flow in shale reservoirs using detail well logs, completion, and production data. By understanding the behavior of the shale reservoir, conducting the hydraulic fracture could be much easier. Moreover, this method has the ability to perform the history matching on the production data. Kalantari-Dehghani et al. [26] coupled numerical reservoir simulator with AI methods to develop a shale proxy model that is able to regenerate numerical simulation results in just a few seconds. They introduced three different well-based tier systems to achieve a comprehensive input data for the ANN. In another work, Kalantari-Dehghani et al. [27] showed that data-driven proxy models at the hydraulic fracture cluster level could be used separately as a reservoir simulator especially in low permeability reservoir such as shale which has a nonlinear behavior.

Ansari et al. [11] established the viability of using machine learning and neural network to construct a smart proxy for a fluidized bed based on CFD data of the same fluidized bed. More details on the approach and the steps are given by Ansari [28]. In a subsequent report, Ansari et al. [1] developed a proxy model for gas pressure and volume fraction in their fluidized bed, based on CFD data. Although reasonable agreement was observed between the trained proxy model and CFD simulation results, further improvements in the training process were deemed necessary in order to improve the quality of the trained neural net proxy model.

Hosseini [29] used a similar approach to model the behavior of flow after dam break with the goal of reducing the computational time for the fluid flow simulations by developing a Smart Proxy Model.

3. METHODS

In this section, the solution methodology and the required steps for constructing the neural network are discussed.

3.1 CFD SIMULATION SETUP

A schematic of the rectangular fluidized bed, used in this study is shown in Figure 3-1. The fluidized bed, which is 0.12 x 0.72 x 0.12 m in X, Y and Z directions has an initial bed height of 0.12 m, and initial bed voidage of 0.42. The bed material has a density of 2000 kg/m^3 and a diameter of 400 µm. Details of the CFD simulation set up was covered in the part one report of this project, [11], and will not be repeated here.

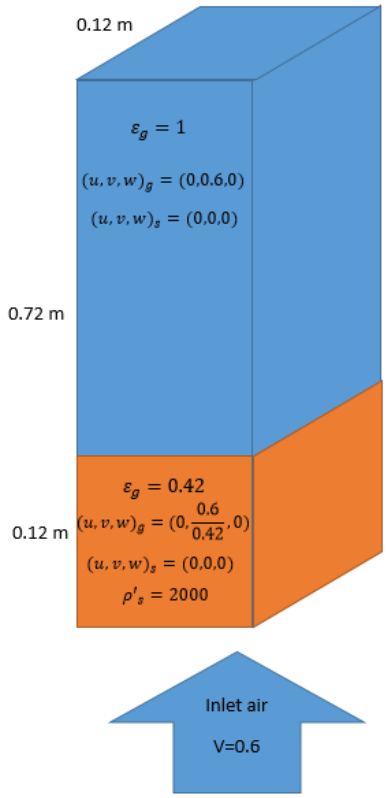

Figure 3-1 Geometry and initial condition of the problem.

3.2 PROBLEM DEFINITION

The MFiX model has been created and executed successfully for multiple inlet velocities. The data generated by the CFD runs with a variety of inlet velocities is used for the training, calibration, and validation process of the neural network model. Furthermore, additional CFD simulations with different inlet velocities are performed and are excluded from the neural network training process. The additional CFD simulations are used to test the predictive capabilities of the smart CFD proxy, in what is referred to as a blind test.

3.2.1 Interpolating the inlet air velocity

The inlet air velocity varies from a minimum value of 0.6 m/s to a maximum value of 1.2 m/s (Figure 3-2). The inlet air velocity is assumed to be uniform across the fluidized bed inlet (Figure 3-1) with air discharging into atmospheric pressure at the outlet.

The goal of this project is to predict the behavior of the fluidized bed at *Layer Level* (cross sectional planes along the length of the fluidized bed) at any given inlet air velocity (within the velocity range used for training) at any time. The neural network model will be trained for seven different inlet velocities. The predictive capability of the trained neural network is evaluated using CFD data, which has not been part of the training process (blind test). Figure 3-3 shows the concept of this project.

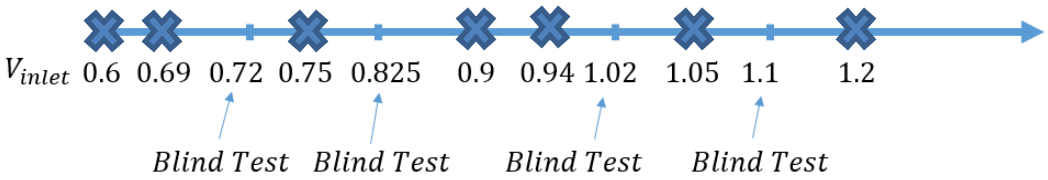

Figure 3-2 Inlet air velocities used in MFIX simulations. Inlet velocities used in ANN training are marked with X.

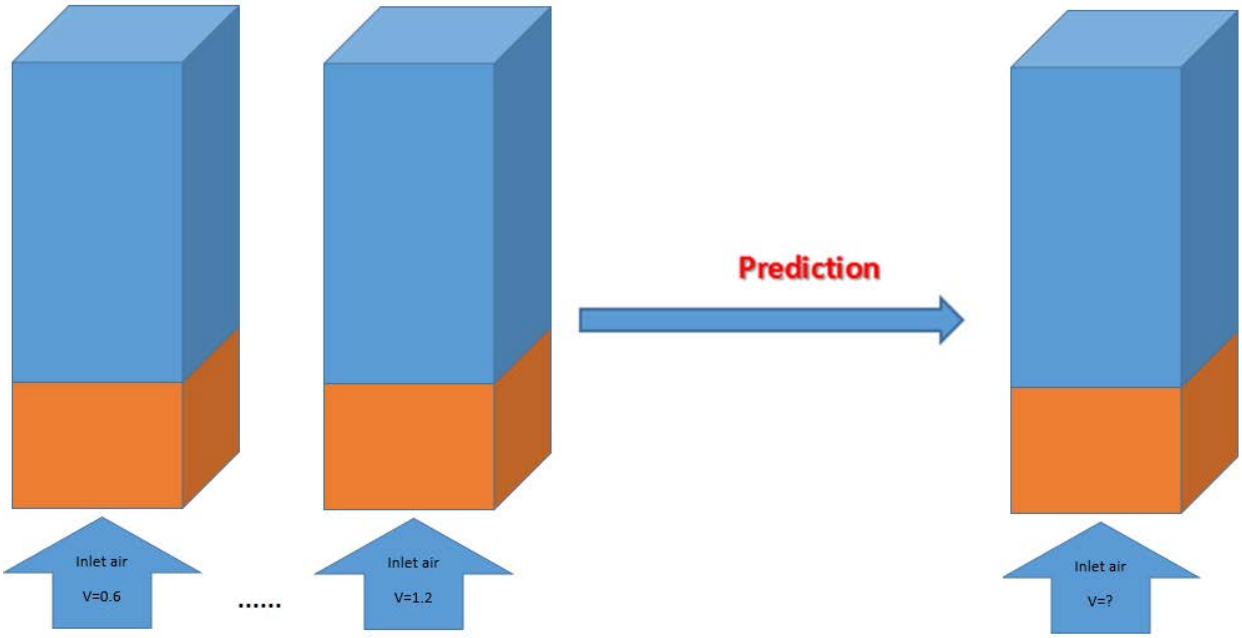

Figure 3-3 Conceptual illustration of problem definition

The process of fluidization, as shown in Figure 3-4, starts with the bed material moving upward like a slug flow, Figure 3-4a, until the maximum bed expansion is reached, Figure 3-4b, and the

bed starts to collapse. In Figure 3-4 color red indicates high voidage (low solid volume fraction) and color blue indicates low voidage (high solid volume fraction). The solid flow is symmetrical until the bed collapses, smaller bubbles are formed, and the bed behaves more chaotically, Figure 3-4c. And ultimately, the bed becomes fully fluidized and chaotic, Figure 3-4d.

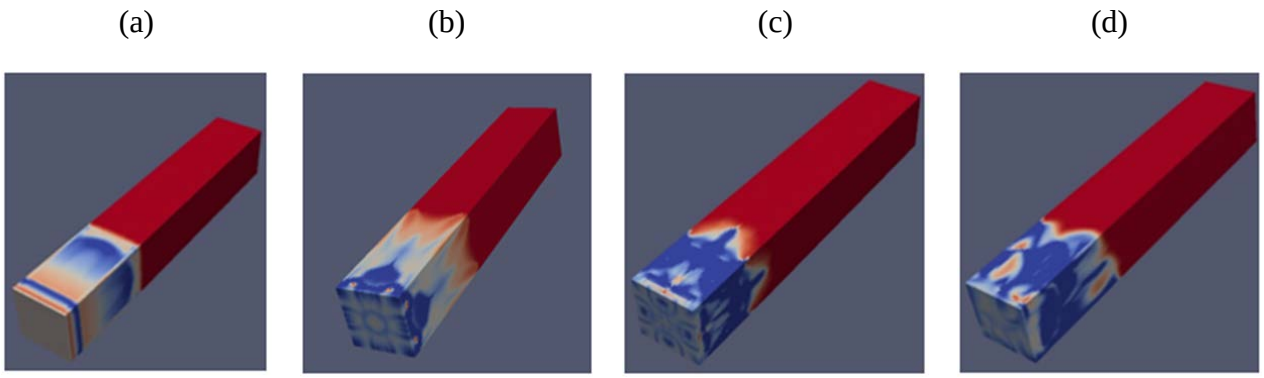

Figure 3-4 Voidage contours at different times encountered in the fluidized bed (for illustration purposes, the bed is titlted horizentoally)

3.3 ARTIFICIAL NEURAL NETWORK SETUP

Once the output files of MFiX are converted to *.csv file they are ready to be reorganized to serve as the input to the Artificial Neural Network (ANN). Every time-step and every inlet velocity has one *.csv file containing 9 columns and 118,098 rows (size of the modeled fluidized bed, 27x162x27 = 118,098 cells). Each column represents one property such as gas pressure and each row corresponds to one cell. Depending on the solution scenario, which will be discussed later, some of these columns and rows or different combination of them (temporally averaging) will be used as input or output.

3.3.1 Neural Network Architecture

Each artificial neural network consists of an input layer, one or more hidden layers, and an output layer. The input and output parameters are chosen based on the nature of the problem and the property which is going to be predicted.

The number of inputs and outputs are chosen based on the problem and the solution scenario which will be discussed in detail in the next section. There is no clear guideline on how many hidden layers and neurons are required at each layer. The type of problem and user experience, along with few rules of thumb are the primary factors in determining the number of hidden layers and neurons. One such rule is that the number of neurons in the first hidden layer shouldn't be less than the number of input parameters. Matlab and its Neural Network toolbox have been used for ANN training.

For the first try, only one hidden layer with 15 neurons is considered. The network characteristics and the activation function were described in the part one report of this series, [11], and will not be repeated here. The type and some internal functions of ANN are listed in Table 3-1.

Table 3-1 ANN model parameters

ANN Parameters	***Current Status***
Network Type	*Feed-forward Back Propagation*
Training Algorithm	*Levenberg-Marquardt*
Transfer Function	*TANSIG*

3.3.2 Input and Output

In the first report of this research, [11], it was shown that non-cascading scenario had a downside which was the need for the MFIX results at each time-step. In order to train the ANN at time step (t), the CFD results at time step (t-1) were used as input to ANN, along with static parameters, such as location of each cell or distance between each cell to the walls. The output for the non-cascading training process was a single dynamic parameter, such as pressure or velocities or volume fraction at time step (t).

In the second report of this research, [1], static parameters, CFD results and other model input parameters such as gas inlet velocity were used at time step (t) to train the ANN for the same time step (t) and different ANNs were trained for different time steps. The output of the neural network was either gas pressure, gas volume fraction or gas velocity. All the trainings were performed at the *Cell Level*. In the *Cell Level* approach, information in each computational cell (control volume) and the surrounding cells are used to construct the ANN. In other words, the ANN was trained using 118,098 (=27*27*162) data points for each inlet velocity.

In this report, the training procedure outlined in our second report [1] is utilized at the *Layer Level*. Training and employing ANN at the layer level leads to improvement in the training time, since only a single average value is trained across each cross section (layer). The speedup in training comes at the expense of less spatial resolution. The average gas pressure at a horizontal plane is used to construct the ANN. Since there are 162 grid points in the vertical direction in the CFD simulations, 162 layers are used for constructing the ANN. Figure 3-5 shows the difference between the cell based approach, where an ANN is constructed for each computational cells, Figure 3-5a, and the layer based approach, where an ANN is constructed for the averaged values across each cross-sectional area, Figure 3-5b.

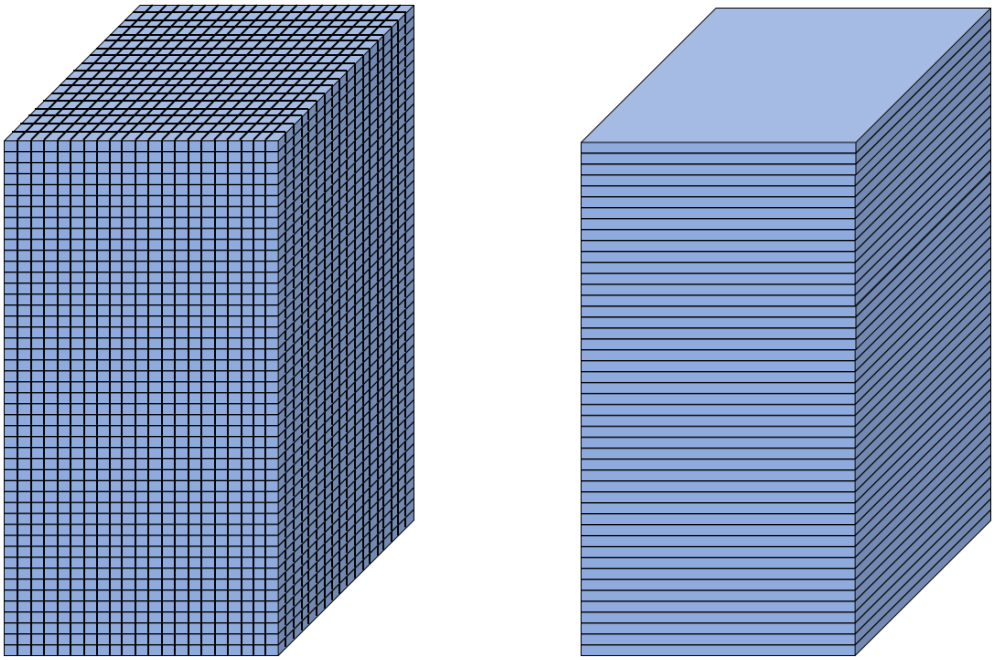

(a) (b)

Figure 3-5 Different training approaches for ANN at (a) Cell Level (b) Layer Level

3.3.3 Data Partitioning

A good ANN is a model that learns the pattern in the given data-set while it is able to predict the behavior of a new given dataset, this model is called “Just Right”. If the ANN does not learn the pattern in the data very well the model is called “Under-fit”. If the ANN learns the pattern of the data very well with a very small error but it is not able to predict the behavior of a new given data-set, the model is called “Over-fit”. Under-fitting occurs for so many reasons such as lack of information (the model should have more parameters and more records). Overfitting occurs when the network learns to mimic almost all the data points exactly but when it comes to the prediction, the model performs poorly for a new given data, in other words, the model memorizes all the data points. Figure 3-6 shows these 3 states of training.

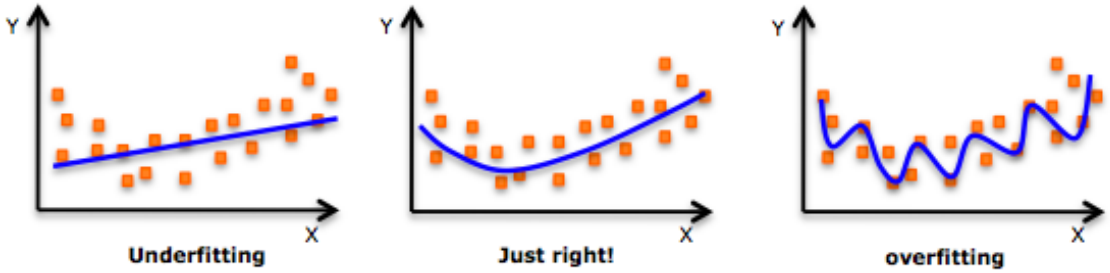

Figure 3-6 Underfitting and overfitting of the data

To overcome the overfitting problem, only a portion of the data is used to train the network. The remaining data points which the model has not seen in the training process, are further divided into two sub groups; calibration and validation.

Training is an iterative process where in each iteration the optimization algorithm tries to move toward the lower error. An iteration is defined as the process through which all the records in the training data set are introduced to the ANN once and the error between the actual (target) output and those predicted by the ANN are calculated and the impact of the calculated error is back-propagated throughout the ANN in order to modify the weights associated with all the connections between neurons in the ANN. The training process stops based on some user defined criteria. This criterion could be the total number of iteration, or the total time of training, or the number of calibration failure or a combination of those. In this project, the combination of all the mentioned criteria are used to terminate the training process.

Calibration data set is used while the training is being carried out. It is used as some criteria to stop the training process when the model is "Just Right". The error in both training data set and calibration dataset usually decreases at the beginning of the training process, however somewhere along the training process, the error in calibration data set stops decreasing while the error continues to decrease in the training data set. The model at this point is usually the best model because it has provided the lowest possible error for the calibration data set (blind data set) and while it has an acceptable error for the training data set. Figure 3-7 shows the training and calibration curves.

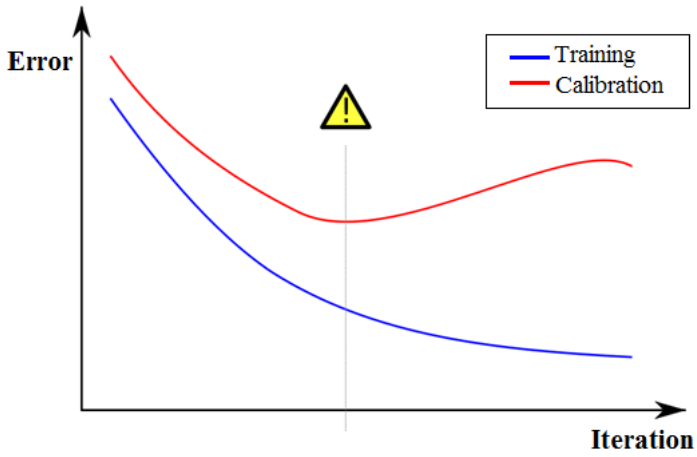

Figure 3-7 Learning curve, training error and calibration error

The validation data set is used upon the completion of the training process when the best ANN is achieved. Although both calibration and validation data sets are blind but having an ANN model with a low calibration error does not mean that the ANN is a good predictor (because the best model is already picked when the calibration error is minimum) unless the ANN error in validation data set is also acceptable. The percentage of the data partitioning used for the preliminary study of this project is shown in Table 3-2.

Table 3-2 Original data partitioning

Data	*Training*	*Calibration*	*Validation*
Percentage of data (%)	*70*	*15*	*15*

3.3.4 Blind Test

A blind test is when some of the data that was not used during the training of ANN, is used to further validate the predictive capability of the trained ANN, Figure 3-8. The difference between calibration and validation during the training process and the complete blind test is that the records in the calibration and validation process during the training are chosen randomly from the original dataset, for example, some of the records of inlet velocity of 0.9 are in the training set and some of them are in calibration and validation set, but all the records of inlet velocity of 0.825 are in the blind test set which makes the prediction much more difficult.

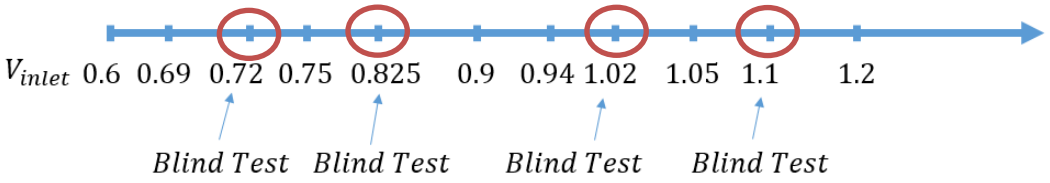

Figure 3-8 Blind test cases carried out at four different inlet velocities

3.4 SOLUTION SCENARIOS

Different scenarios are considered to reach the final goal of this project. The term "*Different scenarios*" refers to having different input and output structures at different time-steps. The training technique is the same throughout all the scenarios. Each scenario has two parts, the training process and the deployment process. During training process, the input parameters and CFD output are fed to the ANN to optimize the network parameters. In deployment, the ANN output will be generated based on the trained ANN and the given input parameters. Deployment could be done with the data used in the training to check the training quality, and it could be done on blind cases to evaluate the predictability and generality of the ANN.

As it was stated earlier, the goal of this research project is to build a smart proxy model at the *Layer Level*, which is constructed from CFD based data. The scenarios outlined below show the systematic steps, which have been taken from the least complex scenario to the more complex scenarios. The scenarios are as follows:

- Training an ANN for gas pressure using 4 static parameters at a single time step, as discussed in section 3.4.1
- Training an ANN in a non-cascading manner at a single time step for gas pressure using 4 static parameters at the target layer and pressure at the next layer, downstream of the target layer, as discussed in section 3.4.2

- Training an ANN in a cascading manner at a single time step for gas pressure using 4 static parameters at the target layer and pressure at the next layer, downstream of the target layer, as discussed in section 3.4.3
- Training an ANN in a non-cascading manner at a single time step for gas pressure using 4 static parameters at the target layer and pressure at the previous layer, upstream of the target layer, as discussed in section 3.4.4
- Training an ANN in a cascading manner at a single time step for gas pressure using 4 static parameters at the target layer and pressure at the previous layer, upstream of the target layer, as discussed in section 3.4.5
- Temporal and spatial averaging of ANN data in Upward (inlet to outlet) Cascading mode from time steps 500 to 1400 and time steps 1500 to 3400 are discussed in section 3.4.6

3.4.1 Training for gas pressure using 4 static parameters

In the Cell Level approach, identification of the cell location was done by using 6 values (distances to the right, left, top, bottom, north, and south walls, as shown in Figure 3-9-a). In order to define the location of each layer in Layer Level approach, we have only 2 distances to the top and bottom walls (Figure 3-9-b). By using these 2 distances, we can teach the ANN how close the exit or inlet planes are to each layer, which helps the ANN to handle the boundary condition. Moving from *Cell Level* to *Layer Level* will reduce the available static parameters from 11 features to 4 features (Figure 3-9).

As depicted in Figure 3-10, a neural network is trained with 4 static parameters (2 distances to the exit and inlet planes to account for boundary effects, the index of the layer, and the inlet velocity) at time step 1400, along with inlet velocity value. Additionally, average gas pressure from CFD results at each inlet velocity is used as output to ANN. For this scenario, Figure 3-10, at each inlet velocity and time step, there are 162 records, for a total of 1,134 (7 velocities *162) records for all the inlet velocities, as shown in Figure 3-2.

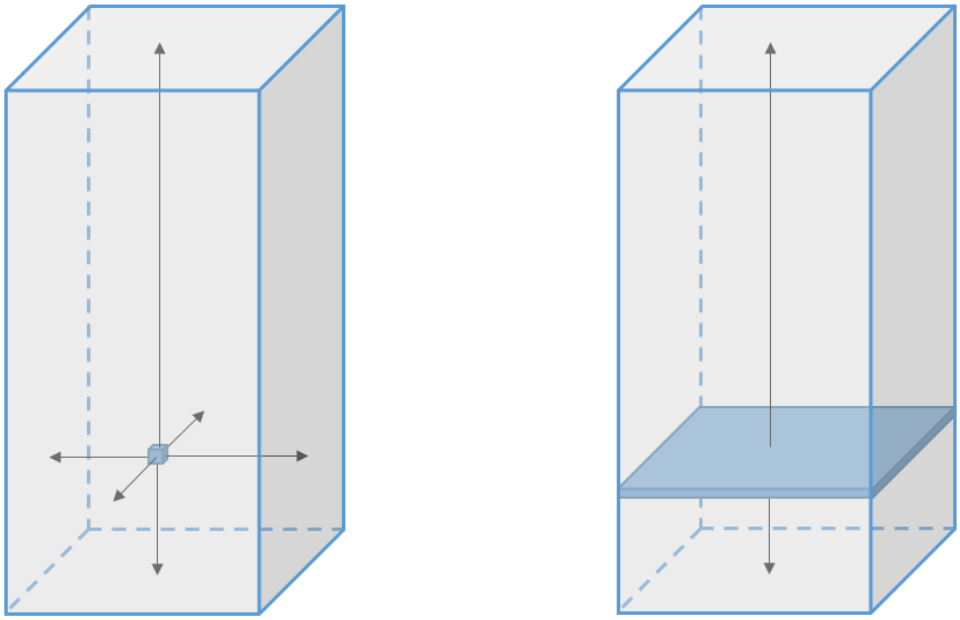

(a) (b)

Figure 3-9 Distances to the wall in Cell Level (a) and in Layer Level (b)

Table 3-3 Moving from Cell Level to Layer Level

	Distance to top	Distance to bottom	Distance to left	Distance to right	Distance to north	Distance to south	I, J, K	Index	Inlet Velocity
Cell Level	✓	✓	✓	✓	✓	✓	✓	✓	✓
Layer Level	✓	✓	✗	✗	✗	✗	✗	✓	✓

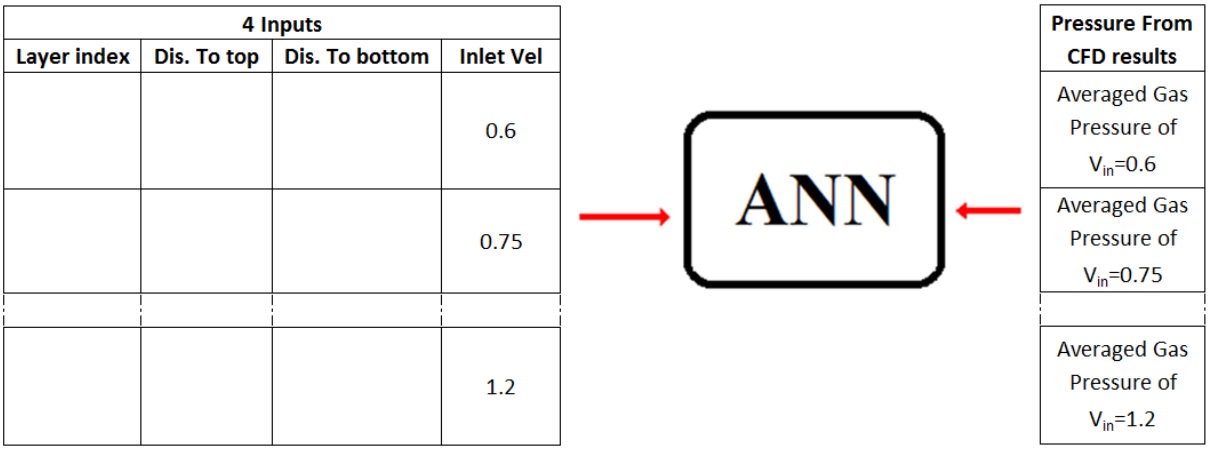

Figure 3-10 Traning for average gas pressure using 4 static parameters at layer level at each time step

Table 3-4 summarizes the ANN numerical values associated with this step of the project. Similar to previous report, Figure 3-11 shows the distribution of gas pressure in the fluidized bed for different inlet velocities., This figure shows that there is enough variation for the neural network to learn from (Figure 3-11 a and b). Data for inlet velocity of 0.825 m/s is kept out of the training and is used for validation, Figure 3-11c. The results of training ANN with 4 static parameters at layer level are presented in section 4.2.

Table 3-4 Neural Network Model parameters

Number of Inputs	*4*
Number of hidden layers	*1*
Number of Hidden Neurons	*8*
Number of records	*1,134*
Number of Output	*1*

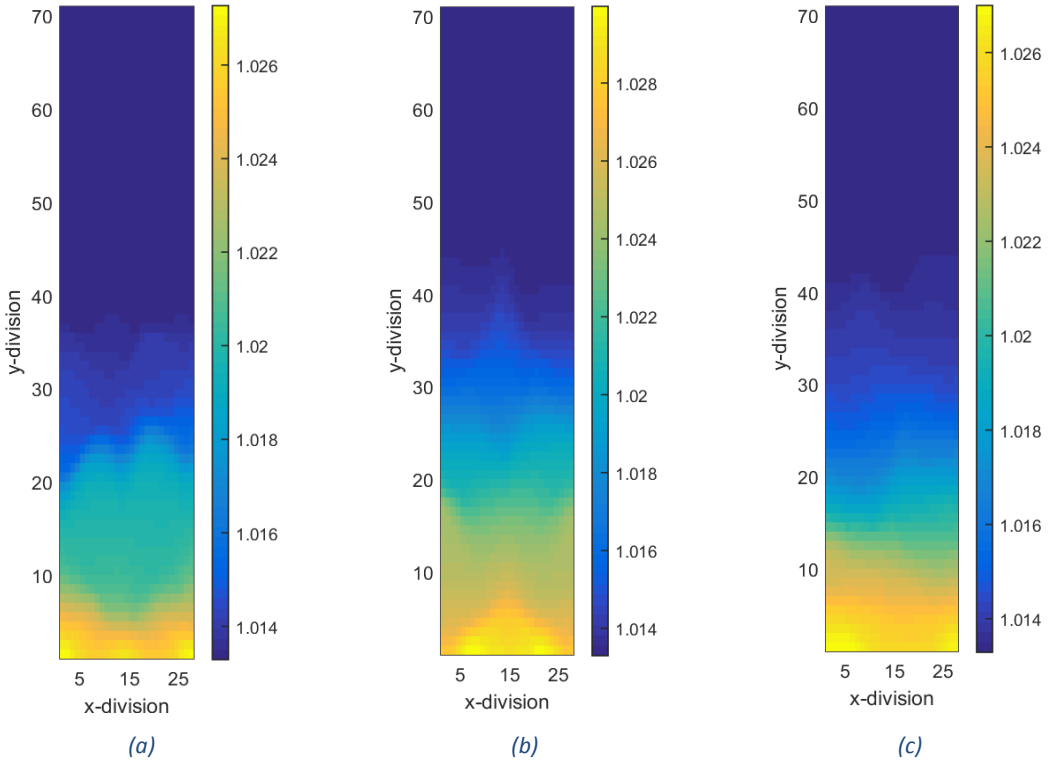

Figure 3-11 Gas pressure at cross sectional plane K = 7 at (a) V_{inlet} = 0.6 m/s (b) V_{inlet} = 1.2 m/s (c) V_{inlet} =0.825 m/s (Pressure unit: 10^5 Pa)

3.4.2 Training and deployment for average gas pressure in Non-Cascading Mode with information flowing from downstream to upstream

In the previous scenario, 4 static parameters are used to train the ANN. To improve the quality of the trained ANN, a dynamic parameter (gas pressure in the current scenario) is used during the training process, as an additional input. In our previous report [11], it was shown that the dynamic parameter used during the training has to be selected from the same time step the ANN is being trained for and not from the previous time step. In the current scenario, if training ANN for level "L", pressure from CFD results at level "L+1" (downstream level) is used as input to the training of ANN. The training scheme discussed above is shown in Figure 3-12. The direction of ANN training is selected to be from fluidized bed outlet to inlet (downstream to upstream). This choice is explained in section 3.4.3. The last layer is a boundary plane (outlet) and therefore does not require any training.

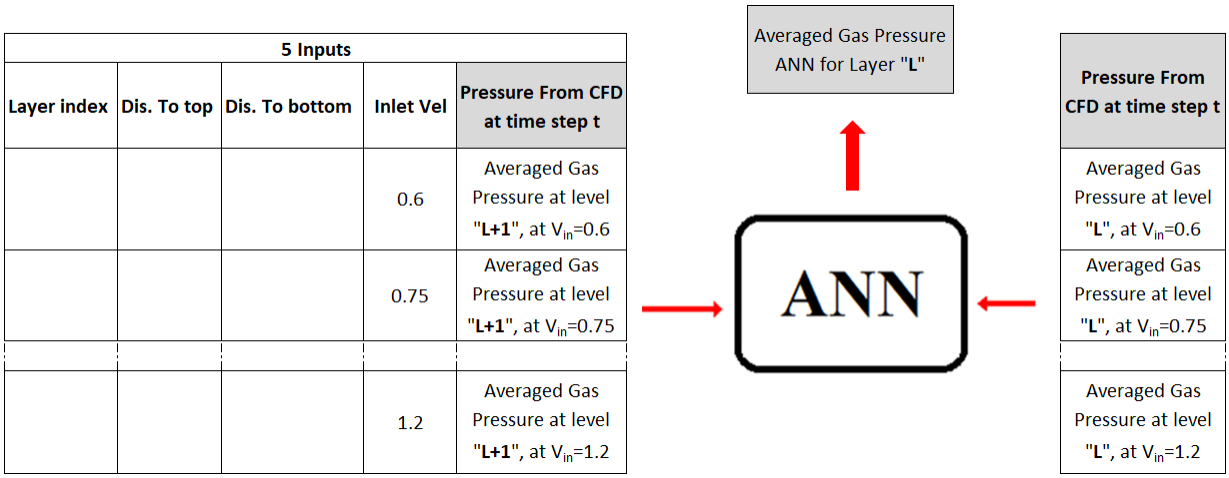

Figure 3-12 Traning for average gas pressure using 5 parameters for target layer "L", with information flowing from downstream to upstream

The deployment process is exactly the same as training except gas pressure at the target level is not an input to the ANN from CFD, rather this gas pressure at the target level is the output of ANN. Figure 3-13 shows the schematic of the deployment process, for the blind test condition of inlet velocity of V_{in} = 0.825 m/s. The results from this scenario is presented in section 4.3.

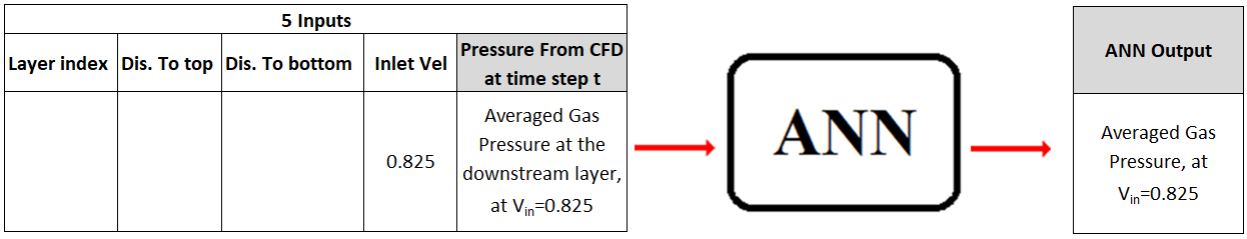

Figure 3-13 ANN deployment for average gas pressure using 5 parameters in non-cascading mode, with information flowing from downstream to upstream

3.4.3 Training and deployment for average gas pressure in Cascading Mode with information flowing from downstream to upstream

The training of ANN in the cascading mode is identical to the training steps described in the previous section, for non-cascading mode. If training ANN for level "L", pressure from CFD results at level "L+1" (downstream level) is used as input to the training of ANN, as shown in Figure 3-12. The only difference between cascading and non-cascading modes occurs at the deployment stage. In non-cascading mode, CFD results at the downstream level are input to the ANN during the deployment, Figure 3-13. However, in the cascading mode, the pressure values at the downstream level of "L+1", when training ANN for the target layer "L" comes from the trained ANN and not the CFD, Figure 3-14. Since in this approach, pressure value at level "L+1"

of trained ANN is used to predict the pressure at level "L", the direction of the information flow has to be from level "L+1" to level "L". In other word, deployment is done from downstream to upstream (outlet to inlet). The deployment process for the cascading mode is shown in Figure 3-15.

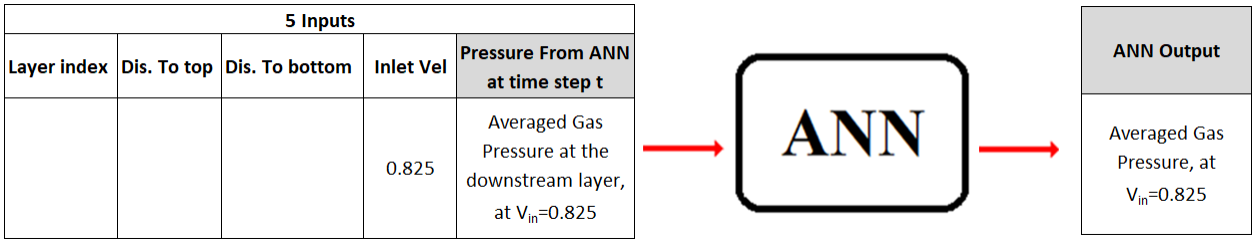

Figure 3-14 ANN deployment for average gas pressure using 5 parameters in cascading mode with information flowing from downstream to upstream

Since the direction of cascading is downward, the top layer (J=162) acts as the boundary condition and $P_{J=161}$ could be obtained using $P_{J=162}$. Then, $P_{J=160}$ is predicted using $P_{J=161}$ and this process will be repeated until the pressure of bottom layer (J=1) is predicted. The only challenge of cascading approach is that the pressure of top layer (J=162) may or may not be known for blind test cases, so the pressure should be estimated at this layer which will be discussed later.

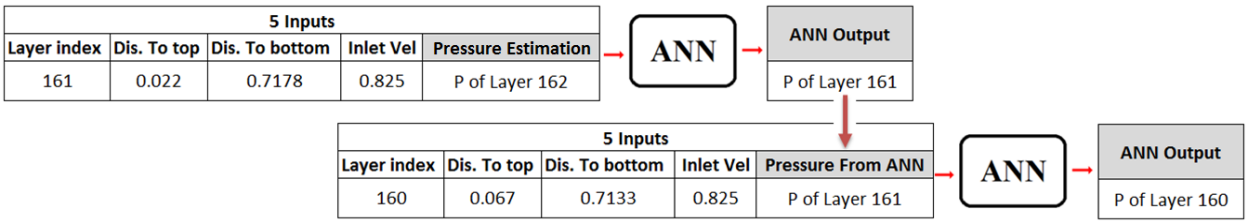

Figure 3-15 Detail of cascading deployment for average gas pressure using 5 parameters when information flows from downstream to upstream

It is worth mentioning that the training process for cascading and non-cascading approaches are identical. In the training process, all the gas pressures (at the target layer and the layer downstream from it) are provided from CFD results. In the non-cascading deployment, the input still comes from CFD, however in the cascading deployment, the ANN output from one layer is used as ANN input for the predication of the next layer. The summary of this discussion is shown in Table 3-5.

Table 3-5 Original data partitioning

Process	***Approach***	***Source of the Data***	
		Input	***Output***
Training	*Non-cascading / cascading*	*CFD*	*CFD*
Deployment	*Non-cascading*	*CFD*	*N/A*
	cascading	*ANN*	*N/A*

The only input that is required for cascading deployment beside the static parameters, is the starting pressure of the top layer (exit plane), as shown in Figure 3-15. Figure 3-16 shows the starting layer and deployment direction for predicting the average pressure at each layer for the cascading approach. The top layer (exit plane of the fluidized bed, shown is green) is a boundary plane and is set to atmospheric pressure, since the fluidized bed discharges into the ambient condition and the flow in the freeboard section of fluidized bed is extremely dilute, which implies negligible gas pressure drop. As such, the average pressure at the exit plane (layer 162) is equal to 101,325 Pa. With this pressure value known, it is easy to see why the direction of ANN deployment is from exit plane to inlet plane for pressure. Additionally, Figure 3-17 shows that, as expected, the average pressure in the freeboard region of the fluidized bed, where there is no solid particle present, remains constant. Since there will be very little change in pressure in the freeboard, the starting layer for the cascading approach during deployment is set to layer 70, Figure 3-18. The average pressure value at layer 70 can be estimated from CFD results to be 101,329.6 Pa, as seen in Figure 3-19. The results of downward cascading starting from layer 70 are shown in section 4.4.

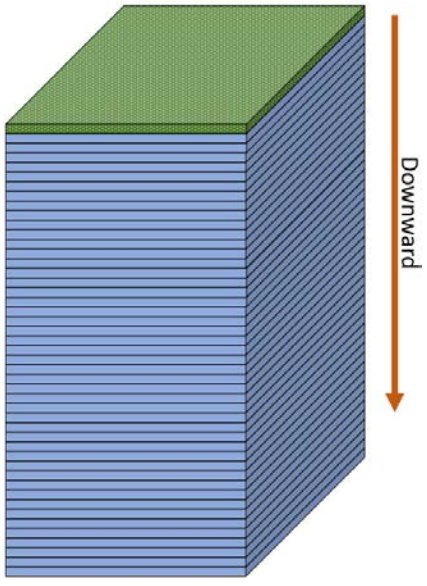

Figure 3-16 Starting layer (exit plane) and direction of cascading deployment

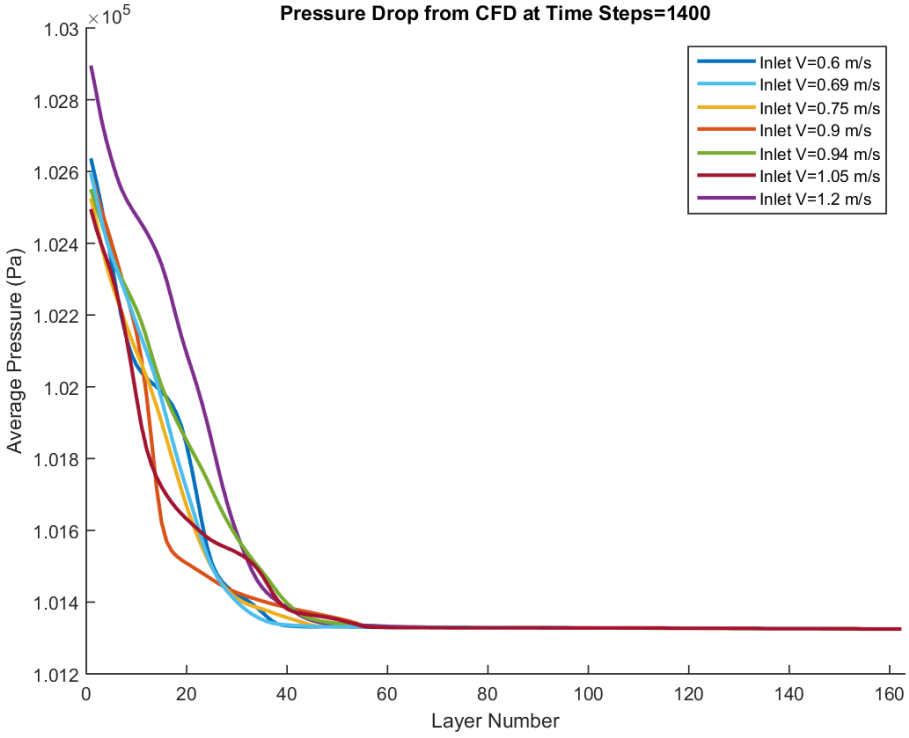

Figure 3-17 Average pressure profile for different inlet velocities used in training

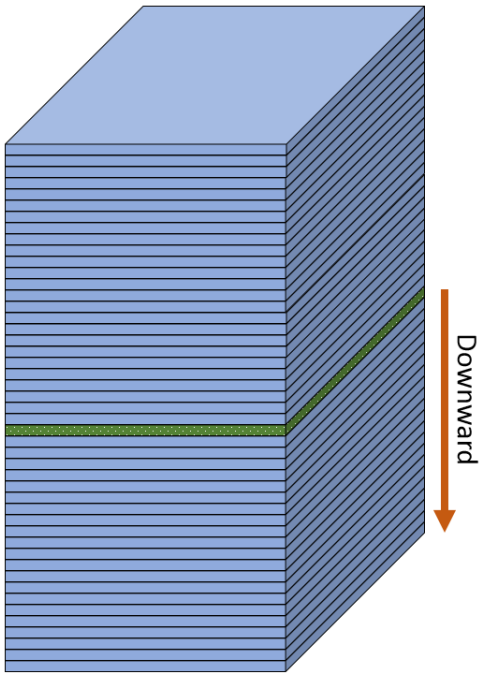

Figure 3-18 Starting layer (layer 70) and direction of Cascading deployment

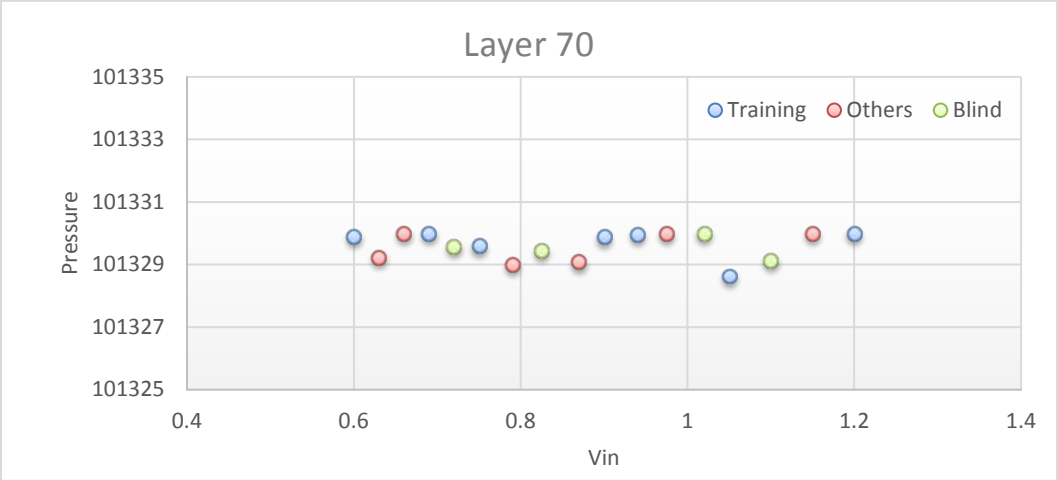

Figure 3-19 Average pressure across layer 70 for different inlet velocities

3.4.4 Training and deployment for averaged gas pressure in Non-Cascading Mode with information flowing from upstream to downstream

As an alternate method to the previous two sections, the direction of training and deployment could be from upstream to downstream of target layer "L", (inlet to outlet). This may be a more institutive direction for training and deployment, since this is the direction of mean flow in the fluidized bed and flow information travel downstream.

5 Inputs				
Layer index	**Dis. To top**	**Dis. To bottom**	**Inlet Vel**	**Pressure From CFD at time step t**
			0.6	Averaged Gas Pressure at level "**L-1**", at V_{in}=0.6
			0.75	Averaged Gas Pressure at level "**L-1**", at V_{in}=0.75
			1.2	Averaged Gas Pressure at level "**L-1**", at V_{in}=1.2

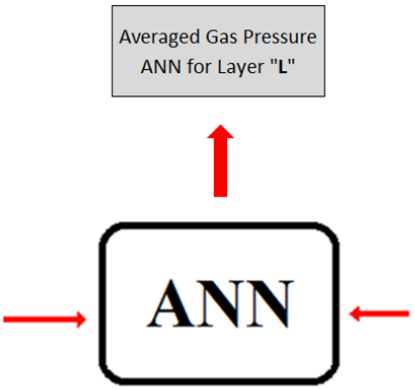

Pressure From CFD at time step t
Averaged Gas Pressure at level "**L**", at V_{in}=0.6
Averaged Gas Pressure at level "**L**", at V_{in}=0.75
Averaged Gas Pressure at level "**L**", at V_{in}=1.2

Figure 3-20 Traning for average gas pressure using 5 parameters with information flowing from upstream to downstream

Figure 3-21 shows the deployment process of the non-cascading approach for one of the blind tests with inlet velocity of V_{in}= 0.825 m/s. The average pressure of the layer "L-1", below the target layer of "L" is obtained from the CFD results and the ANN will predict the average pressure at target layer of "L". All the inlet velocities that are used in the training process can be used to confirm the training quality of the ANN.

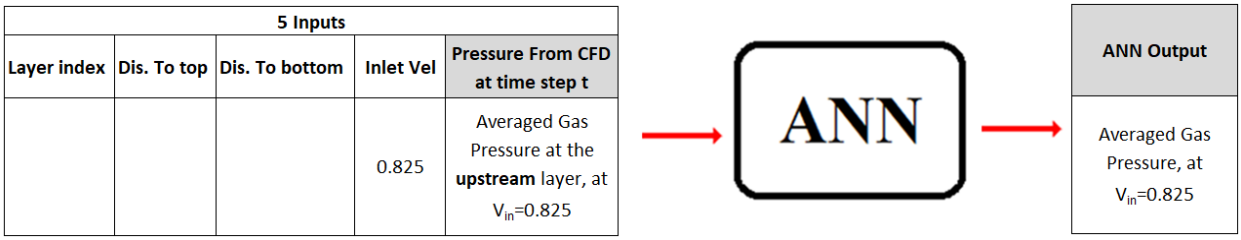

Figure 3-21 ANN deployment for average gas pressure using 5 parameters in non-cascading mode with information flowing from upstream to downstream

As mentioned before, the importance of the non-cascading approach is only to show how well the ANN could predict if the correct input is used. But for the practical application, cascading approach should be employed. The results of the training using upward non-cascading approach are presented in section 4.5.

3.4.5 Training and deployment for averaged gas pressure in Cascading Mode with information flowing from upstream to downstream

The training of cascading approach is identical to non-cascading approach, Figure 3-20. As mentioned before, the only difference between cascading and non-cascading is at deployment. The average gas pressure from CFD results is used during non-cascading deployment, while the average pressure from ANN is used in the cascading approach. Figure 3-22 depicts this process.

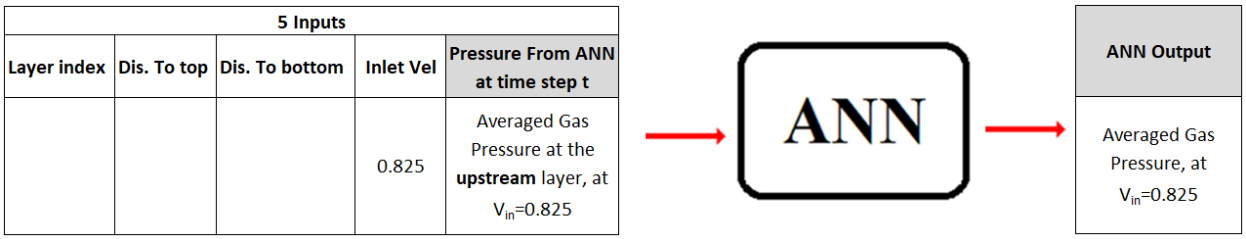

Figure 3-22 ANN deployment for average gas pressure using 5 parameters in cascading mode when information flows from upstream to downstream

In cascading approach, the pressure of below layer is not available and it should be calculated based on previous layer. The deployment sequence for cascading approach is shown in Figure 3-23. Since the direction of deployment for layer "L" is from upstream to downstream, the bottom layer (J=1) acts as the boundary condition and $P_{J=2}$ could be obtained using $P_{J=1}$. Then, $P_{J=3}$ is predicted using $P_{J=2}$ and this process will be repeated until it reaches to the top layer (J=162).

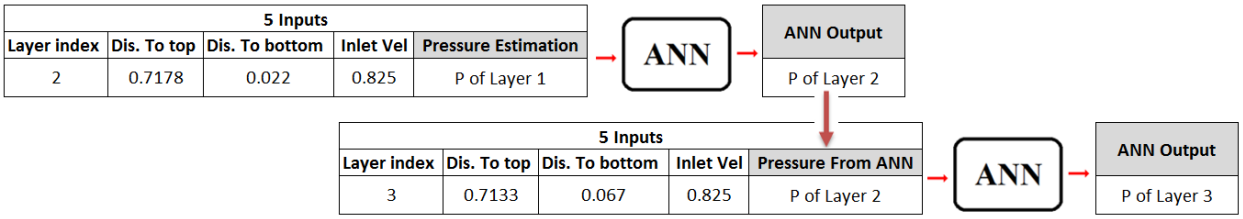

Figure 3-23 Detail of cascading deployment for average gas pressure using 5 parameters when information flows from upstream to downstream

Figure 3-24 shows the starting point and the direction of deployment. Since the pressure at the bottom layer is not known (not a prescribed boundary condition), the average value of pressure at layer 1, from all CFD simulations are used at a reasonable starting point, as shown in Figure 3-25. This average value, which is 102,644 Pa and will be the pressure estimate for layer 1, during cascading deployment, as shown in Figure 3-23. The results of the upward cascading with layer 1 as the starting point are presented in section 4.6.

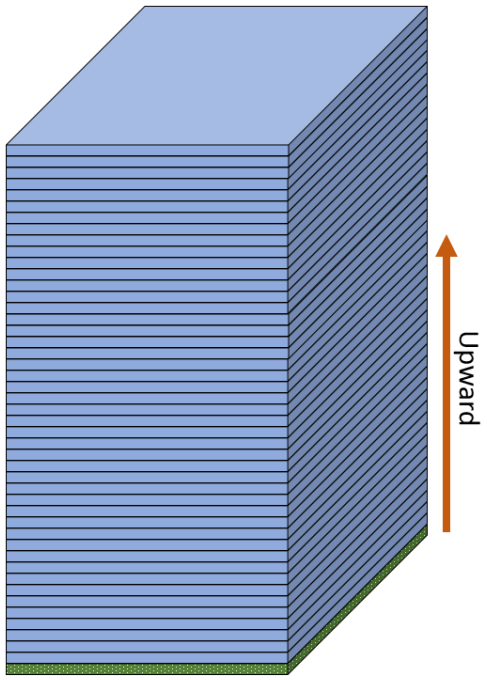

Figure 3-24 Starting layer (inlet plane) and direction of Cascading deployment

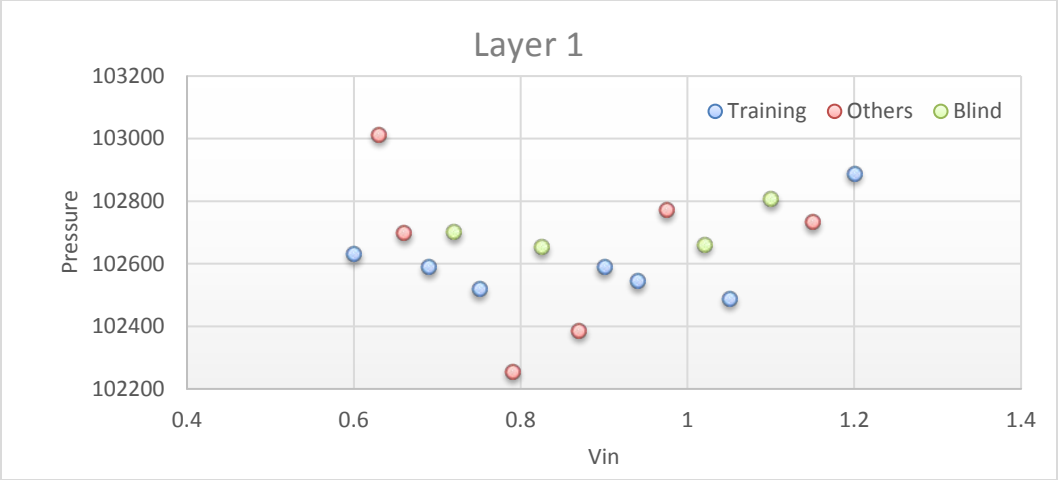

Figure 3-25 Average pressure across the bottom layer at different inlet velocities

3.4.6 Time average

Flow in a fluidized bed is highly transient and chaotic. As such, even multiple CFD simulations of the same flow conditions yield different instantaneous flow field, although the time averaged flow field must be the same. For this reason, the performance of a fluidized bed is typically accessed based on the time and/or space averaged behavior of the various variables such as pressure, velocities and volume fraction of gas and solid particles.

More than one ANN is needed in order to perform time average analysis of the smart proxy results. This is achieved by constructing 10 ANNs for time steps 500 to 1400, at an increment of 100 time steps and 20 ANNs for time steps 1500 to 3400 at an increment of 100 time steps, using the training approach outlined in Figure 3-20. Each time step is 0.001 seconds of simulation time. Figure 3-26 shows the two-time periods used for time averaging, for time steps 500 to 1400, and for time steps 1500 to 3400, representing flow conditions depicted in Figure 3-4(a) to (b) and Figure 3-4(c) to (d) respectively. Section 4.7 shows the results of time averaging step.

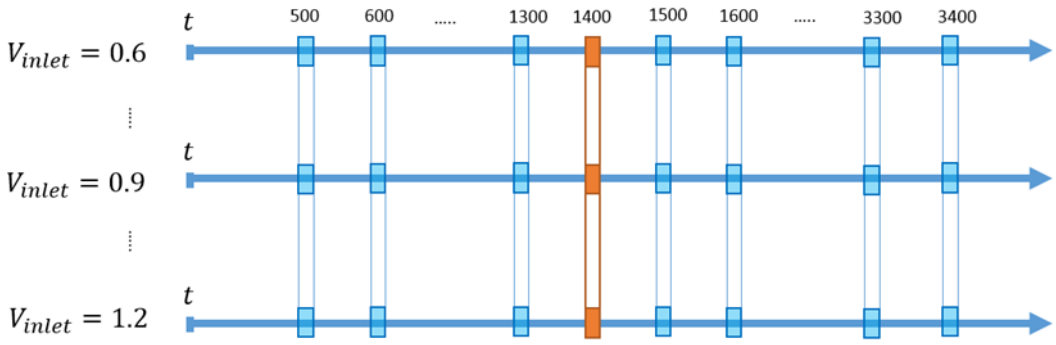

Figure 3-26 Time steps selected for time average

4. RESULTS AND DISCUSSIONS

The results of the various scenarios outlined in the previous section are discussed in this section with the related figures.

4.1 PRESENTATION OF THE RESULT

All the various scenarios in the previous section were built using data from 7 different MFIX runs. In this chapter, the pressure drop curves are provided both for training cases and for blind test cases. Once a good training is achieved, ANN is deployed on several blind test cases to evaluate the predictability of the ANN model. Figure 3-8 showed all the inlet velocities that have been used in the training and deployment process.

Average pressure across each layer for both CFD simulations and ANN, as shown in Figure 4-1, is used for comparison, to assess the prediction accuracy of trained ANN.

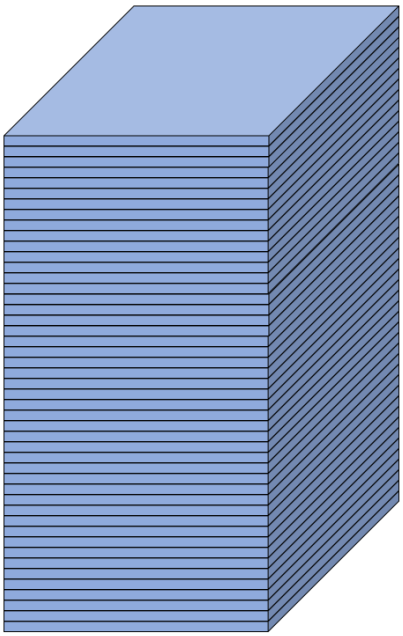

Figure 4-1 Cross sectional planes (layers) used in data analysis

4.2 GAS PRESSURE USING 4 STATIC PARAMETERS

Four static parameters, as shown in Figure 3-10 were used for the training of the ANN to mimic the gas pressure at time step 1400. Figure 4-2 and Figure 4-3 show the comparison between the trained ANN and CFD results for the training data with inlet velocity of V_{in} = 0.6 m/s and 1.2 m/s respectively. Since the flow in the freeboard section of the fluidized bed (layers 70 and above) is extremely dilute, gas pressure drop in the freeboard is very small, as seen in Figure 4-2 and Figure 4-3. Therefore, the pressure profile in the freeboard will not be included in the preceding figures. Additional figures for the rest of the inlet velocities are provided in Appendix I. It is clear from these figures that the ANN performs well in the inlet velocities that are part of the training. Figure

4-4 through Figure 4-6 show the quality of the ANN for blind test cases, when inlet velocities of V_{in} = 0.72, 0.825, and 1.02 m/s are used, respectively.

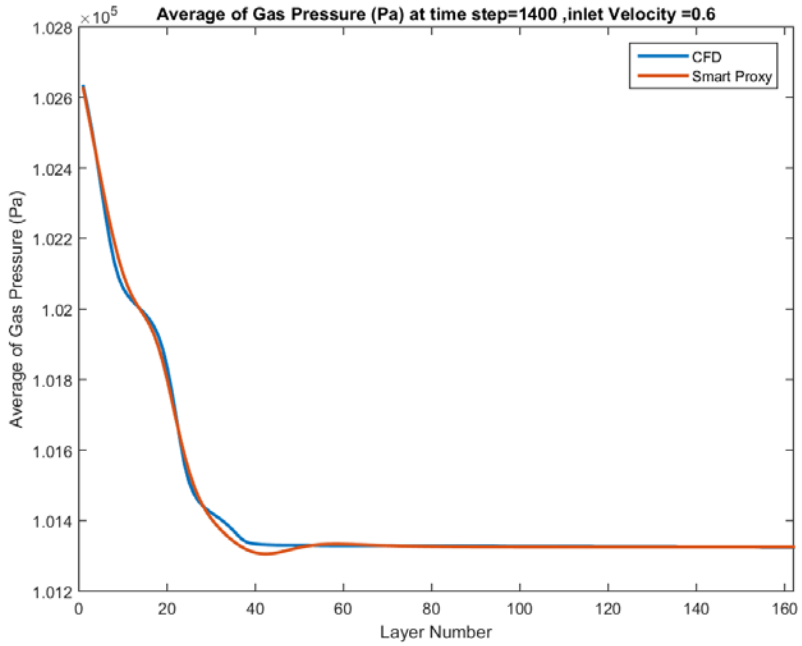

Figure 4-2 Spatially averaged CFD and smart proxy results for gas pressure at time step = 1400 and V_{in}=0.6 m/s (with 4 static parameters)

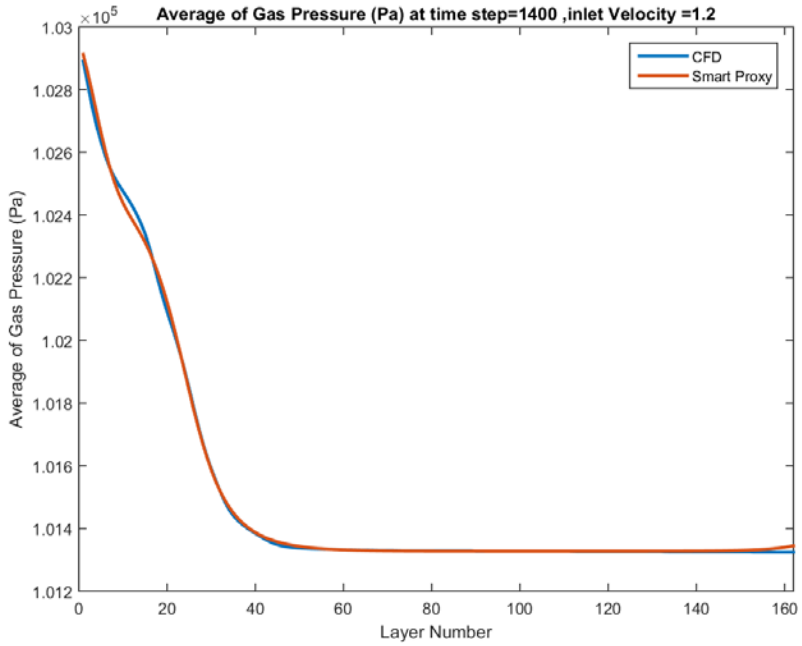

Figure 4-3 Spatially averaged CFD and smart proxy results for gas pressure at time step = 1400 and V_{in}=1.2 m/s (with 4 static parameters)

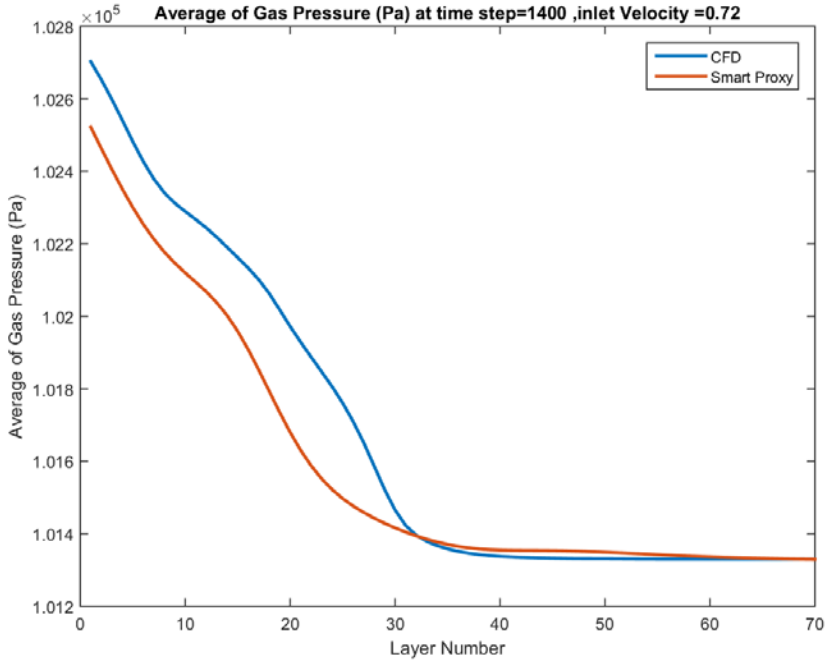

Figure 4-4 Spatially averaged CFD and smart proxy results for gas pressure at time step = 1400 for blind test condition of V_{in}=0.72 m/s (with 4 static parameters)

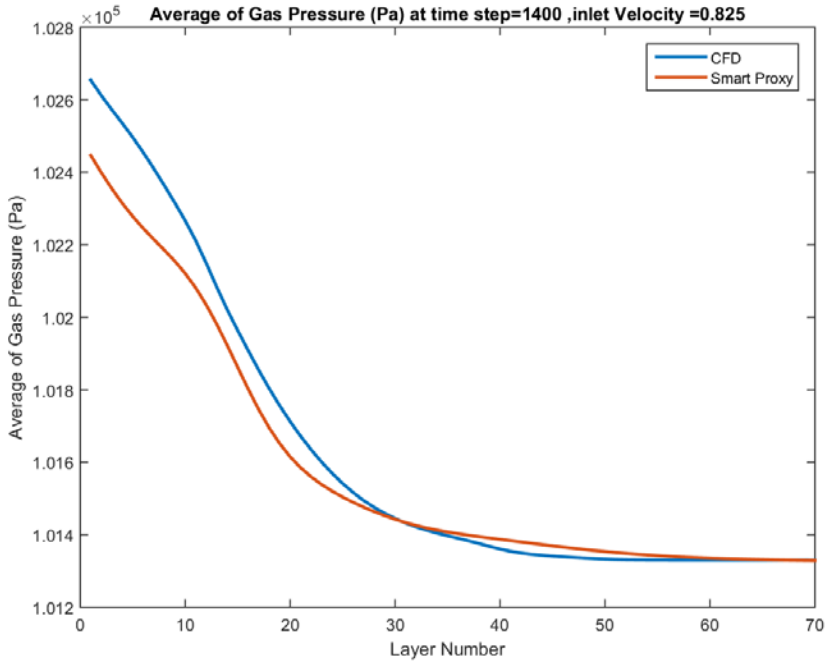

Figure 4-5 Spatially averaged CFD and smart proxy results for gas pressure at time step = 1400 for blind test condition of V_{in}=0.825 m/s (with 4 static parameter)

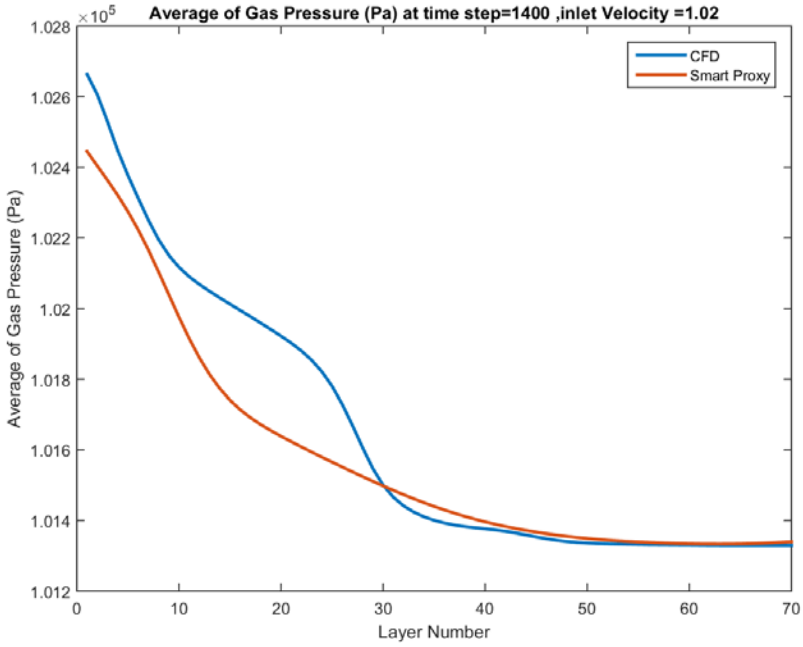

Figure 4-6 Spatially averaged CFD and smart proxy results for gas pressure at time step = 1400 for blind test condition of V_{in}=1.02 m/s (with 4 static parameters)

Although there is good agreement between CFD results and smart proxy results in the training cases, there is a poor agreement for the blind test cases. Figure 4-4 to Figure 4-6 show that the ANN is predicting a much more dilute flow in the vicinity of inlet and the lower portion of the bed, compare to CFD prediction results. The pressure drop across the bed predicted by ANN is subsequently lower than in CFD. This indicates that the amount of solid particles predicted by ANN is less than the actual amount of solid in the bed (as predicted by CFD results). This fact shows that the ANN can mimic the data which is used in the training but it has not learnt enough to be used as a predictive model. It means that the network does not have enough information to predict a blind test. To resolve this issue, additional parameter, average pressure at the downstream or upstream layer, is added to the training data set.

4.3 AVERAGE GAS PRESSURE, WITH INFORMATION FLOWING FROM DOWNSTREAM TO UPSTREAM IN NON-CASCADING MODE

To improve the quality of ANN, one more parameter is added to the training which is the average pressure of downstream layer (according to Figure 3-12). Figure 4-7 shows the quality of the training for gas pressure at time step 1400, when inlet velocity of V_{in} = 0.6 is used. As expected, this figure shows a significant improvement in the training result in compare to when 4 static parameters are used (Figure 4-2). Adding one dynamic parameter to the input along with the 4 static parameters helps the ANN to mimic the CFD results with higher accuracy. Figure 4-8 shows the deployment quality when inlet velocity of V_{in} = 0.825 is used. This figure shows an excellent match between CFD and the smart proxy results. The non-cascading deployment proves that the

ANN can be used as a predictive model for the blind test cases if the ANN is trained properly. This approach could be further tested when cascading approach is used.

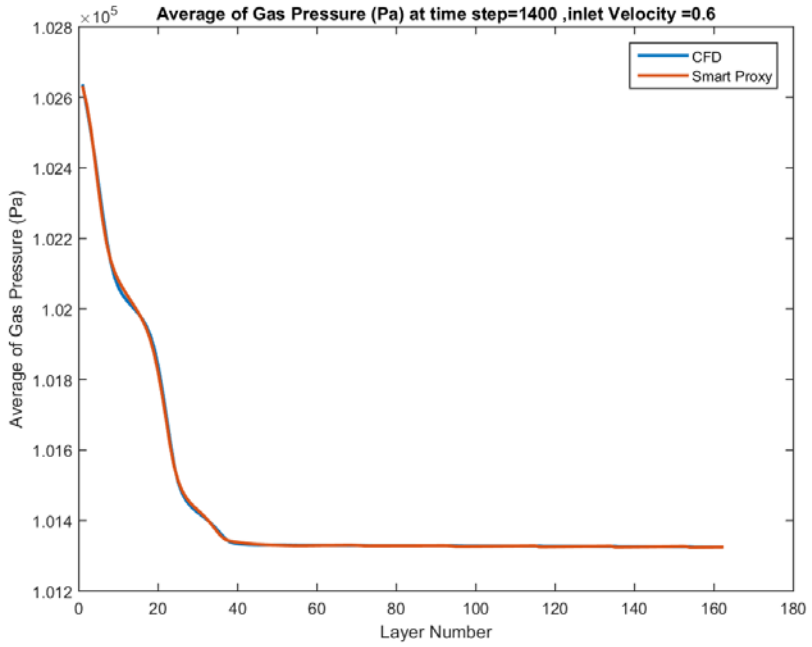

Figure 4-7 Spatially averaged CFD and smart proxy results for gas pressure at time step = 1400 and V_{in}=0.6 m/s

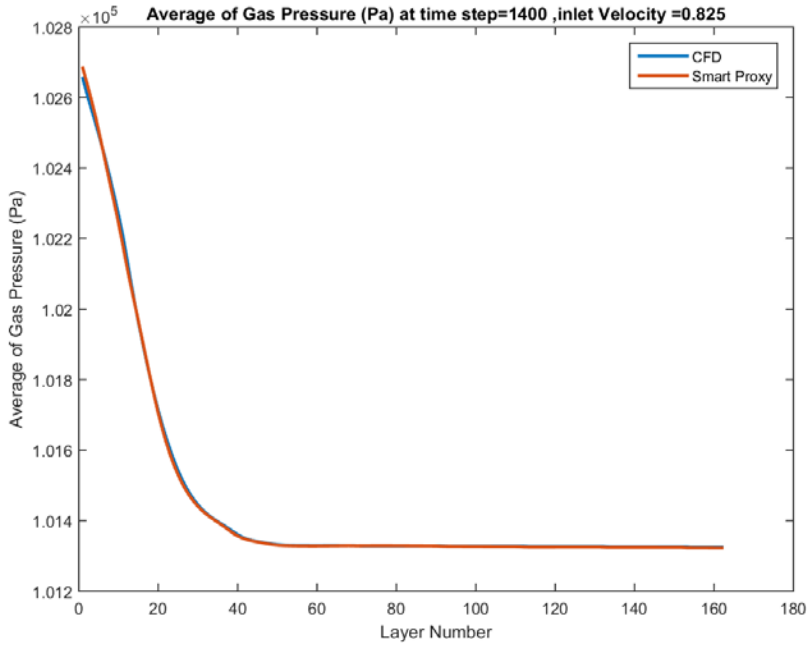

Figure 4-8 Spatially averaged CFD and smart proxy results for gas pressure at time step = 1400 for blind test condition of V_{in}=0.825 m/s

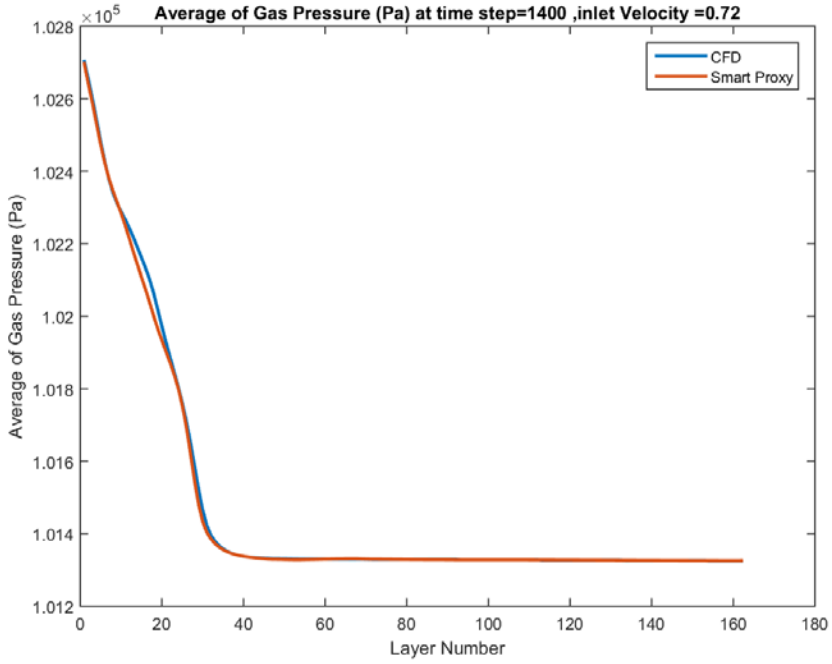

Figure 4-9 Spatially averaged CFD and smart proxy results for gas pressure at time step = 1400 for blind test condition of V_{in}=0.72 m/s

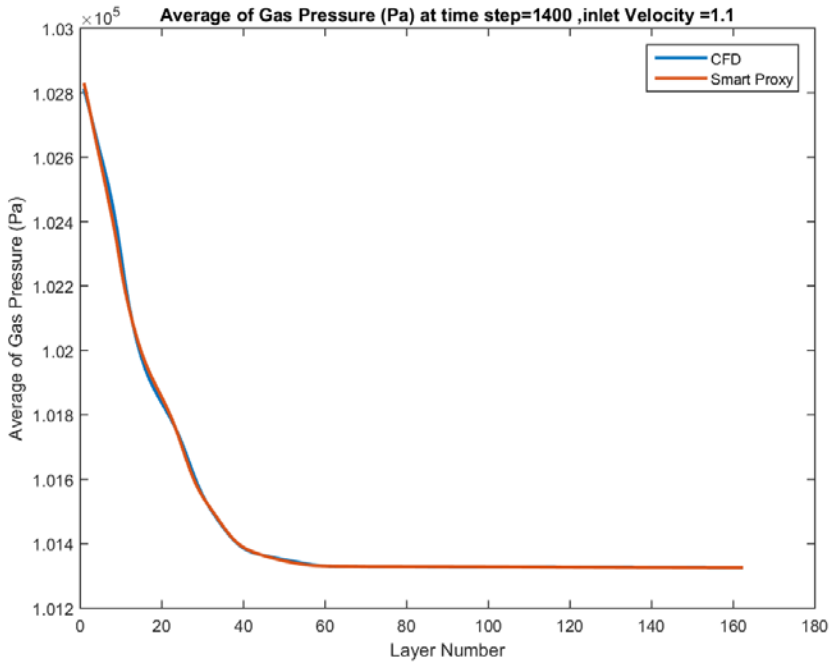

Figure 4-10 Spatially averaged CFD and smart proxy results for gas pressure at time step = 1400 for blind test condition of V_{in}=1.1 m/s

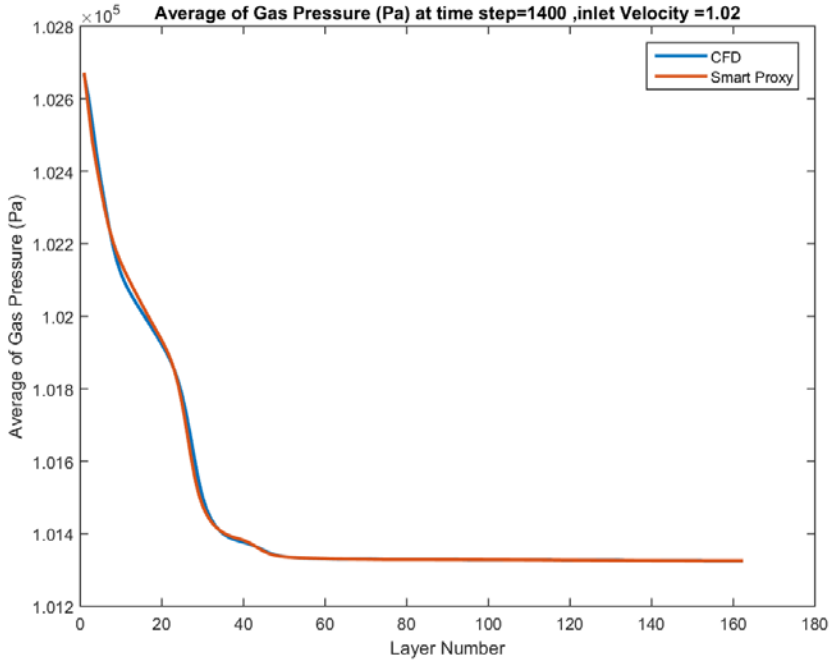

Figure 4-11 Spatially averaged CFD and smart proxy results for gas pressure at time step = 1400 for blind test condition of V_{in}=1.02 m/s

4.4 AVERAGE GAS PRESSURE, WITH INFORMATION FLOWING FROM DOWNSTREAM TO UPSTREAM IN CASCADING MODE

After successful deployment in the non-cascading approach, the same trained ANN described in section 4.3 is used in the cascading mode according to Figure 3-14 and Figure 3-15. Figure 4-12 shows the cascading deployment when inlet velocity of V_{in} = 0.6 m/s, which is part of the training data set, is used at time-step 1400. The starting layer for deployment is exit plane (layer J=162) and the direction of deployment is from downstream (exit plane) to upstream (inlet plane). The result of smart proxy deviates from CFD results after couple of layers. The ANN model is not performing well even though inlet velocity of 0.6 m/s is part of the training data set. The lack of fidelity between ANN predication and CFD results indicate that the training process is not as optimal as it can be.

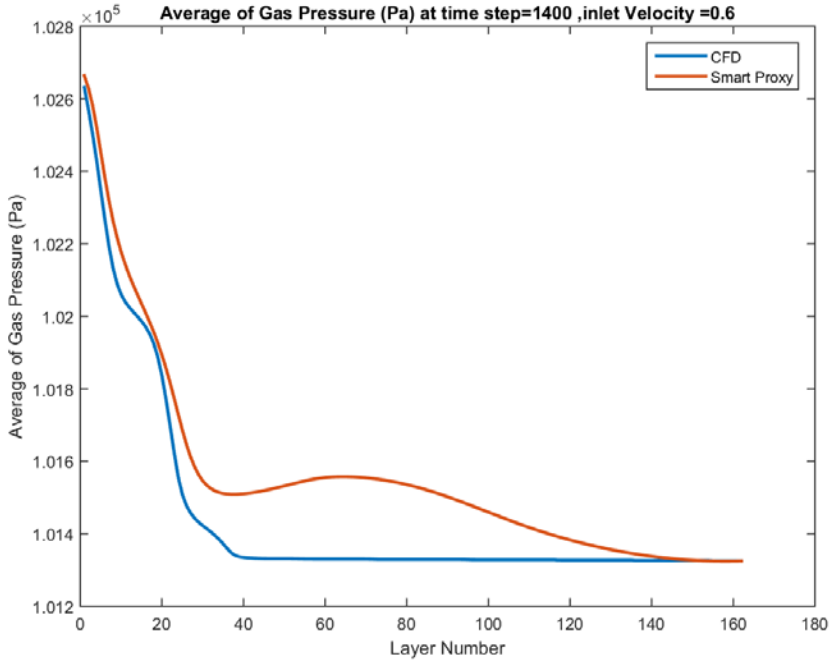

Figure 4-12 Spatially averaged CFD and smart proxy results for gas pressure at time step = 1400 and V_{in}=0.6 m/s with starting layer = 162

As mentioned in the section 3.4.3, since the fluidized bed discharges into atmospheric condition, the outlet pressure should be atmospheric and hence constant. Additionally, since the gas pressure drop in the freeboard region of the bed is minimal, due to lack of solid particles, layer 70 (Figure 4-12) is chosen as the start of deployment plane.

Figure 4-13 shows the results of the smart proxy and CFD when the ANN is deployed from downstream (layer 70) to upstream (layer 1) in a cascading manner, for inlet velocity of V_{in} = 0.6 (m/s) and time-step of 1400. The agreement between CFD results and ANN prediction has not improved. Figure 4-12 and Figure 4-13 show that training and deployment of ANN from downstream (exit plane) to upstream (inlet plane) does not yield a high-fidelity ANN model.

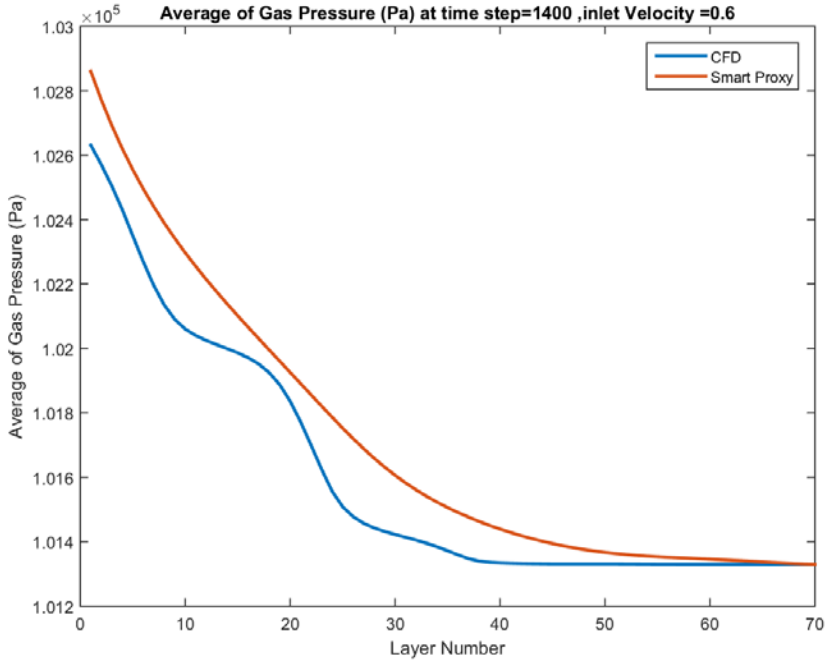

Figure 4-13 Spatially averaged CFD and smart proxy results for gas pressure at time step = 1400 and V_{in}=0.6 m/s, with starting layer=70

4.5 GAS PRESSURE WITH TRAINING AND DEPLOYMENT FROM UPSTREAM TO DOWNSTREAM IN NON-CASCADING MODE

After an unsuccessful deployment in the previous sections, the direction of ANN training and deployment is changed to training and deploying from upstream layer (inlet plane) to downstream plane (exit plane), according to Figure 3-20. The input to the training process is shown in Figure 3-21. Figure 4-14 shows the quality of the training for average gas pressure at time step 1400, when inlet velocity of V_{in} = 0.6 is used. As expected, this figure shows a good agreement between CFD and smart proxy. Figure 4-15 shows the deployment quality when inlet velocity of V_{in} = 0.825, from blind test cases, is used. This figure shows an acceptable match between CFD results and the smart proxy.

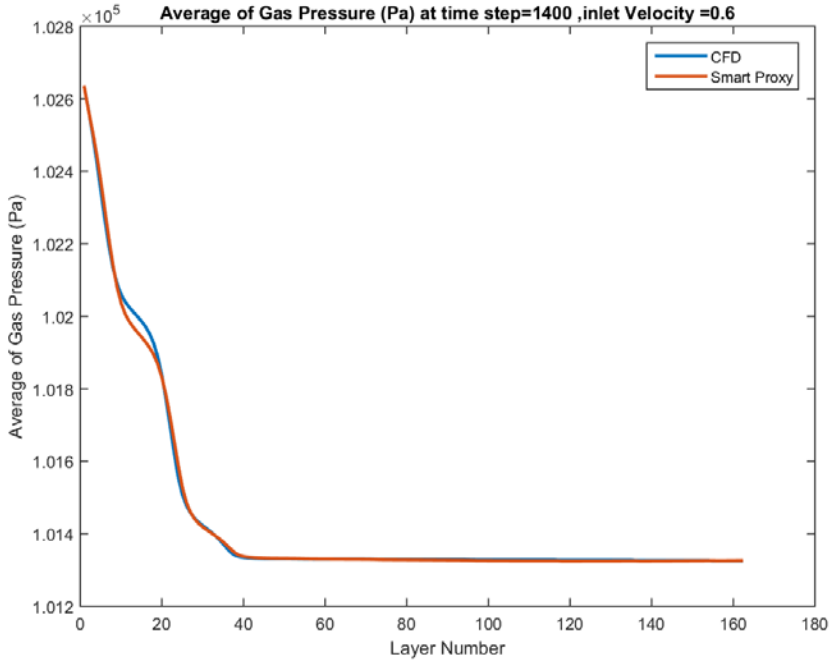

Figure 4-14 Spatially averaged CFD and smart proxy results for gas pressure at time step = 1400 and V_{in}=0.6 m/s

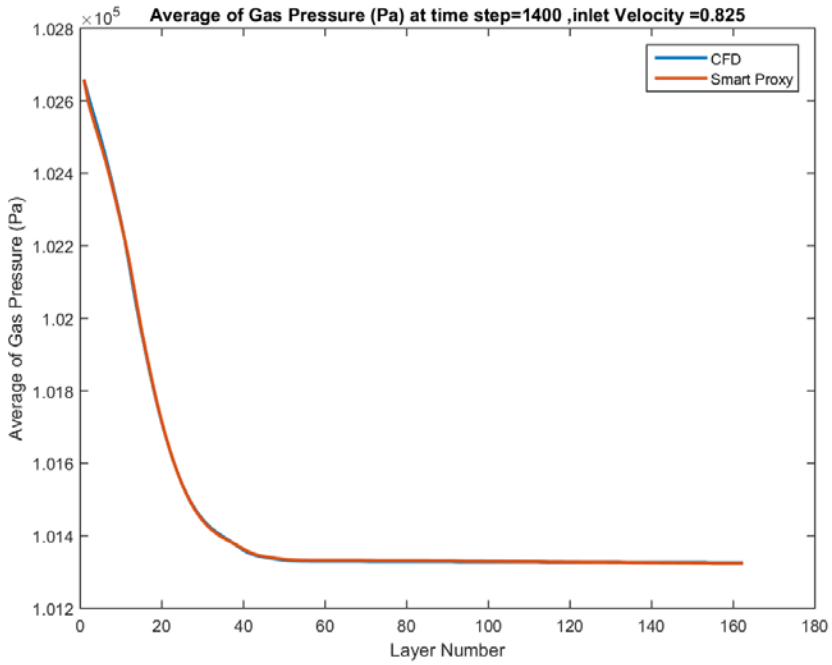

Figure 4-15 Spatially averaged CFD and smart proxy results for gas pressure at time step = 1400 for blind test condition of V_{in}=0.825 m/s

4.6 AVERAGE GAS PRESSURE WITH INFORMATION FLOWING FROM UPSTREAM TO DOWNSTREAM IN CASCADING MODE

The ANN from section 4.6 is used for the cascading approach based on Figure 3-23. Figure 4-16 shows the ANN deployment in the cascading mode for the inlet velocity of V_{in} = 0.6 m/s and time-step of 1400. This inlet velocity is part of the training data set used to train the ANN. The direction of training and deployment is from inlet plane (layer 1) to exit plane (layer 162). Changing the cascading direction improves the results significantly, although there are some discrepancies between ANN prediction and CFD results in the bed.

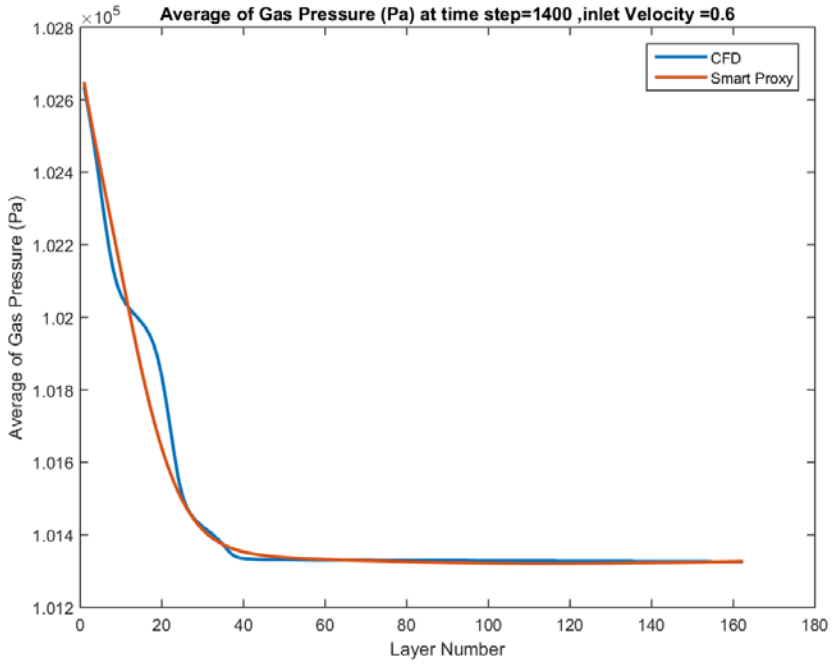

Figure 4-16 Spatially averaged CFD and smart proxy results for gas pressure at time step = 1400 and V_{in}=0.6 m/s

Next, the ANN is used for the blind test cases to evaluate the smart proxy predictability. Figure 4-17 shows the comparison between CFD results and ANN prediction, in upstream to downstream cascading deployment when the V_{in} = 0.825 m/s from blind test cases is used. As shown, the smart proxy and CFD have a good agreement. The only input to the ANN is the inlet velocity and the average gas pressure at the starting layer of J=1, as discussed in detail in section 3.4.5. The gas pressure of starting layer is assumed to be 102,644 kPa which is the average pressure at layer 1 from all CFD simulations (Figure 3-25).

Figure 4-18 and Figure 4-19 show the predictive capability of the trained ANN, when deployed for two additional blind test cases with inlet velocities of V_{in} = 0.72 and 1.02 m/s and time-step of 1400.

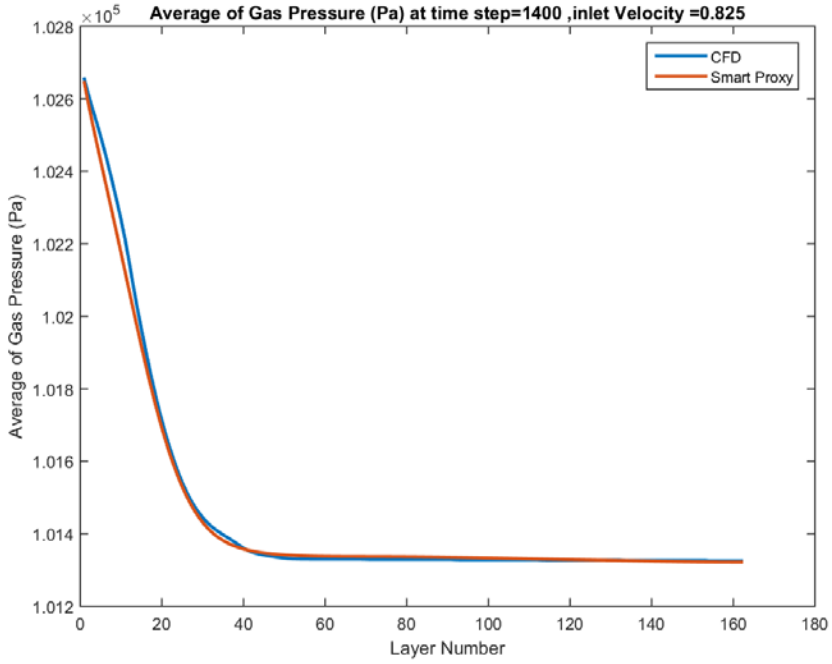

Figure 4-17 Spatially averaged CFD and smart proxy results for gas pressure at time step = 1400 for blind test condition of V_{in}=0.825 m/s

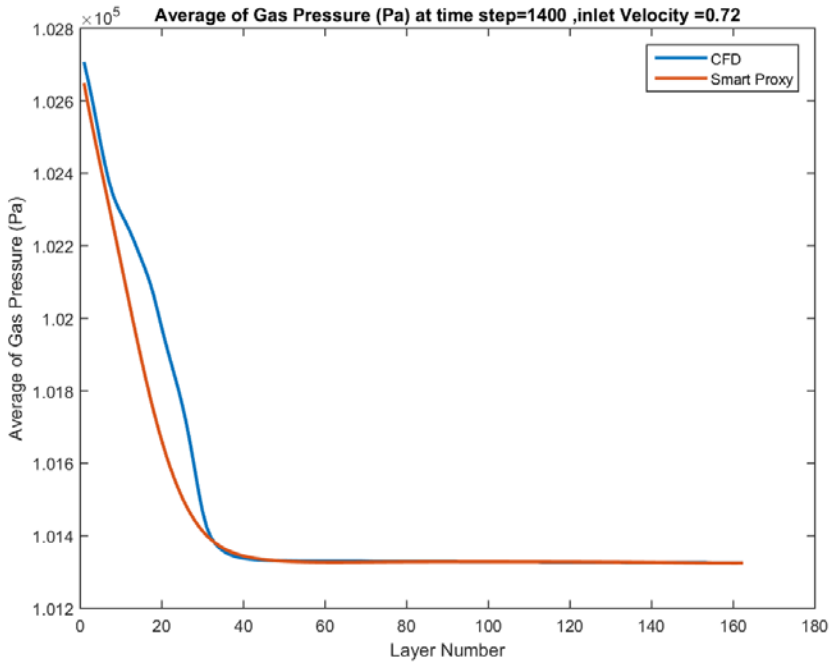

Figure 4-18 Spatially averaged CFD and smart proxy results for gas pressure at time step = 1400 for blind test condition of V_{in}=0.72 m/s

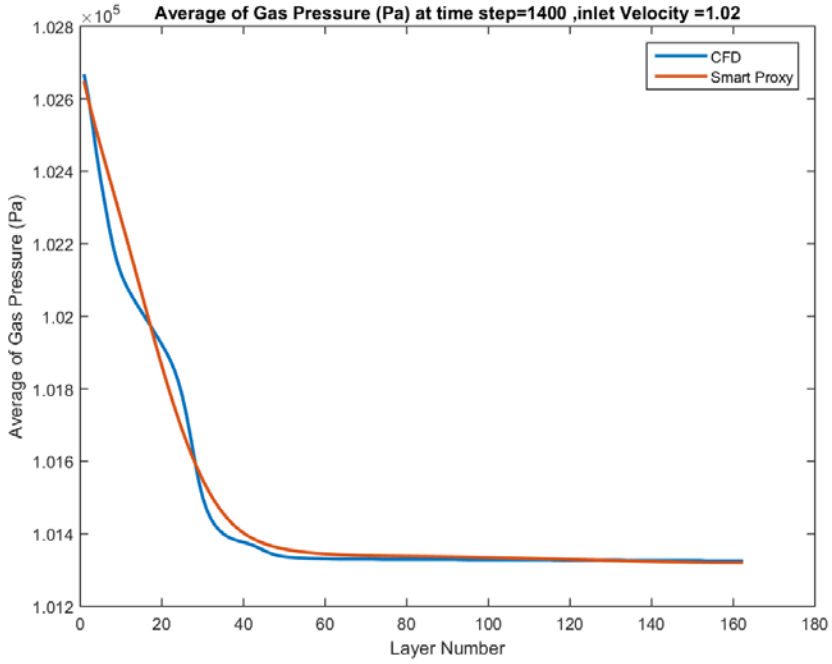

Figure 4-19 Spatially averaged CFD and smart proxy results for gas pressure at time step = 1400 for blind test condition of V_{in}=1.02 m/s

The above results show an acceptable agreement between CFD and smart proxy results. The smart proxy results show some deviation from CFD results in the bed. This may be due to the fact that pressure at the starting layer of 1 is the average of all CFD simulations and may differ from the actual average pressure at layer 1 for individual cases.

4.7 TIME AVERAGE

The approach developed in the section 3.4.6 is used to train a series of ANNs at time steps 500 to 1400 with an increment of 100, as shown in Figure 4-20.

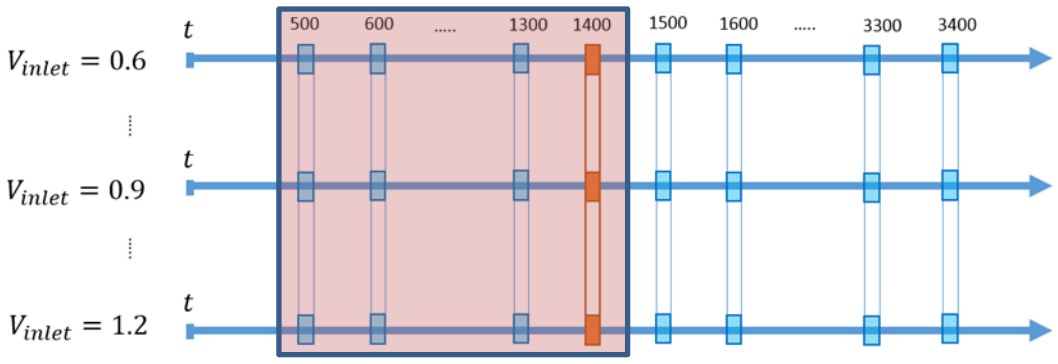

Figure 4-20 Time steps used in time average between time steps 500 to 1400

Figure 4-21 shows all the smart proxy results for different time-steps for inlet velocity of 0.825 m/s (a blind test case). All time steps have the same average pressure of 102,644 Pa as their starting point at layer 1. The black curve in Figure 4-21 shows the time average curve for time steps 500 to 1400. The comparison between CFD and smart proxy for all the time-steps from 500 to 1400 are provided in Appendix II.

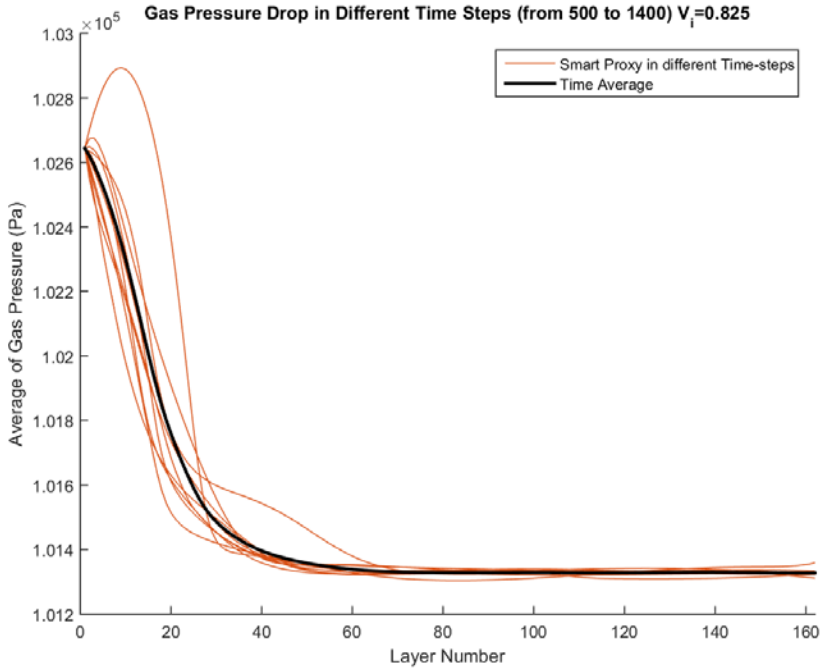

Figure 4-21 Spatial average profile of smart proxy results for gas pressure for times 500 through 1400 and blind test condition of V_{in} = 0.825 m/s

Comparison between the time averaged CFD results across each layer and time averaged ANN results across each layer is shown in Figure 4-22. The RMSE in Figure 4-22 is 38 Pa, which is less than 3% of the pressure drop across the fluidized bed. Additional deployment for blind test cases of inlet velocities of 1.02 and 1.1 m/s are shown in Figure 4-23 and Figure 4-24, respectively. The comparison between CFD and smart proxy for all the time-steps from 500 to 1400 are provided in Appendix III and IV for V_{in} = 1.02 and 1.1 (m/s), respectively.

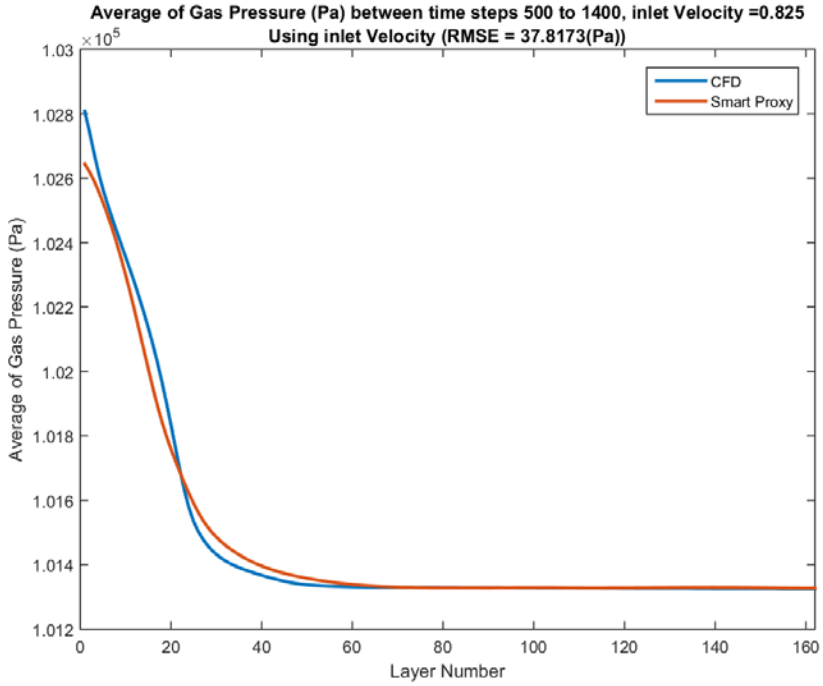

Figure 4-22 Spatial average profile of CFD and smart proxy results for gas pressure, averaged over time steps 500 to 1400 at blind test condition of V_{in} = 0.825 m/s

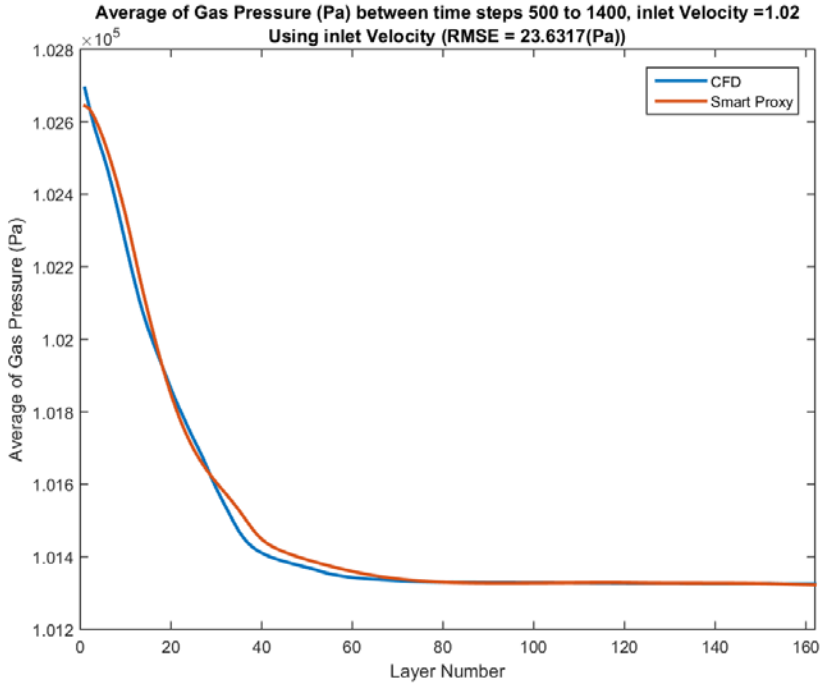

Figure 4-23 Spatial average profile of CFD and smart proxy results for gas pressure, averaged over time steps 500 to 1400 for blinf test condition of V_{in} = 1.02 m/s

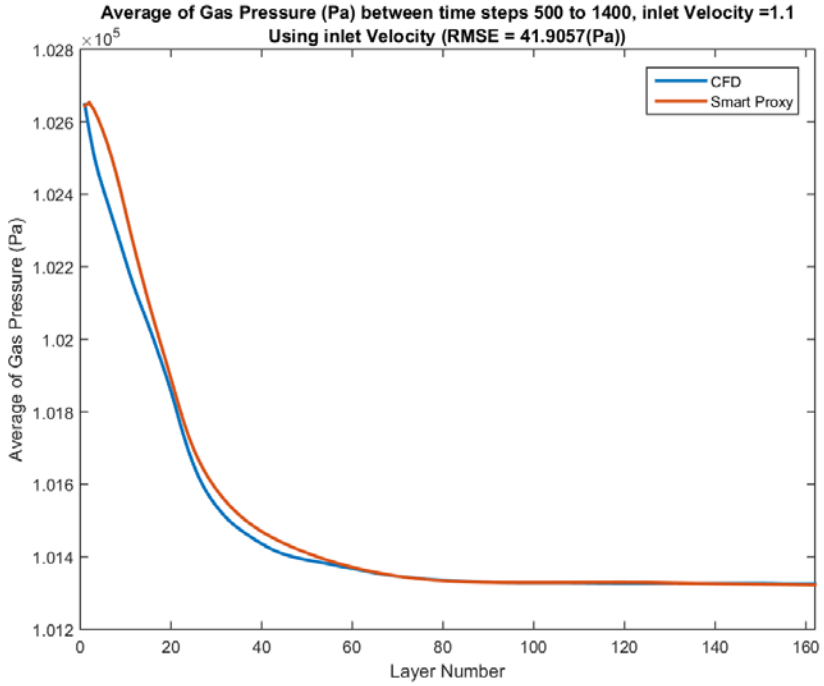

Figure 4-24 Spatial average profile of CFD and smart proxy results for gas pressure, averaged over time steps 500 to 1400 for blind test condition of V_{in} = 1.1 m/s

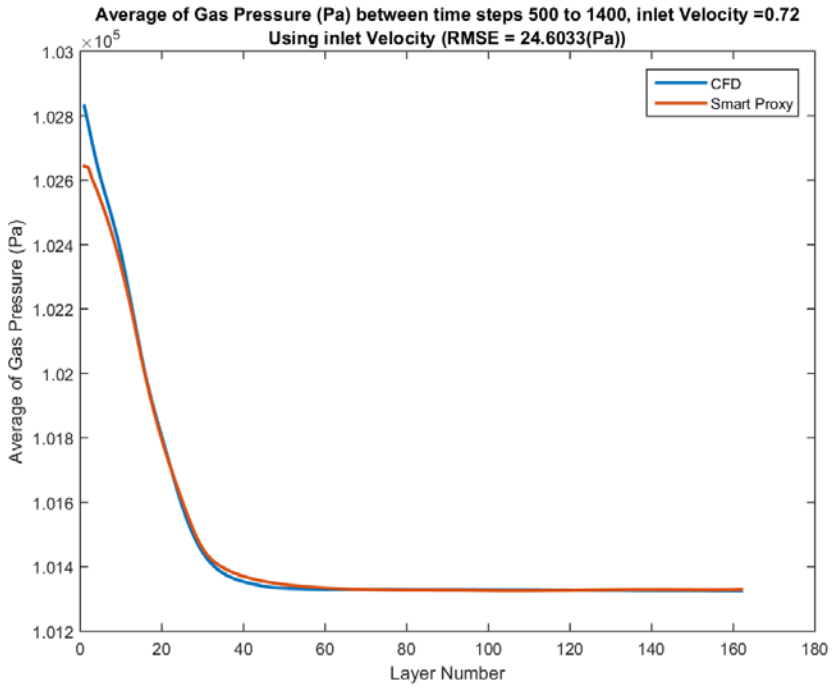

Figure 4-25 Spatial average profile of CFD and smart proxy results for gas pressure, averaged over time steps 500 to 1400 for blinf test condition of V_{in} = 0.72 m/s

The smart proxy model is able to capture the behavior of the time-steps 500 through 1400 reasonably well, when flow is more of a slugging flow. The following figures illustrate the performance of the ANN, over time steps 1500 to 3400, when flow becomes fluidized. Series of ANNs are constructed at time steps 1500 to 3400 at an increment of 100, as shown in Figure 4-26. Once the ANNs are trained, three blind tests, as outlined in Figure 3-8 are carried out.

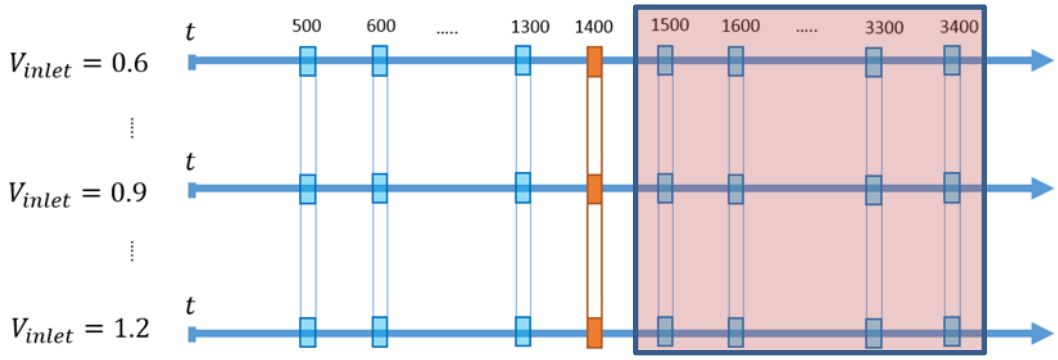

Figure 4-26 Time steps used for time averaging between time steps 1500 to 3400

Figure 4-27 shows all the smart proxy results for different time-steps for inlet velocity of 0.825 m/s (a blind test case). The black curve in Figure 4-21 shows the time average pressure across all layers between time steps 1500 to 3400. The comparison between CFD and smart proxy results for the time-steps 1500 to 3400 are provided in Appendix II.

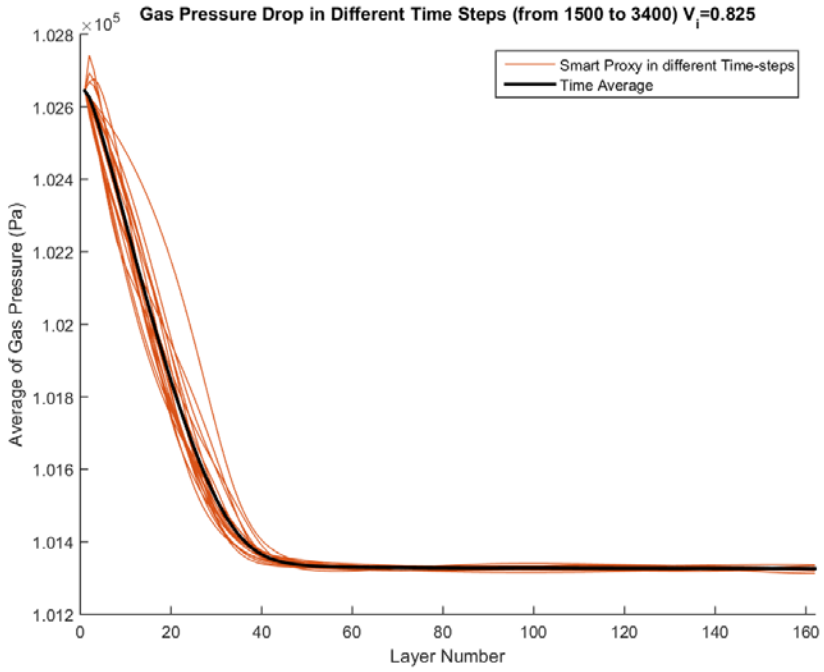

Figure 4-27 Spatial average profile of smart proxy results for gas pressure for time steps 1500 to 3400 at blind test condition of V_{in} = 0.825 m/s

The comparison of time averaged pressure values across each layer from CFD results and ANN prediction in deployment mode for three blind test cases with inlet velocities of 0.825, 1.02 and 1.1 m/s between time steps of 1500 to 3400 are shown in Figure 4-28 through Figure 4-30, respectively. The comparison between CFD and smart proxy results for the time-steps 1500 to 3400 are provided in Appendix II, III and IV for V_{in} = 0.825, 1.02 and 1.1 (m/s), respectively.

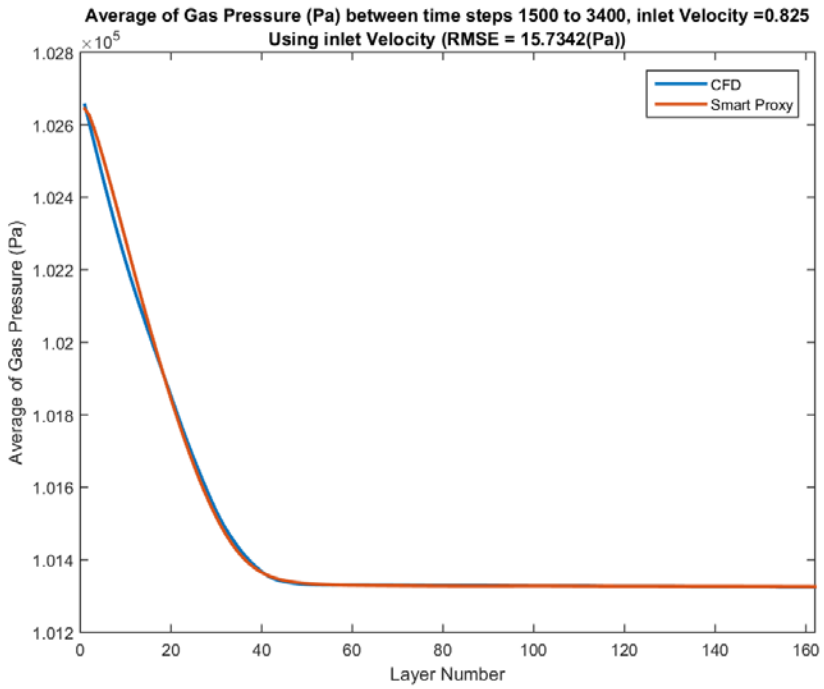

Figure 4-28 Spatial average profile of CFD and smart proxy results for gas pressure, averaged over time steps 1500 to 3400 for blind test condition of V_{in} = 0.825 m/s

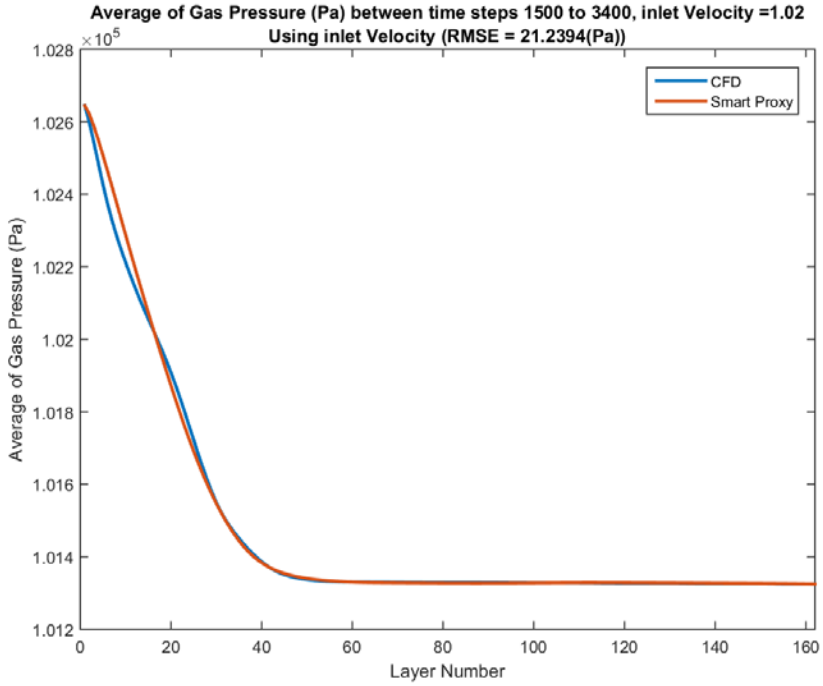

Figure 4-29 Spatial average profile of CFD and smart proxy results for gas pressure, averaged over time steps 1500 to 3400 for blind test condition of V_{in} = of 1.02 m/s

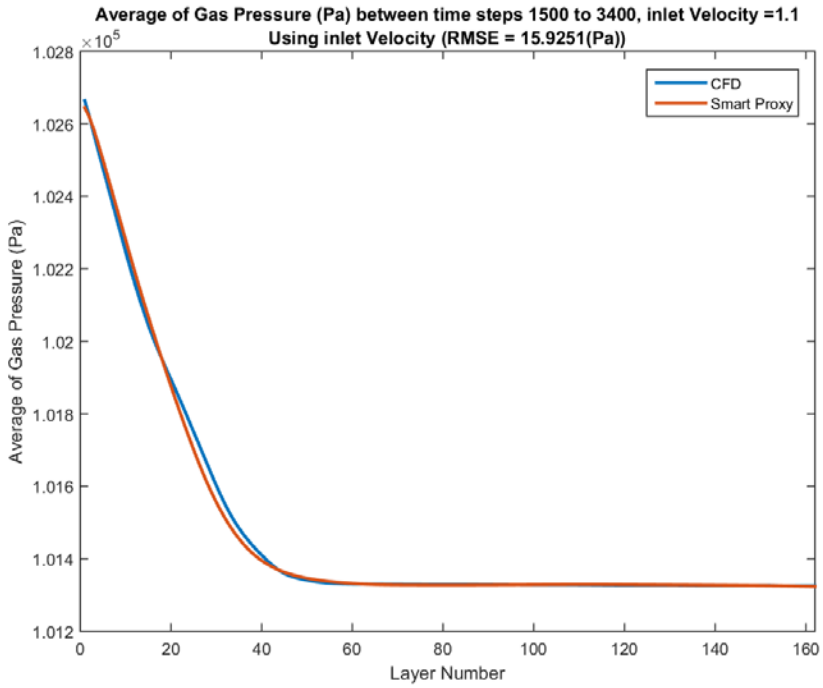

Figure 4-30 Spatial average profile of CFD and smart proxy results for gas pressure, averaged over time steps 1500 to 3400 for blind test condition of V_{in} = 1.1 m/s

5. CONCLUSIONS

A data-driven smart proxy has been developed to mimic CFD results for gas pressure in a fluidized bed at the *Layer Level*, with a reasonable accuracy and faster execution time. In the *Cell Level* training, the average time for training an ANN was about 2 to 3 minutes (for optimized ANN) [1]. However, after changing the approach to *Layer Level*, the training time reduced to less than 1 minute, since the size of training data was reduced dramatically. The size of training data set reduced from 118,098 data points (rows) and 11 parameters (columns) in Cell Level approach to 162 data points (rows) and 4 parameters (columns) in Layer Level approach. The *Layer Based* approach, in comparison with *Cell Based* approach provides more accurate results for the pressure drop, however, the disadvantage of *Layer Based* approach is that all cell information are lost. Table 5-1 shows the RMSE of different blind test cases when *Cell Based* and *Layer Based* approach are used to simulate the time average results. Table 5-1 shows a significant improvement for the temporally averaged results when the model is built at the *Layer Level.*

Table 5-1 RMSE for Cell-based and Layer-based approaches

Blind cases	*Cell Based*	*Layer Based*
V_{in} = 0.825 (m/s)	29.7	15.7
V_{in} = 1.02 (m/s)	38.0	21.2
V_{in} = 1.1 (m/s)	76.2	15.9

Table 5-2 shows the comparison of run time of multiphase CFD and smart proxy. This proxy requires incredibility less amount of time to execute than CFD simulation does, with a reasonable error (less than 3% based on Equ. 2-4). The results of this project are very promising and they show that artificial intelligence and machine learning can expedite application of non-intrusive uncertainty quantification techniques to CFD based multiphase flow modeling.

Table 5-2 Execution time for CFD and smart proxy

Method	*Execution Time*
CFD	*4 seconds simulation = 3 days on 4 CPUs*
Smart Proxy	*4 seconds simulation = 60 s = 1 min*

5.1 RECOMMENDATIONS AND FUTURE WORKS

This study shows that the smart proxy is a feasible technology to handle complex, multi-physics, nonlinear flows. The next step for this project is to train an ANN for gas volume fraction and gas velocity at the *Layer Level*. Additionally, the use of geometry as a model variable in training an

ANN may be explored. This could expedite the process of scale up, which is very time consuming, when approached with CFD modeling.

6. REFERENCES

[1] Ansari, A., Mohaghegh, S., Shahnam, M., Dietiker, J.F., and Li, T., "Data Driven Smart Proxy for CFD, Application of Big Data Analytics & Machine Learning in Computational Fluid Dynamics, Part Two: Model Building at the Cell Level," NETL-PUB-21634, United States:N. p., Web. doi:10.2172/1431303, 2018.

[2] Gel, A., Garg, R., Tong, C., Shahnam, M., and Guenther, C., "Applying uncertainty quantification to multiphase flow computational fluid dynamics," *Powder Technology,* vol. 242, pp. 27-39, 2013.

[3] Gel, A., Shahnam, M. and Subramaniyan, A.K., "Quantifying uncertainty of a reacting multiphase flow in a bench-scale fluidized bed gasifier. A Bayesian approach," *Powder Technology,* vol. 311, pp. 484-495, 2017.

[4] Gel, A., Shahnam, M., Musser, J, Subramaniyan, A.K. and Dietiker, J.F., "Non-intrusive Uncertainty Quantification of Computational Fluid Dynamics Simulations of a Bench-scale Fluidized Bed Gasifier," *Industrial & Engineering Chemistry Research,* no. DOI: 10.1021/acs.iecr.6b02506, 2016.

[5] Shahnam, M., Gel, A., Dietiker, J.-F., Subramaniyan, A. K. and Musser, J., "The Effect of Grid Resolution and Reaction Models in Simulation of a Fluidized Bed Gasifier through Non-intrusive Uncertainty Quantification Techniques," *ASME Journal of Verification, Validation and Uncertainty Quantification,* 2016.

[6] Fullmer, W. and Hrenya, C., "Quantitative assessment of fine-grid kinetic theory based predictions of mean-slip in unbounded fluidization," *AIChE Journal,* Vols. DOI 10.1002/aic, 62, no. 2016, pp. 11-17.

[7] Amini, S., Mohaghegh, S.D., Gaskari, R. and Bromhal, G.S., "Pattern Recognition and Data Driven Analytics for Fast and Accurate Replication of Complex Numerical Reservoir Models at Grid Block Level," in *SPE Intelligent Energy Conference and Exhibition*, Utrecht, The Netherlands, 2014.

[8] Mohaghegh, S. D., "Converting Detail Reservoir Simulation Model into Effective Reservoir Management Tools Using SRMs: Case Study - Three Green Fields in Saudi Arabia," *International Journal of Oil, Gas and Coal Technology,* pp. 115-131, 2014.

[9] Mohaghegh, S.D., Abdulla, F., Abdou, M., Gaskari, R. and Maysami, M., "Smart Proxy: An Innovative Reservoir Management Tool, Case Study of a Giant Mature Oilfield in UAE," in *Abu Dhabi International Petroleum Exhibition and Conference,* Abu Dubai, 2015.

[10] Shahkarami, A., Mohaghegh, S.D., Gholami, V., Haghighat, A. and Moreno, D., "Modeling Pressure and Saturation Distribution in a CO2 Storage Project Using a Surrogate Reservoir

Model (SRM)," *Greenhouse Gas Science and Technology, Society of Chemical Industry, John Wiley & Sons, LTD,* pp. 289-315, doi:10.1002/ghg, 2013.

[11] Ansari, A., Mohaghegh, S., Shahnam, M., Dietiker, J.F., Takbiri Borujeni, A., Fathi, E., "Data Driven Smart Proxy for CFD, Application of Big Data Analytics & Machine Learning in Computational Fluid Dynamics, Part One: Proof of Concept," NETL-PUB-21574, NETL Technical Report Series; U.S. Department of Energy, National Energy Technology Laboratory: Morgantown, WV, 2017." United States. doi:10.2172/1417305. http://www.osti.gov/scitech/servlets/purl/1417305, 2017.

[12] NETL Multiphase Flow Science, "MFiX software suite," National Energy Technology Laboratory, Morgantown, WV, 2016. [Online]. Available: http://mfix.netl.doe.gov.

[13] Van der Hoef, M. A., Van Sint Annaland, M., Andrews, A. T., Sundaresan, S. and Kuipers, J. A. M., "Numerical Simulation of Dense Gas-Solid Fluidized Beds: A Multiscale Modeling Strategy," *Annual Review of Fluid Mechanics,* vol. 40, no. doi:101146/annurev.fluid.40111406.102130, pp. 47-70, 2008.

[14] Van der Hoef, M. A., Ye, M., Van Sint Annaland, M., Andrews, A. T., Sundaresan, S. and Kuipers, J. A. M., "Multiscale Modeling of Gas-Fluidized Beds," *Advances in Chemical Engineering,* vol. 31, no. 6, pp. 65-149, 2006, doi:10.1016/S0065-2377(06)31002-2..

[15] Deen, N. G., Van Sint Annaland, M., Van der Hoef, M. A. and Kuipers, J. A., M., "Review of Discrete Particle Modeling of Fluidized Beds," *Chemical Engineering Science, doi:10.1016/j.ces.2006.08.014,* vol. 62, no. 1-2, pp. 28-44, 2007.

[16] Syamlal, M., Rogers, W., O'Brien, T. J., "MFiX Documentation Theory Guide," [Online]. Available: https://mfix.netl.doe.gov/download/mfix/mfix_legacy_manual/Theory.pdf.

[17] Benyahia, S., Syamlal, M., "Summary of MFiX Equations," 2012. [Online]. Available: https://mfix.netl.doe.gov/download/mfix/mfix_current_documentation/MFIXEquations2012-1.pdf.

[18] A. Samuel, "Some Studies in Machine Learning using the Game Checkers," *IBM Journal,* vol. 3, no. 3, pp. 535-554, 1959.

[19] Alpaydin, E., Introduction to Machine Learning, The MIT Press, second edition, 2010.

[20] Haykin, S., Neural Networks - A Comprehensive Foundation, IEEE Press, 1994.

[21] Mohaghegh, S., Ameri, S., Artificial Neural Network as a Valuable Tool for Petroleum Engineers, Network, 1995.

[22] Mohaghegh, S., Arefi, R., Ameri, S., Rose, Deanna, "Design and Development of an Artificial Neural Network for Estimation of Formation Permeability," *SPE Computer Applications, doi:10.2118/28237-PA,* vol. 7, no. 6, pp. 151 - 155, 1995.

[23] Alizadehdakhel, A., Rahimi, M., Sanjari, J., Abdulaziz, A., "CFD and Artificial Neural Network Modeling of Two-phase Flow Pressure Drop," *International Communication in Heat and Mass Transfer,* vol. 36, no. doi.org/10.1016/j.icheatmasstransfer.2009.05.005, pp. 850 - 856, 2009.

[24] Esmaili, S., Mohaghegh, S., "Full Field Reservoir Modeling of Shale Assets using Advance Data-driven Analytics," *Geoscience Frontiers, Elsevier Ltd,* no. doi:10.1016/j.gsf.2014.12.006, 2015.

[25] S. D. Mohaghegh, Data Driven Reservoir Modeling, Richardson, Texas: Society of Petroleum Engineers (SPE), 2017.

[26] Kalantari-Dahaghi, A., Mohaghegh, S., Esmaili, S., "Coupling Numerical Simulation and Machine Learning to Model Shale Gas Production at Different Time Resolutions," *Journal of Natural Gas Science and Engineering,* vol. 25, pp. 380 - 392, 2015.

[27] Kalantari-Dahaghi, A., Mohaghegh, S., Esmaili, S., "Data Driven Proxy at Hydraulic Fracture Cluster Level: A Technique for Efficient CO2 Enhanced Gas Recovery and Storage Assessment in Shale Reservoir," *Journal of Natural Gas Science and Engineering,* vol. 27, no. doi:10.1016/j.jngse.2015.06.039, pp. 515 - 530, 2015.

[28] Ansari, A., "Developing a Smart Proxy for Fluidized Bed Using Machine Learning," Master Thesis, West Virginia University, Morgantown, 2016.

[29] Hosseini Boosari, S.S., "Developing a Smart Proxy for Predicting the Fluid Dynamic in DamBreak Flow Simulation by using Artificial Intelligence," West Virginia University, Morgantown, 2017.

7. APPENDIX I: GAS PRESSURE USING 4 STATIC PARAMETERS

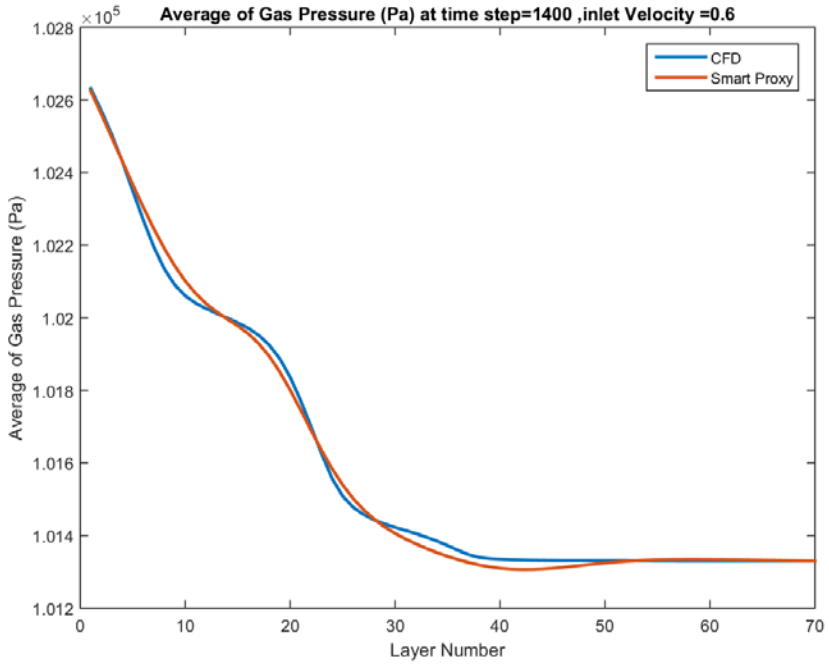

Figure 7-1 Spatially averaged CFD and smart proxy results for gas volume fraction at time step = 1400 and V_{in}=0.6 m/s (using 4 static parameters)

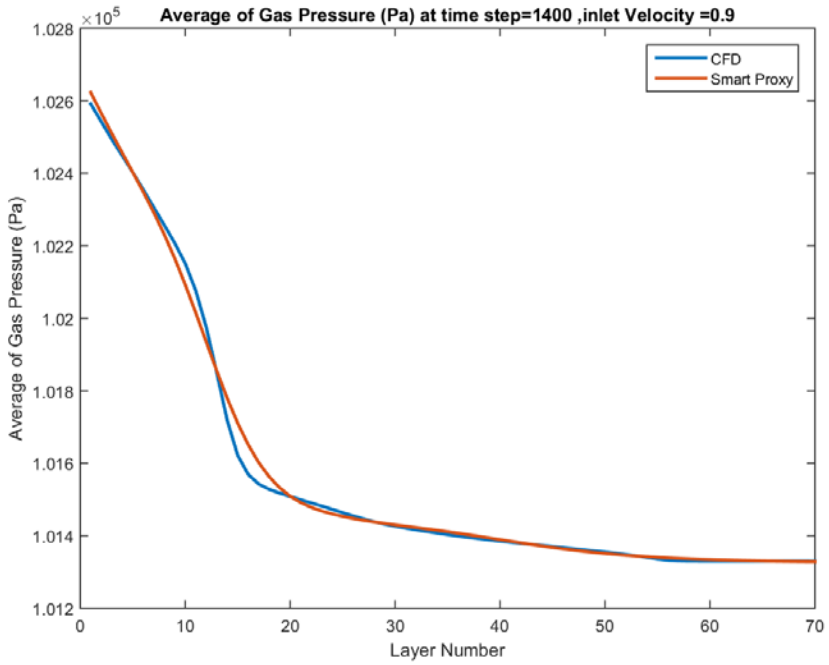

Figure 7-2 Spatially averaged CFD and smart proxy results for gas volume fraction at time step = 1400 and V_{in}=0.9 m/s (using 4 static parameters)

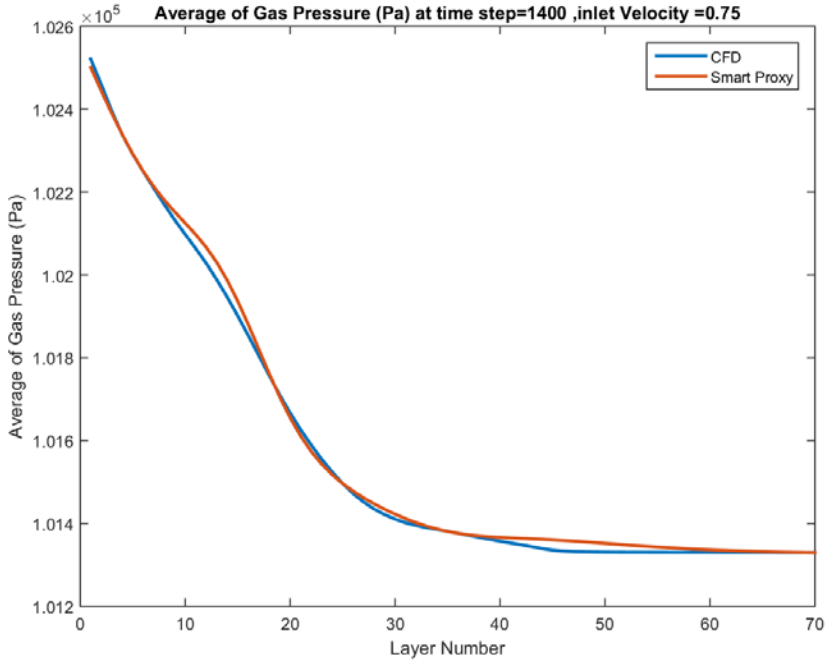

Figure 7-3 Spatially averaged CFD and smart proxy results for gas volume fraction at time step = 1400 and V_{in}=0.75 m/s (using 4 static parameters)

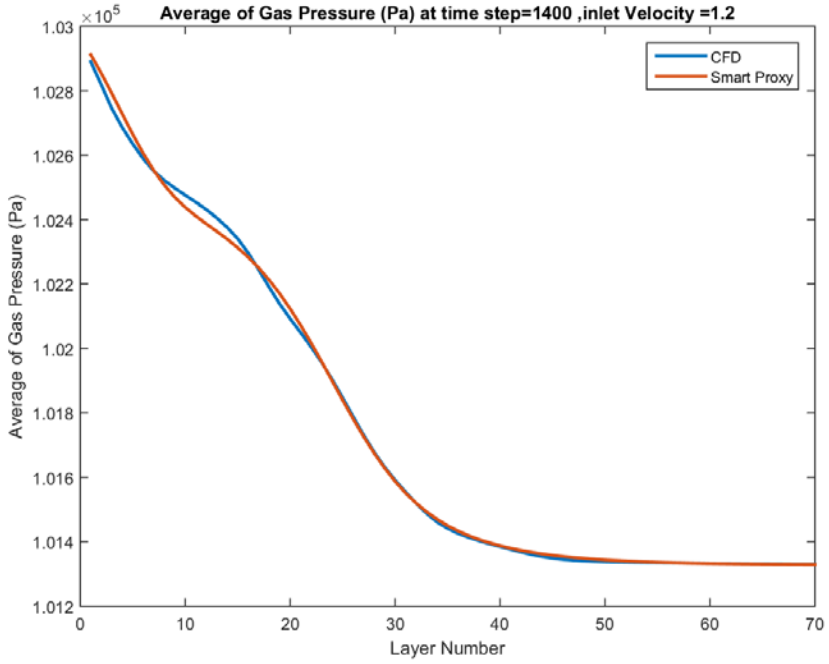

Figure 7-4 Spatially averaged CFD and smart proxy results for gas volume fraction at time step = 1400 and V_{in}=1.2 m/s (using 4 static parameters)

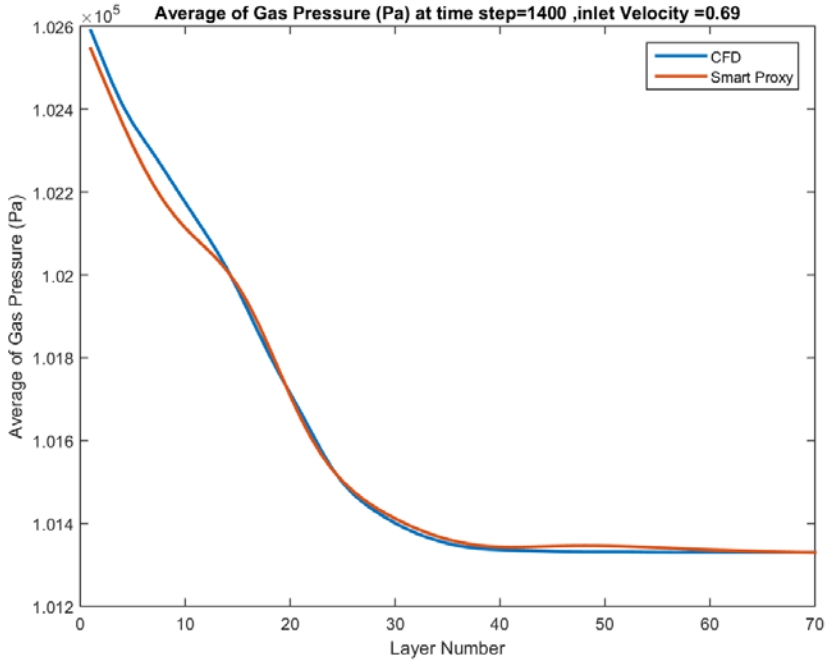

Figure 7-5 Spatially averaged CFD and smart proxy results for gas volume fraction at time step = 1400 and V_{in}=0.69 m/s (using 4 static parameters)

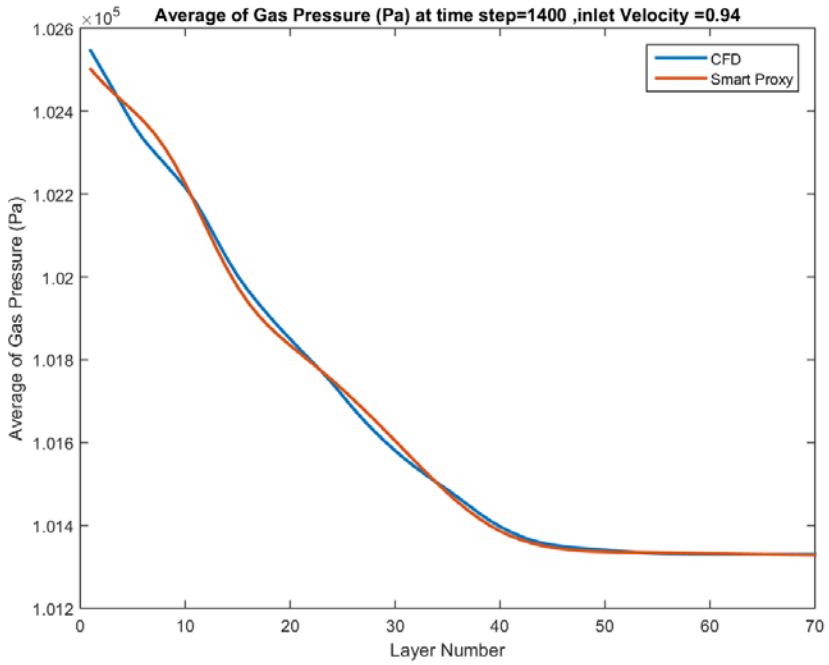

Figure 7-6 Spatially averaged CFD and smart proxy results for gas volume fraction at time step = 1400 and V_{in}=0.94 m/s (using 4 static parameters)

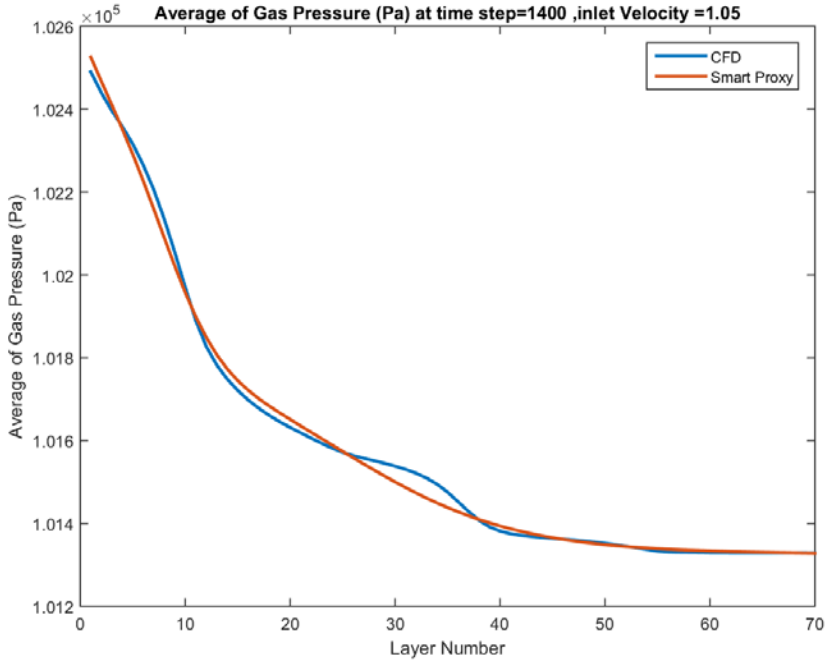

Figure 7-7 Spatially averaged CFD and smart proxy results for gas volume fraction at time step = 1400 and V_{in}=1.05 m/s (using 4 static parameters)

8. APPENDIX II: AVERAGE GAS PRESSURE PROFILE AT BLIND TEST CONDITION OF V_{IN} = 0.825 M/S WITH INFORMATION CASCADING FROM UPSTREAM TO DOWNSTREAM AT TIME STEPS 500 TO 3400

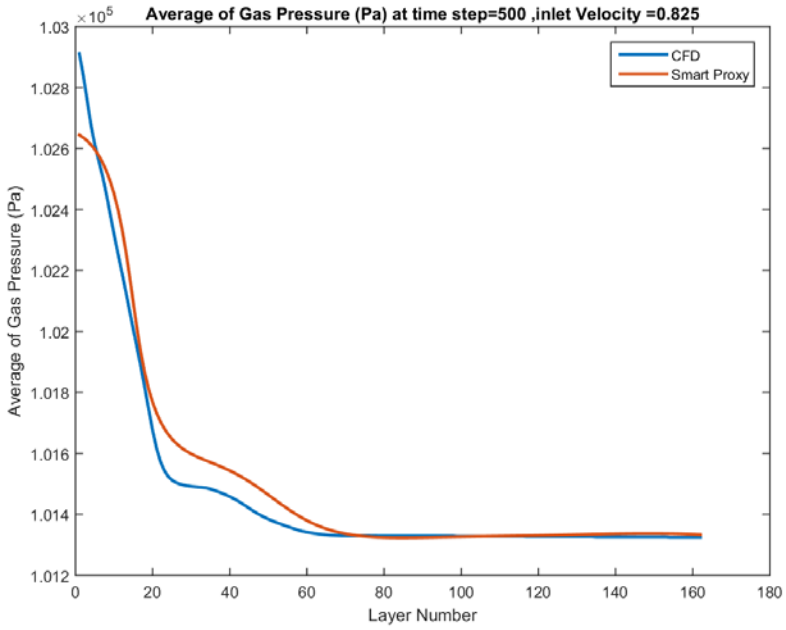

Figure 8-1 Spatially averaged CFD and smart proxy results for gas pressure at time step = 500 for blind test condition of V_{in}=0.825 m/s

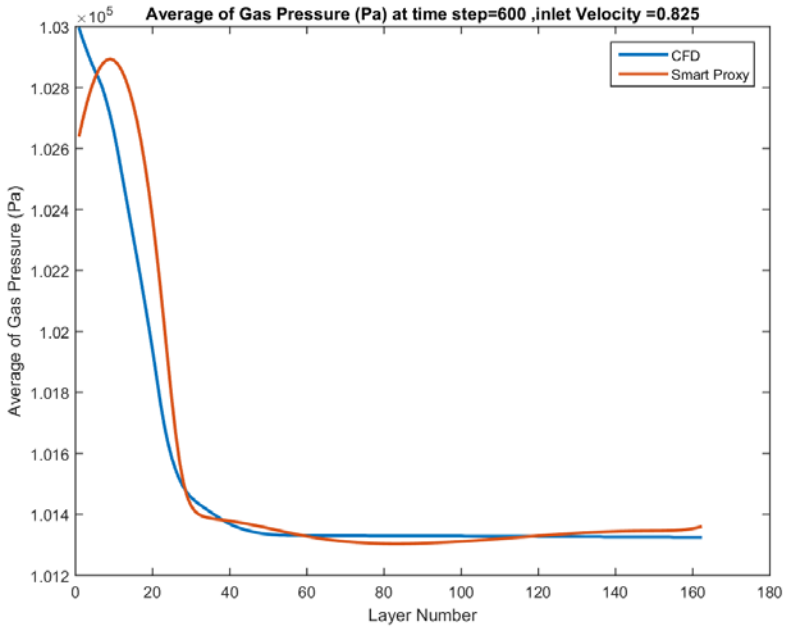

Figure 8-2 Spatially averaged CFD and smart proxy results for gas pressure at time step = 600 for blind test condition of V_{in}=0.825 m/s

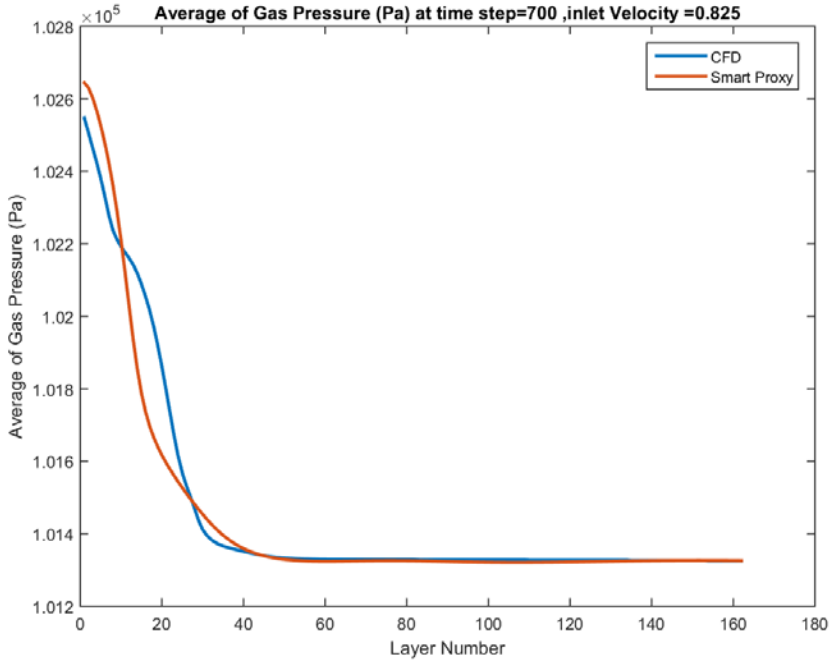

Figure 8-3 Spatially averaged CFD and smart proxy results for gas pressure at time step = 700 for blind test condition of V_{in}=0.825 m/s

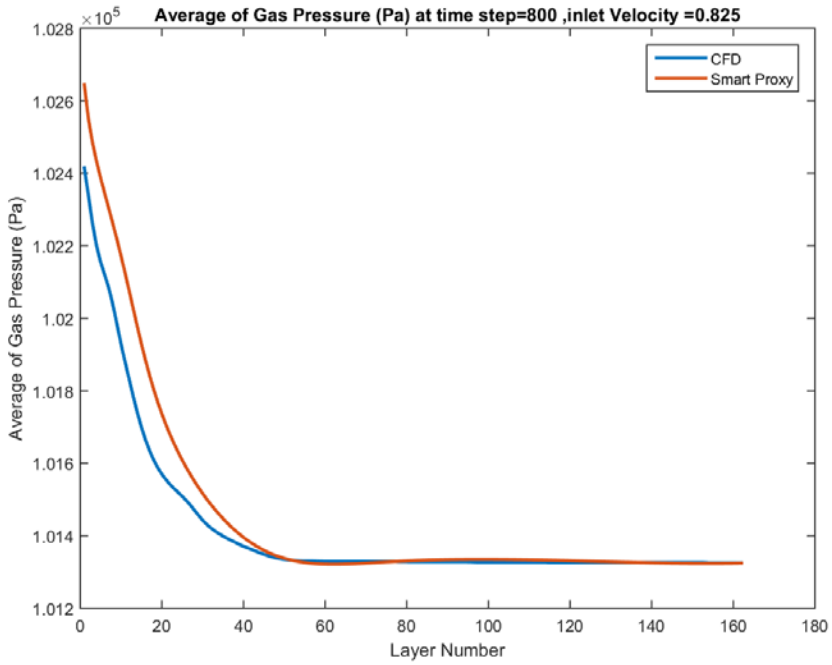

Figure 8-4 Spatially averaged CFD and smart proxy results for gas pressure at time step = 800 for blind test condition of V_{in}=0.825 m/s

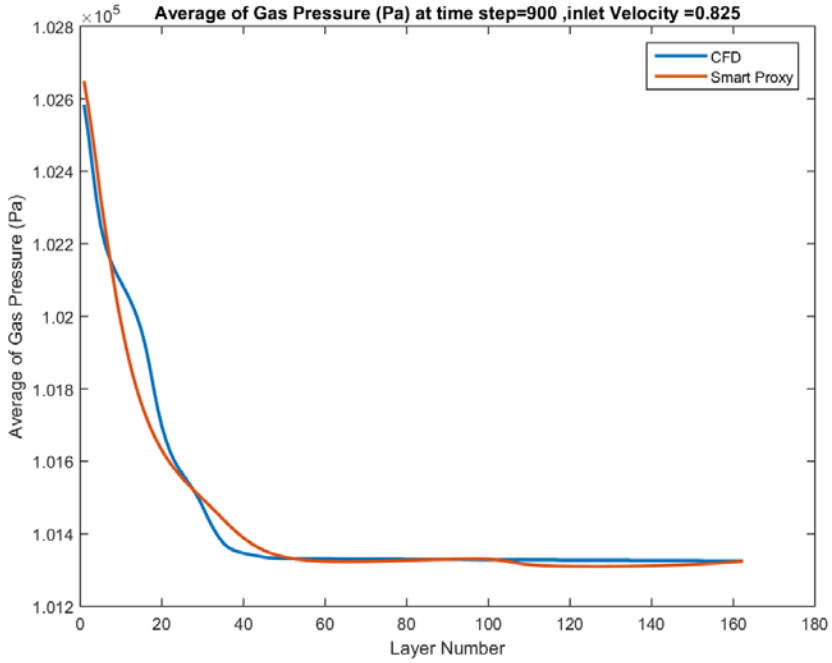

Figure 8-5 Spatially averaged CFD and smart proxy results for gas pressure at time step = 900 for blind test condition of V_{in}=0.825 m/s

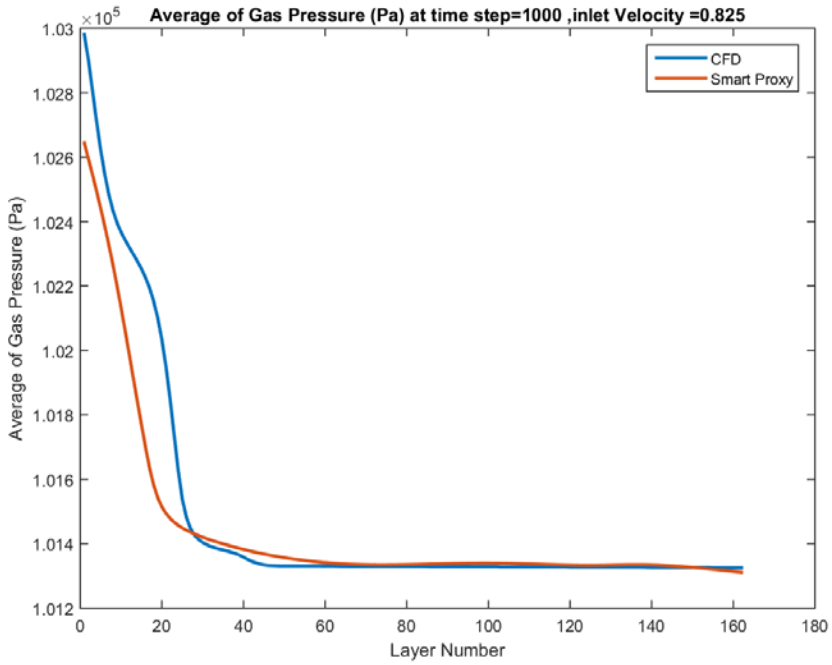

Figure 8-6 Spatially averaged CFD and smart proxy results for gas pressure at time step = 1000 for blind test condition of V_{in}=0.825 m/s

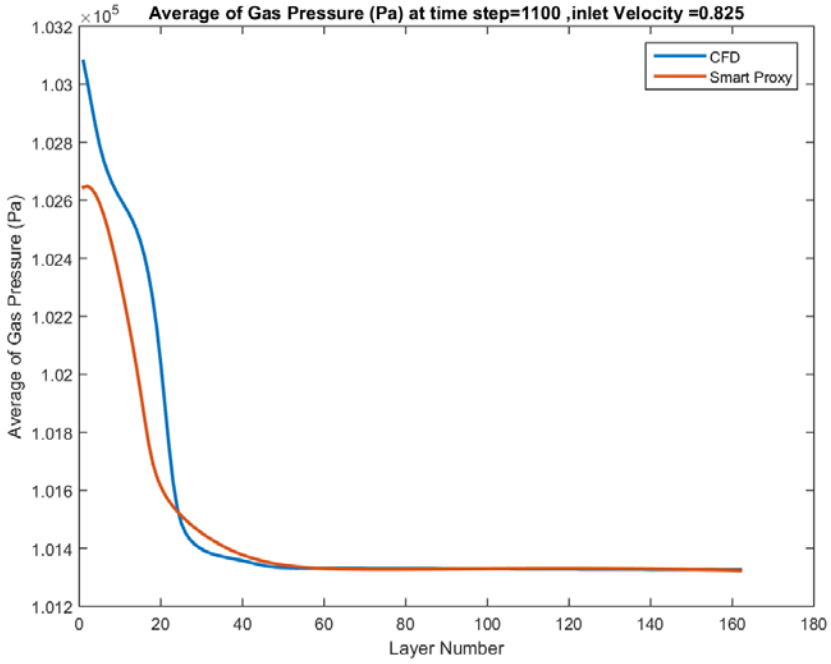

Figure 8-7 Spatially averaged CFD and smart proxy results for gas pressure at time step = 1100 for blind test condition of V_{in}=0.825 m/s

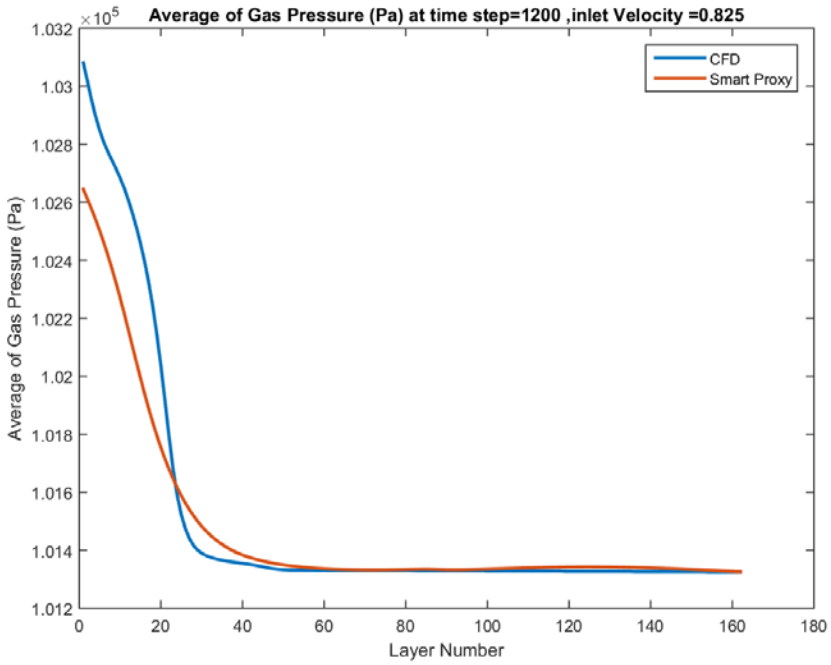

Figure 8-8 Spatially averaged CFD and smart proxy results for gas pressure at time step = 1200 for blind test condition of V_{in}=0.825 m/s

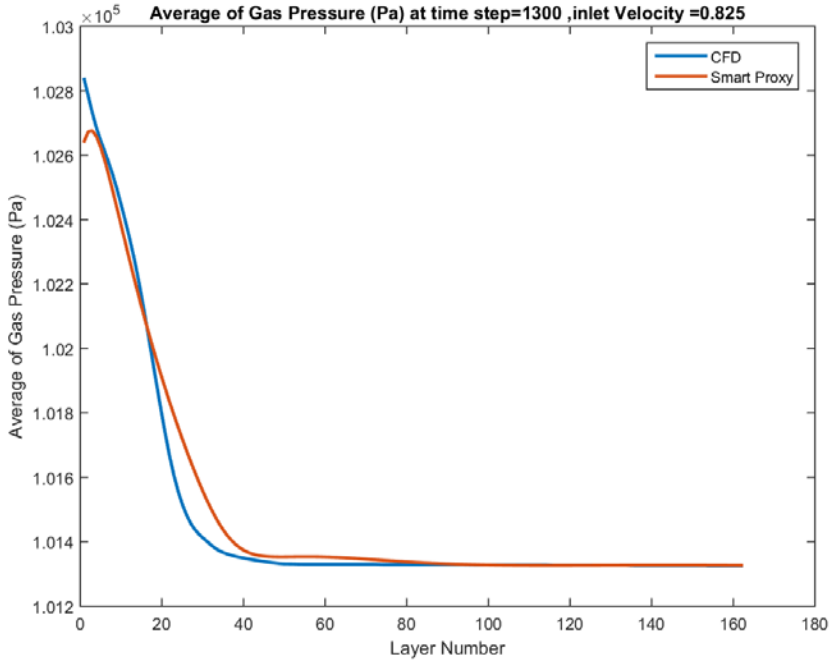

Figure 8-9 Spatially averaged CFD and smart proxy results for gas pressure at time step = 1300 for blind test condition of V_{in}=0.825 m/s

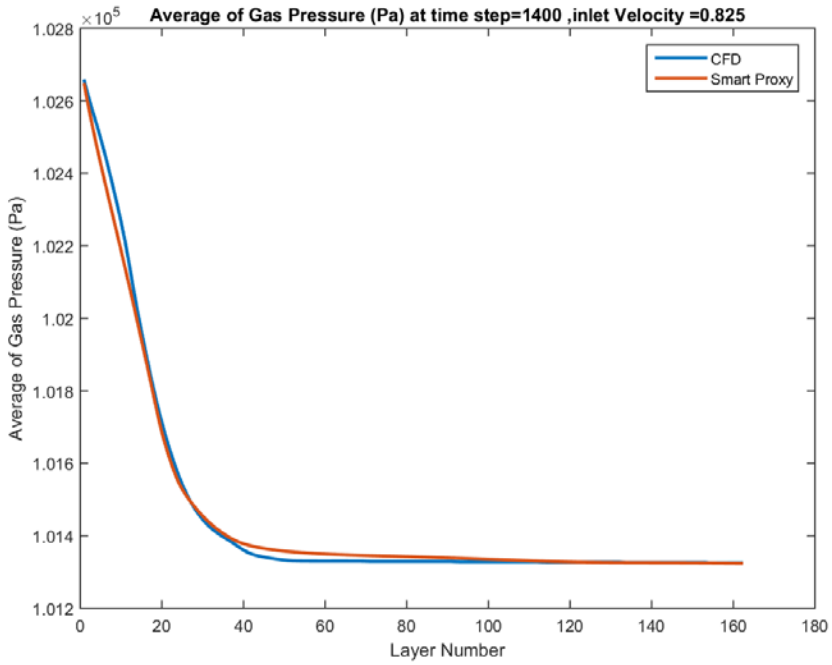

Figure 8-10 Spatially averaged CFD and smart proxy results for gas pressure at time step = 1400 for blind test condition of V_{in}=0.825 m/s

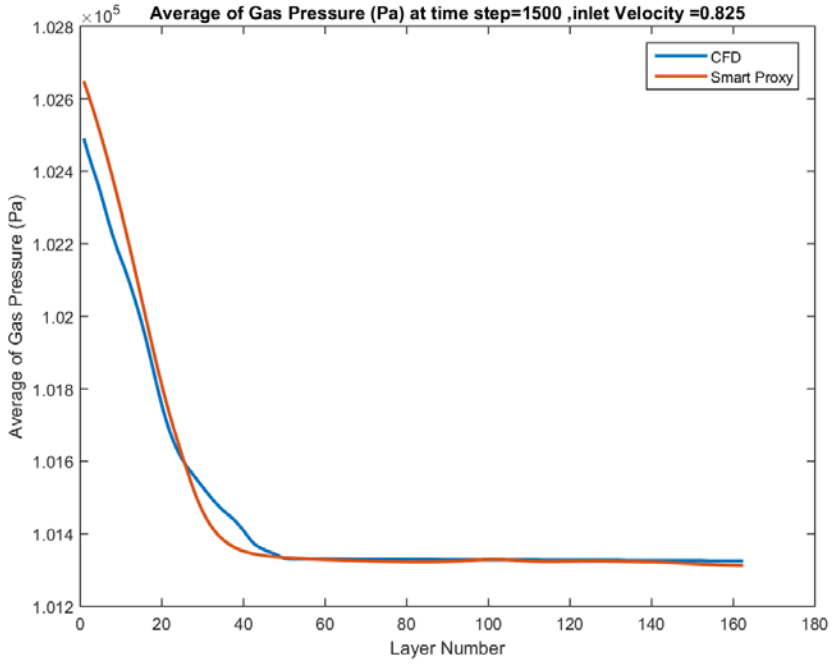

Figure 8-11 Spatially averaged CFD and smart proxy results for gas pressure at time step = 1500 for blind test condition of V_{in}=0.825 m/s

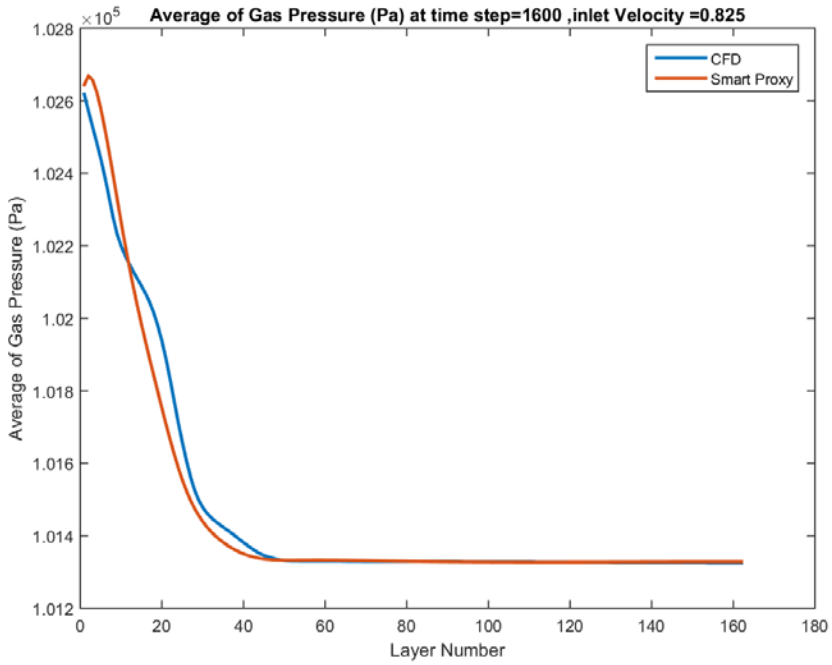

Figure 8-12 Spatially averaged CFD and smart proxy results for gas pressure at time step = 1600 for blind test condition of V_{in}=0.825 m/s

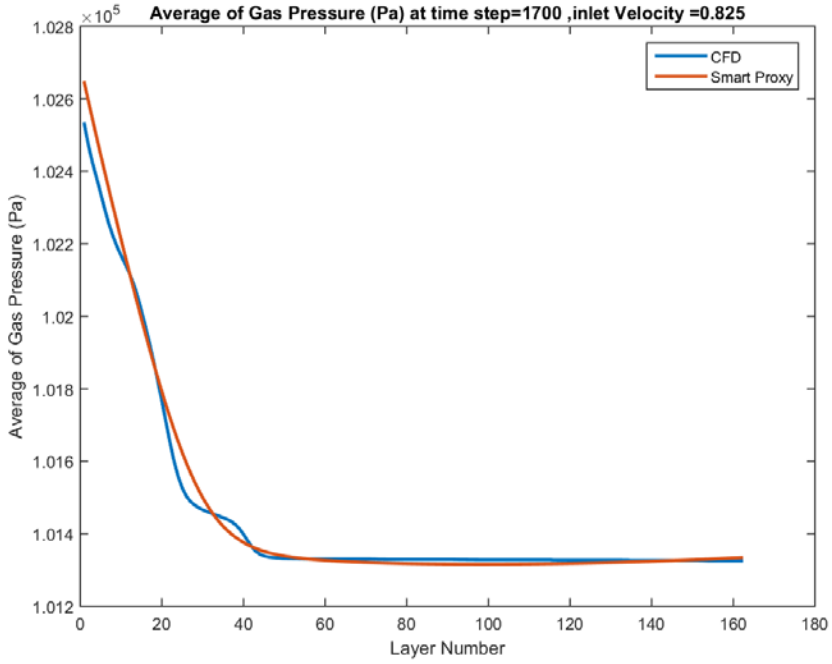

Figure 8-13 Spatially averaged CFD and smart proxy results for gas pressure at time step = 1700 for blind test condition of V_{in}=0.825 m/s

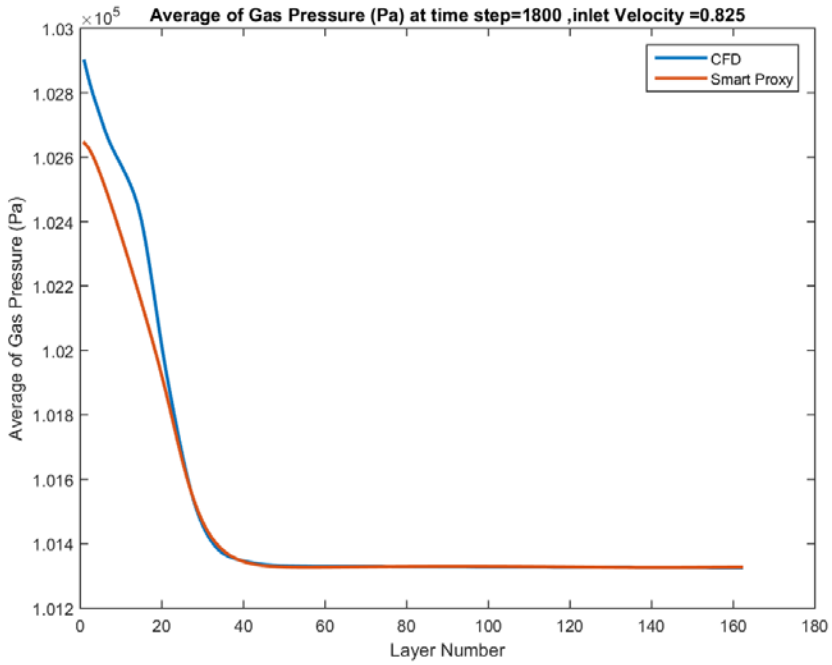

Figure 8-14 Spatially averaged CFD and smart proxy results for gas pressure at time step = 1800 for blind test condition of V_{in}=0.825 m/s

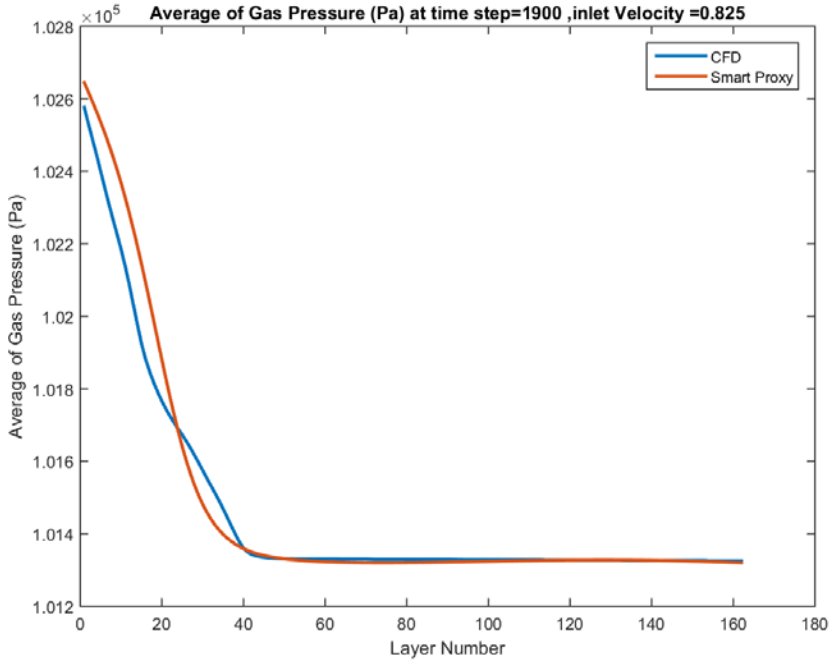

Figure 8-15 Spatially averaged CFD and smart proxy results for gas pressure at time step = 1900 for blind test condition of V_{in}=0.825 m/s

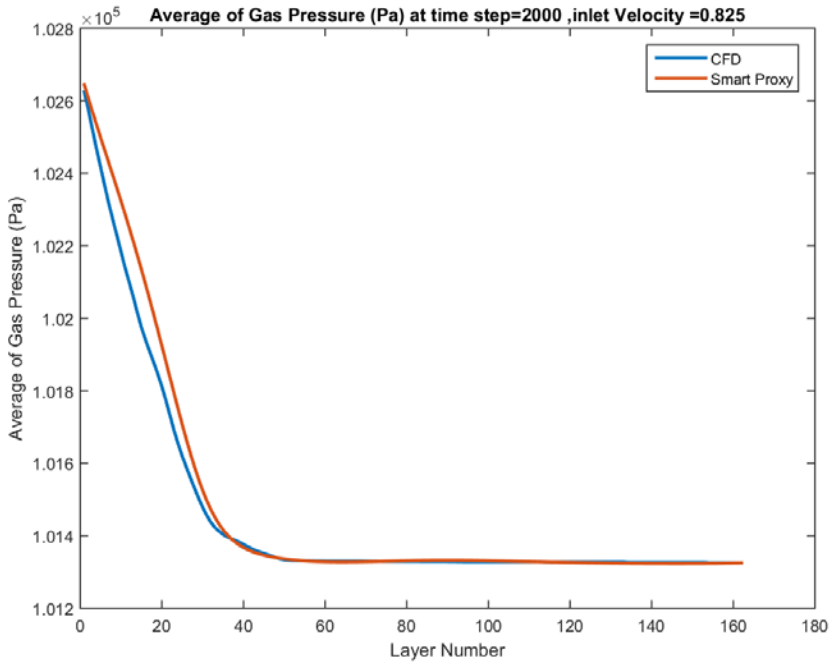

Figure 8-16 Spatially averaged CFD and smart proxy results for gas pressure at time step = 2000 for blind test condition of V_{in}=0.825 m/s

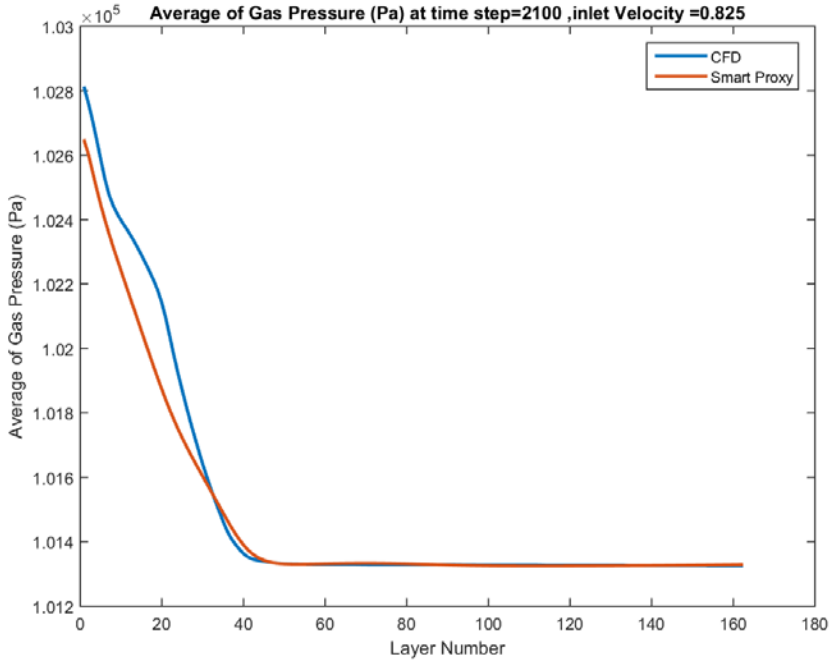

Figure 8-17 Spatially averaged CFD and smart proxy results for gas pressure at time step = 2100 for blind test condition of V_{in}=0.825 m/s

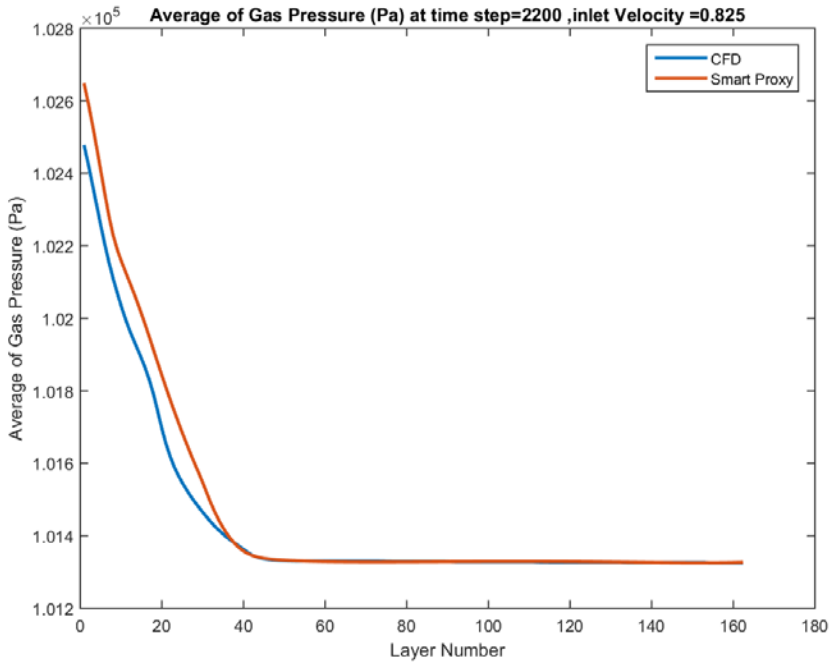

Figure 8-18 Spatially averaged CFD and smart proxy results for gas pressure at time step = 2200 for blind test condition of V_{in}=0.825 m/s

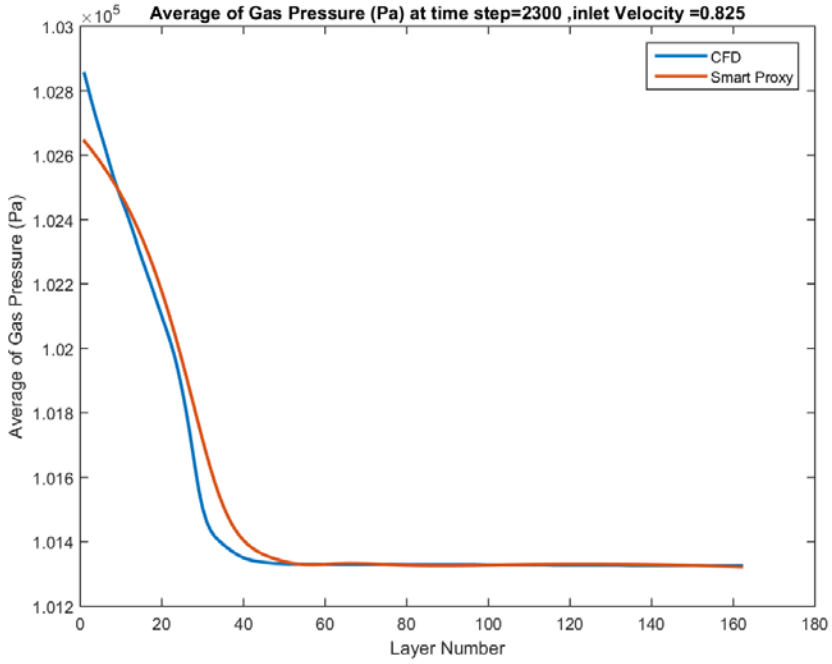

Figure 8-19 Spatially averaged CFD and smart proxy results for gas pressure at time step = 2300 for blind test condition of V_{in}=0.825 m/s

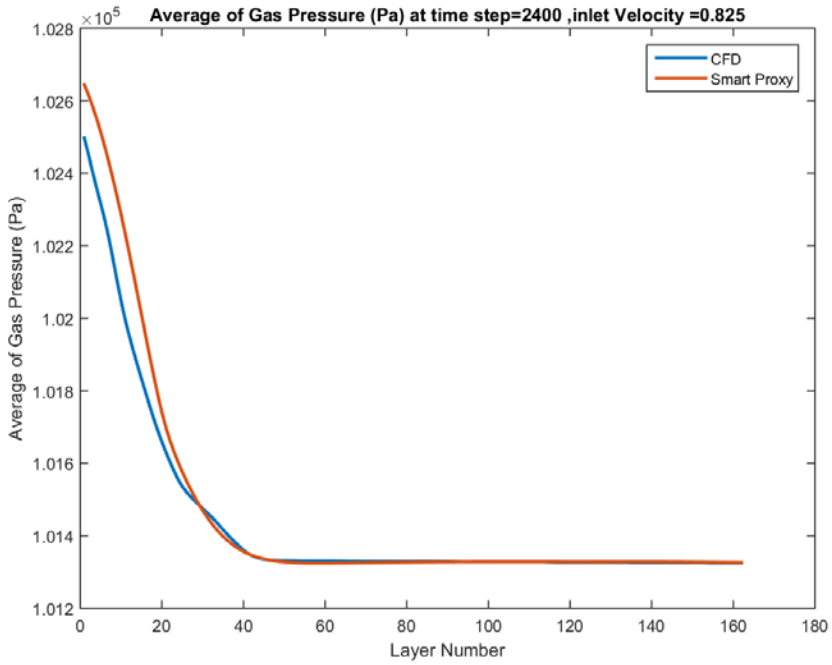

Figure 8-20 Spatially averaged CFD and smart proxy results for gas pressure at time step = 2400 for blind test condition of V_{in}=0.825 m/s

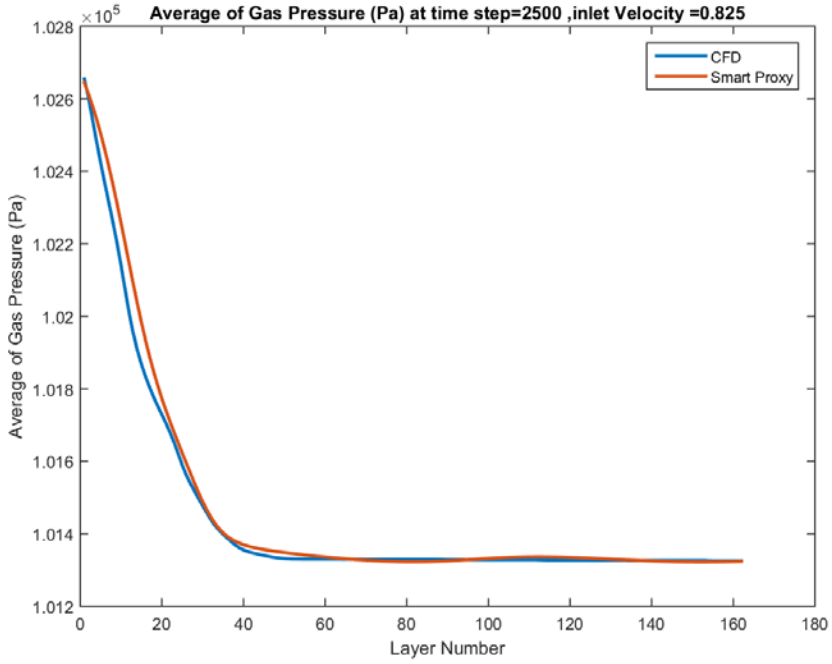

Figure 8-21 Spatially averaged CFD and smart proxy results for gas pressure at time step = 2500 for blind test condition of V_{in}=0.825 m/s

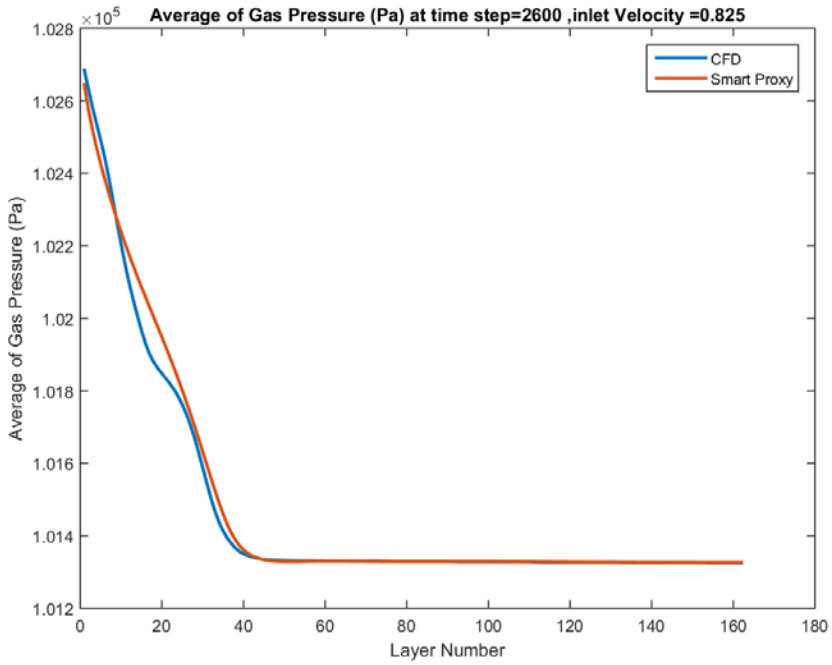

Figure 8-22 Spatially averaged CFD and smart proxy results for gas pressure at time step = 2600 for blind test condition of V_{in}=0.825 m/s

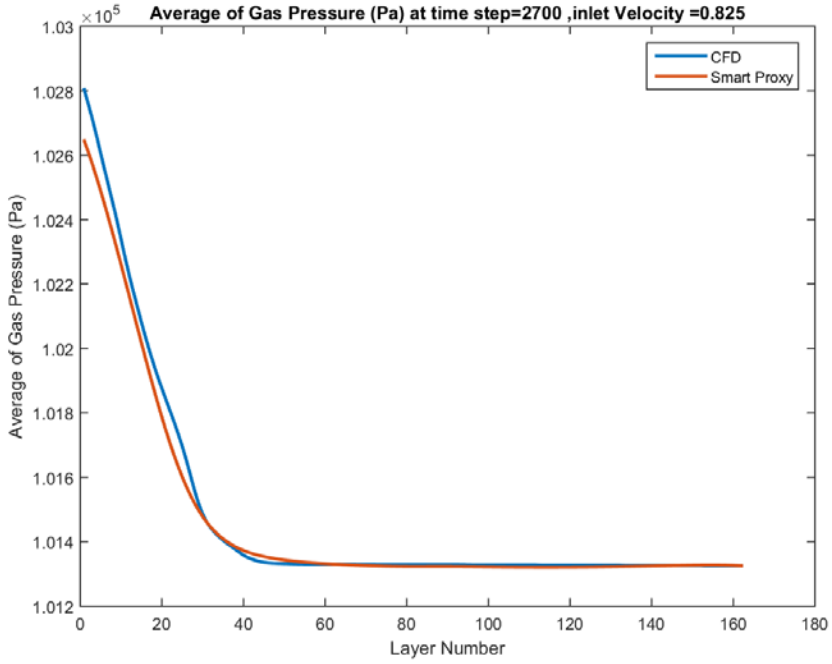

Figure 8-23 Spatially averaged CFD and smart proxy results for gas pressure at time step = 2700 for blind test condition of V_{in}=0.825 m/s

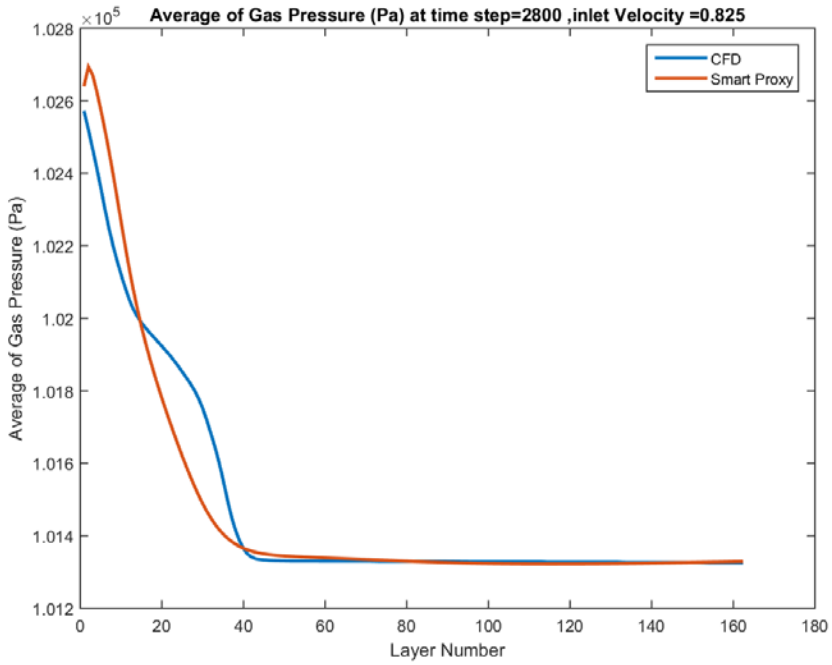

Figure 8-24 Spatially averaged CFD and smart proxy results for gas pressure at time step = 2800 for blind test condition of V_{in}=0.825 m/s

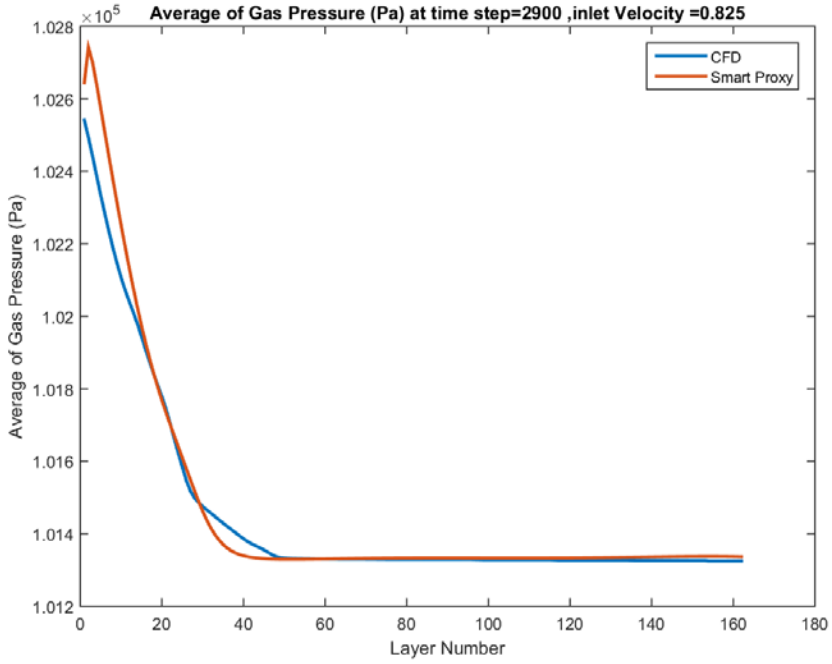

Figure 8-25 Spatially averaged CFD and smart proxy results for gas pressure at time step = 2900 for blind test condition of V_{in}=0.825 m/s

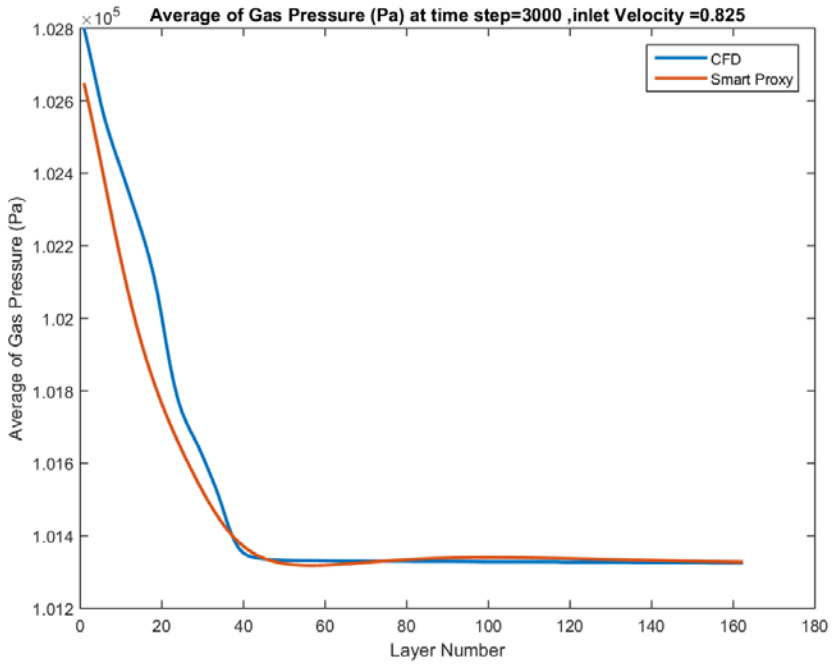

Figure 8-26 Spatially averaged CFD and smart proxy results for gas pressure at time step = 3000 for blind test condition of V_{in}=0.825 m/s

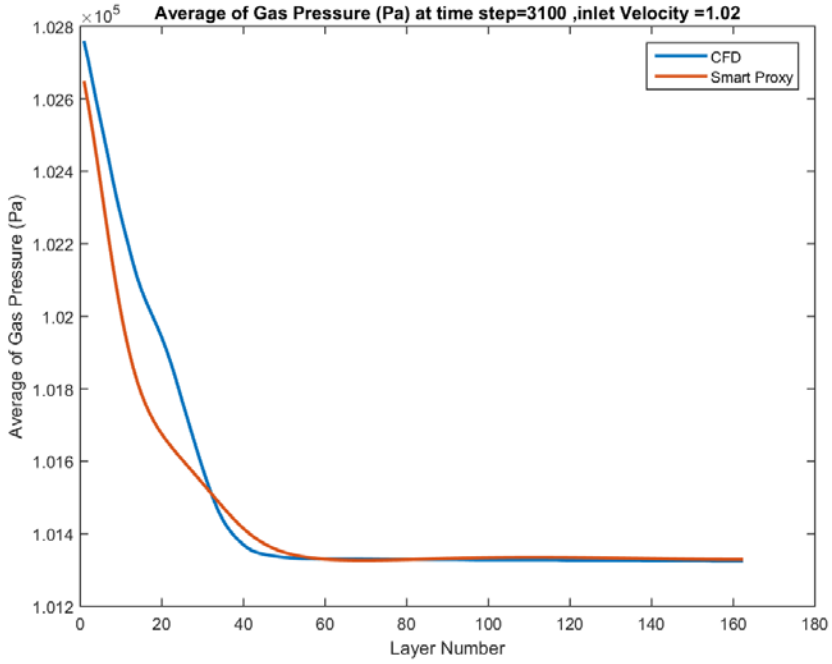

Figure 8-27 Spatially averaged CFD and smart proxy results for gas pressure at time step = 3100 for blind test condition of V_{in}=0.825 m/s

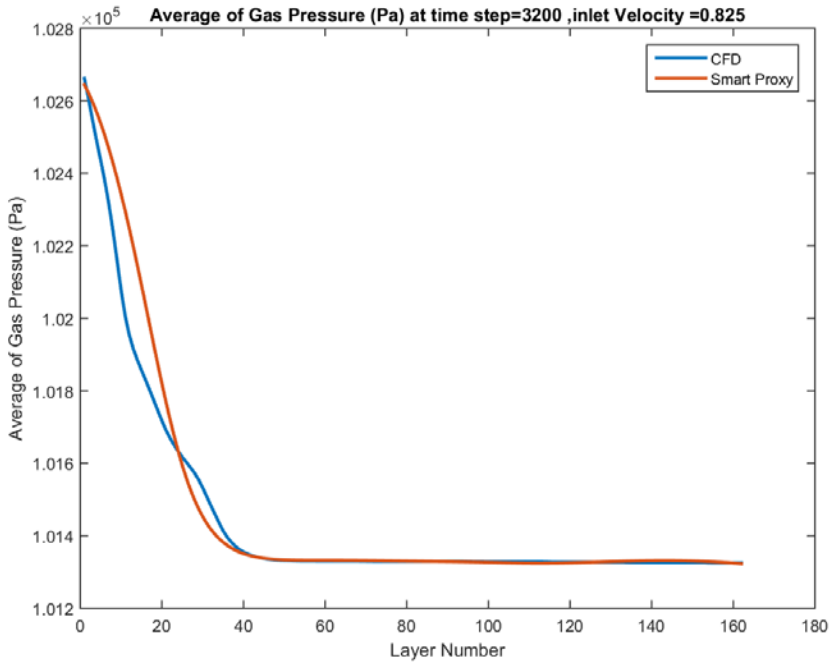

Figure 8-28 Spatially averaged CFD and smart proxy results for gas pressure at time step = 3200 for blind test condition of V_{in}=0.825 m/s

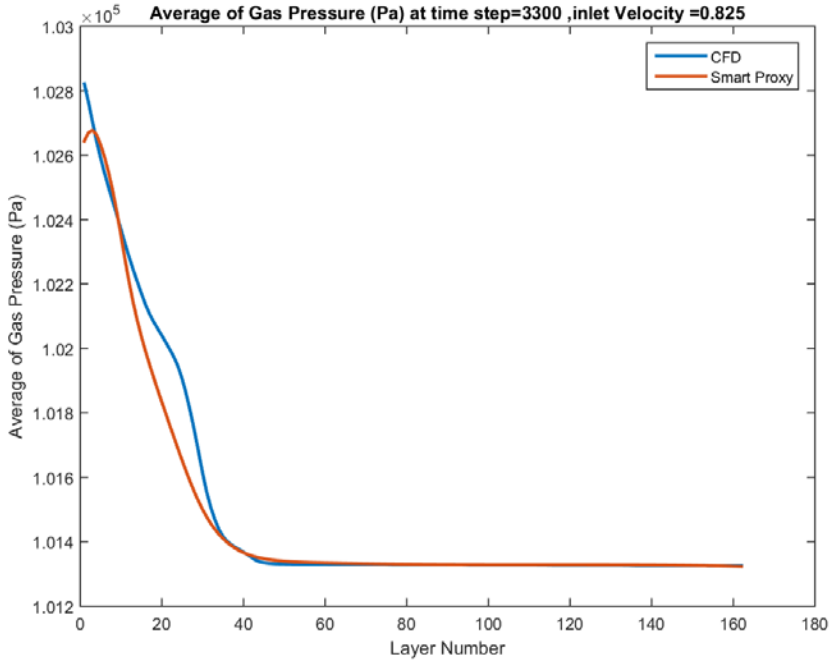

Figure 8-29 Spatially averaged CFD and smart proxy results for gas pressure at time step = 3300 for blind test condition of V_{in}=0.825 m/s

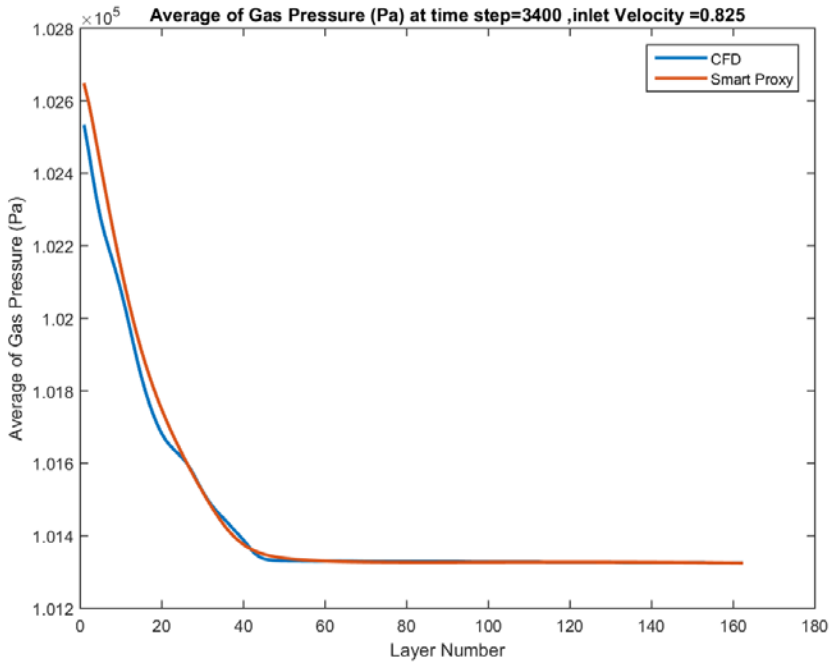

Figure 8-30 Spatially averaged CFD and smart proxy results for gas pressure at time step = 3400 for blind test condition of V_{in}=0.825 m/s

9. APPENDIX III: GAS PRESSURE PROFILE AT BLIND TEST CONDITION OF V_{IN}=1.02 M/S, WITH INFORMATION CASCADING FROM UPSTREAM TO DOWNSTREAM FOR TIME STEPS 500 THROUGH 3400

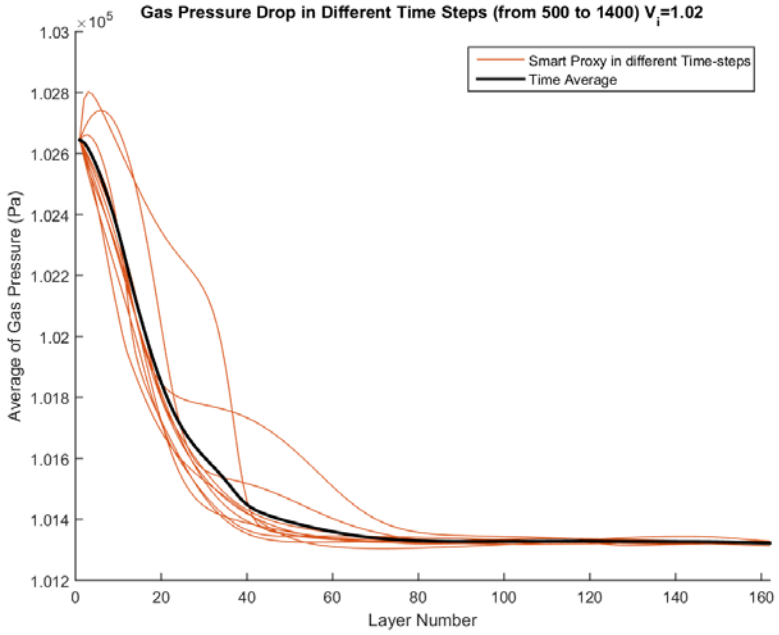

Figure 9-1 Spatial average profile of smart proxy results for gas pressure for time steps 500 through 1400 at blind test condition of V_{in} = 1.02 m/s

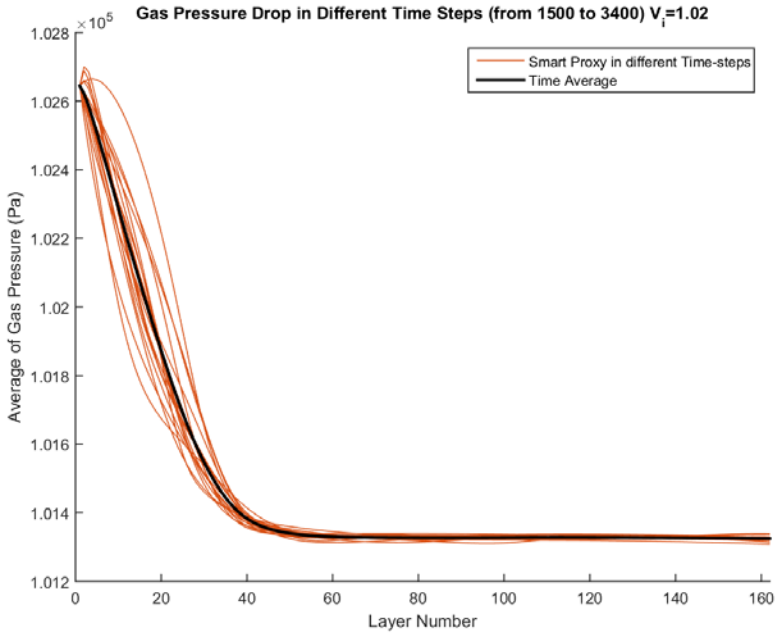

Figure 9-2 Spatial average profile of smart proxy results for gas pressure for time steps 1500 through 3400 at blind test condition of V_{in} = 1.02 m/s

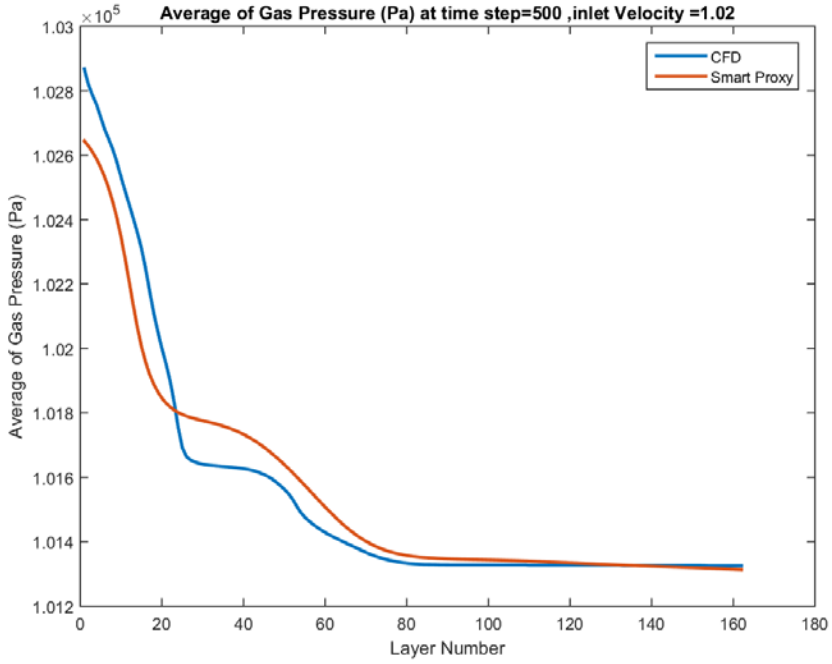

Figure 9-3 Spatially averaged CFD and smart proxy results for gas pressure at time step = 500 for blind test condition of V_{in}=1.02 m/s

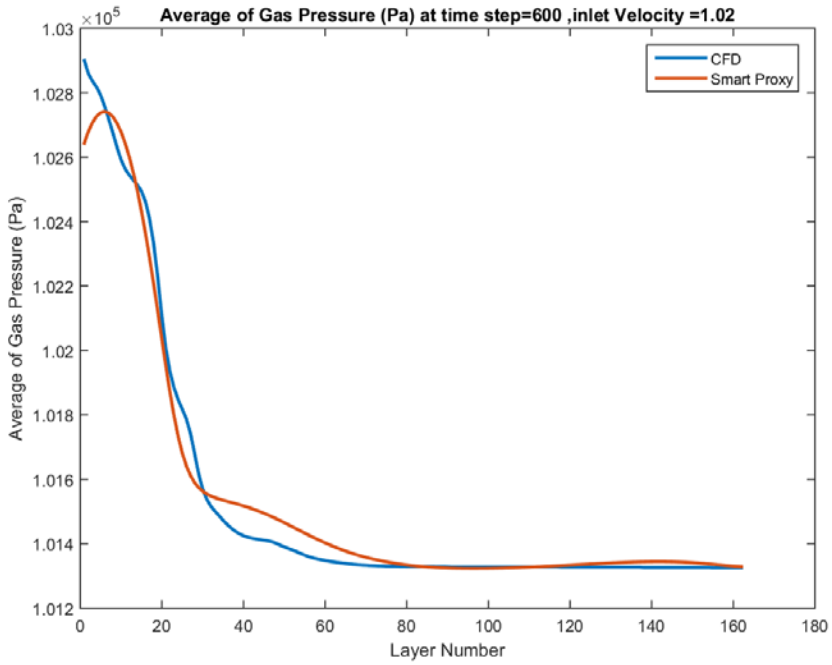

Figure 9-4 Spatially averaged CFD and smart proxy results for gas pressure at time step = 600 for blind test condition of V_{in}=1.02 m/s

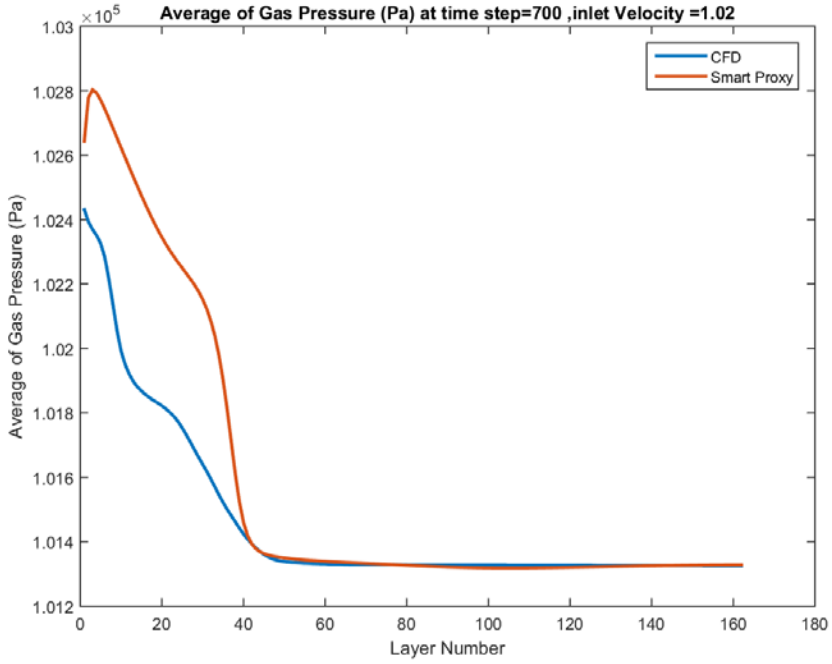

Figure 9-5 Spatially averaged CFD and smart proxy results for gas pressure at time step = 700 for blind test condition of V_{in}=1.02 m/s

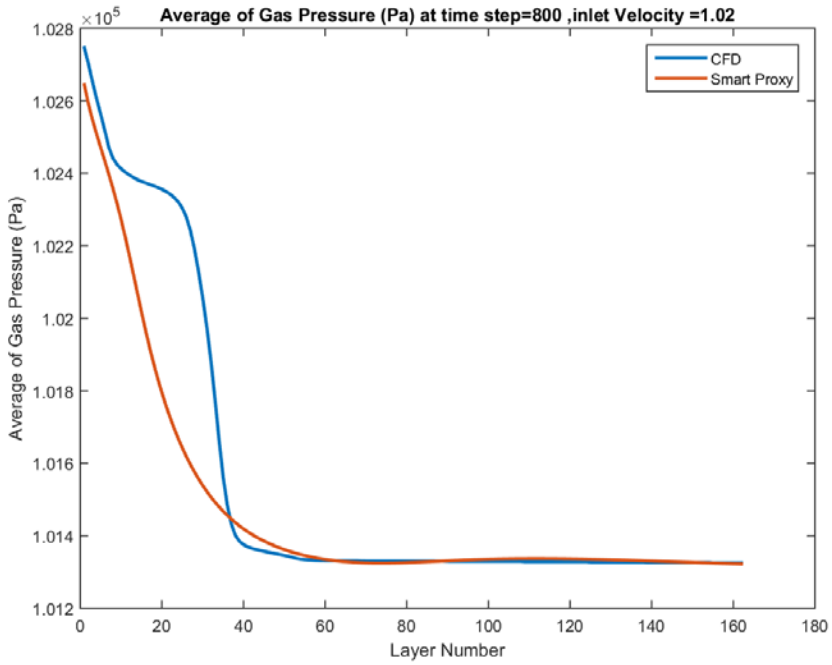

Figure 9-6 Spatially averaged CFD and smart proxy results for gas pressure at time step = 800 for blind test condition of V_{in}=1.02 m/s

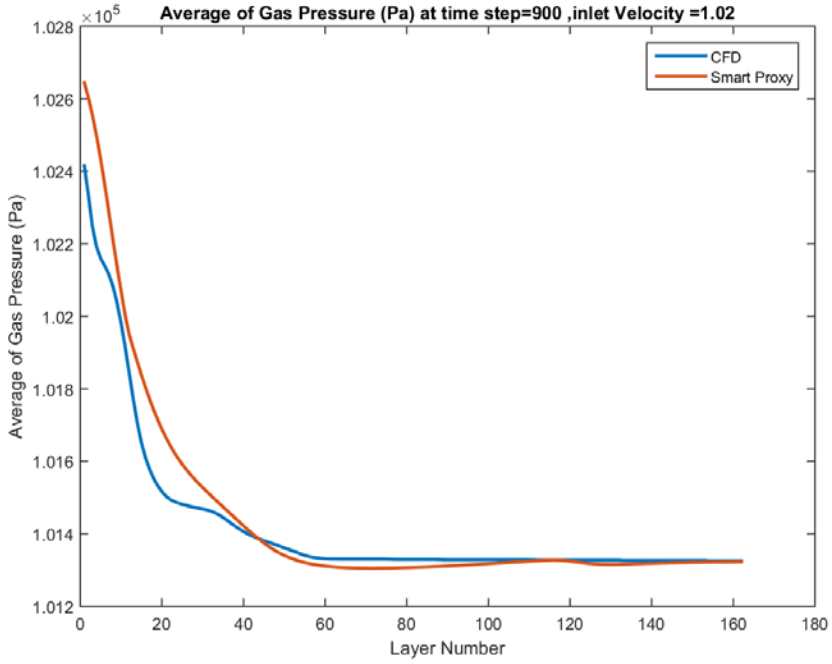

Figure 9-7 Spatially averaged CFD and smart proxy results for gas pressure at time step = 900 for blind test condition of V_{in}=1.02 m/s

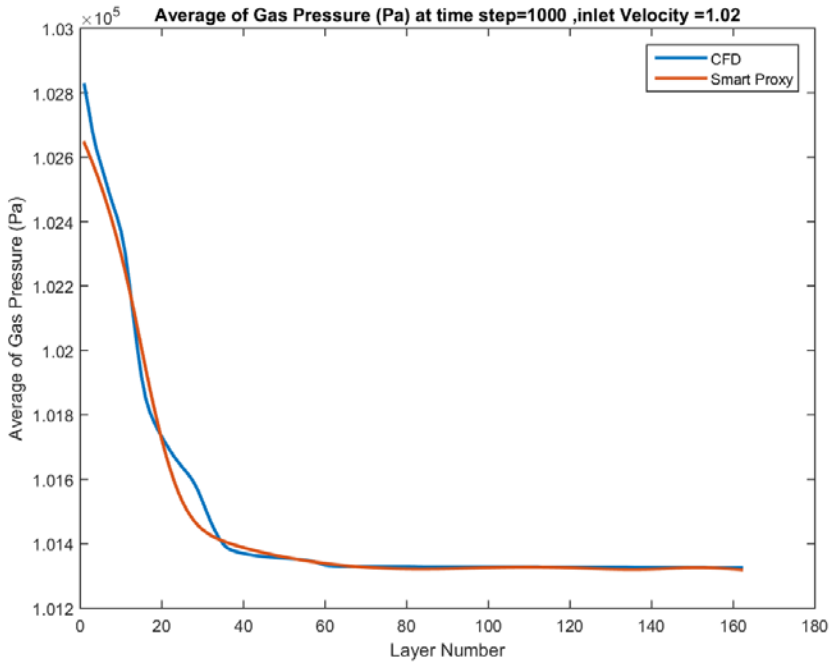

Figure 9-8 Spatially averaged CFD and smart proxy results for gas pressure at time step = 1000 for blind test condition of V_{in}=1.02 m/s

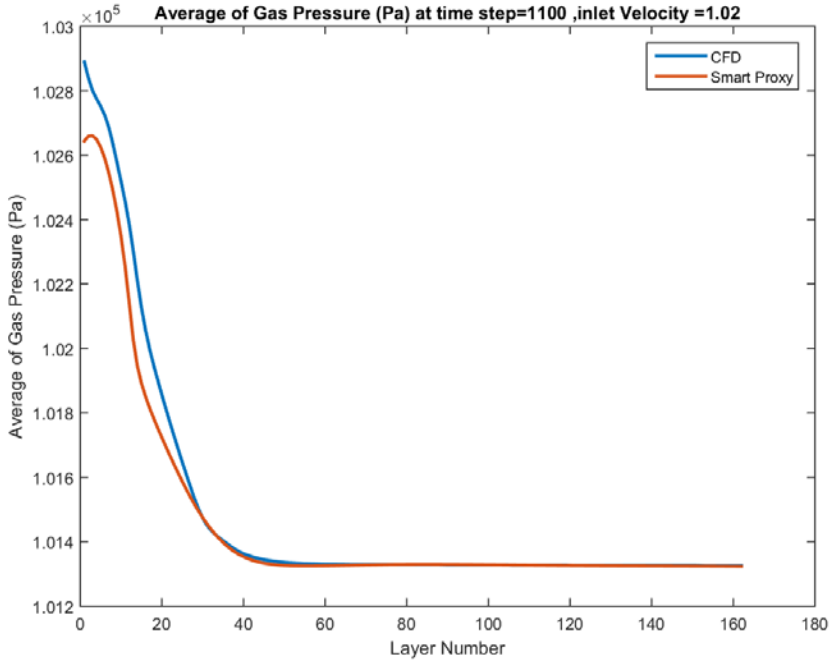

Figure 9-9 Spatially averaged CFD and smart proxy results for gas pressure at time step = 1100 for blind test condition of V_{in}=1.02 m/s

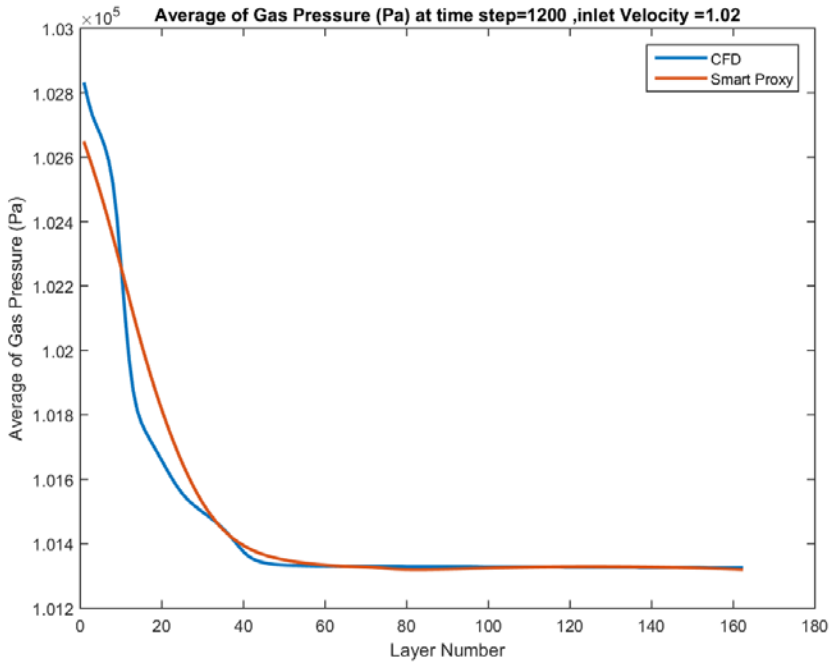

Figure 9-10 Spatially averaged CFD and smart proxy results for gas pressure at time step = 1200 for blind test condition of V_{in}=1.02 m/s

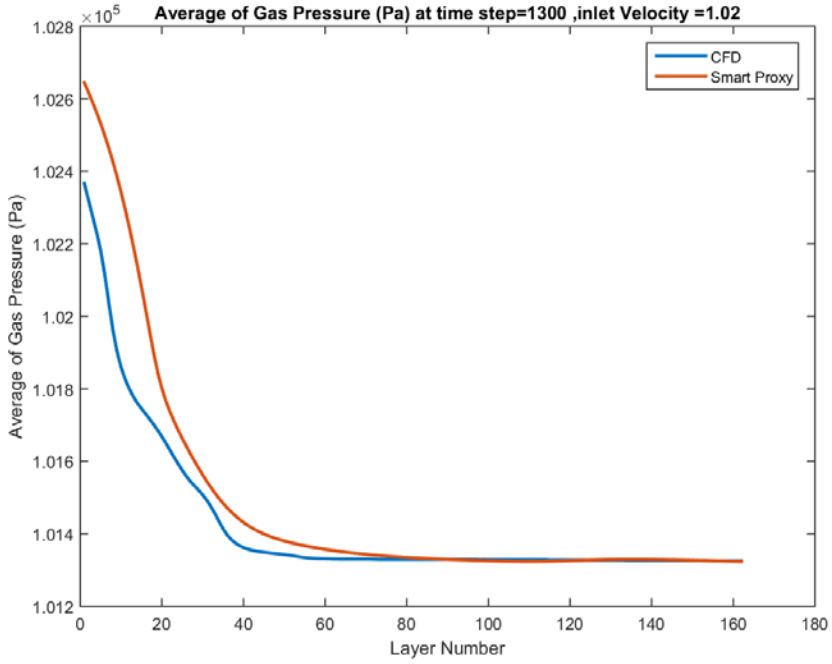

Figure 9-11 Spatially averaged CFD and smart proxy results for gas pressure at time step = 1300 for blind test condition of V_{in}=1.02 m/s

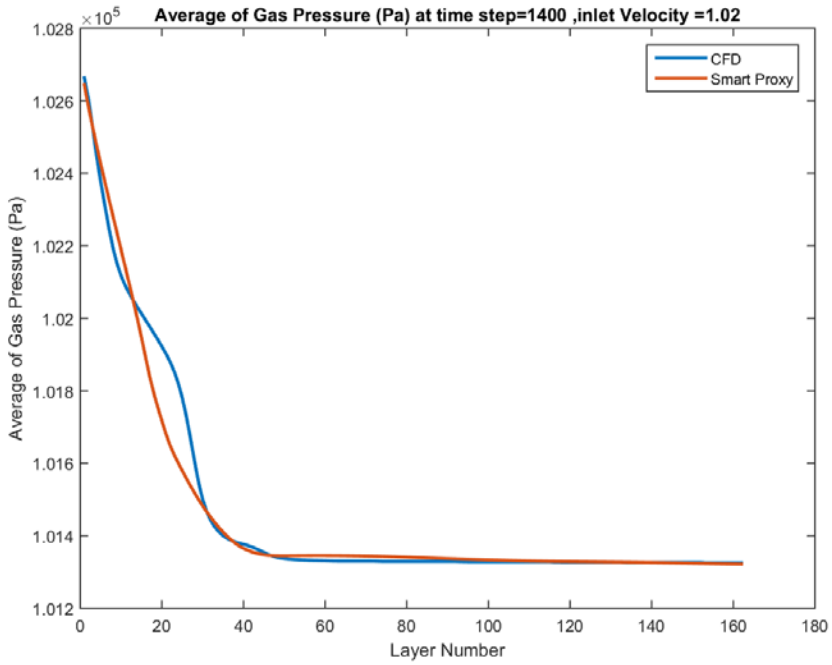

Figure 9-12 Spatially averaged CFD and smart proxy results for gas pressure at time step = 1400 for blind test condition of V_{in}=1.02 m/s

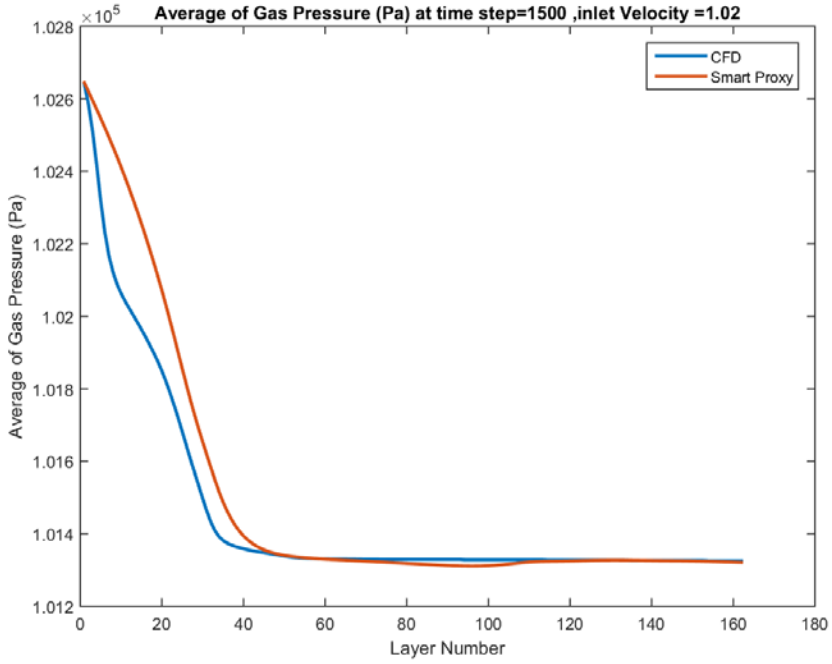

Figure 9-13 Spatially averaged CFD and smart proxy results for gas pressure at time step = 1500 for blind test condition of V_{in}=1.02 m/s

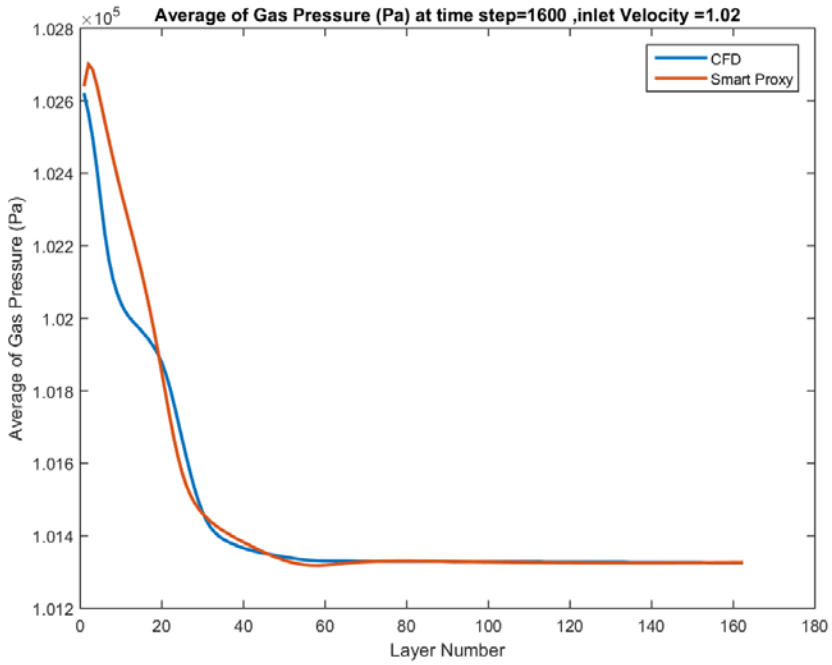

Figure 9-14 Spatially averaged CFD and smart proxy results for gas pressure at time step = 1600 for blind test condition of V_{in}=1.02 m/s

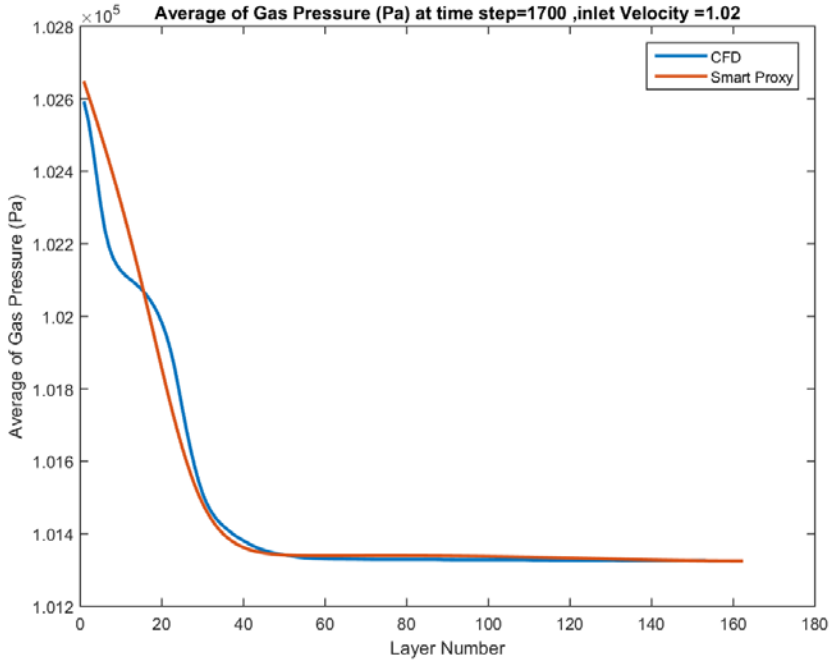

Figure 9-15 Spatially averaged CFD and smart proxy results for gas pressure at time step = 1700 for blind test condition of V_{in}=1.02 m/s

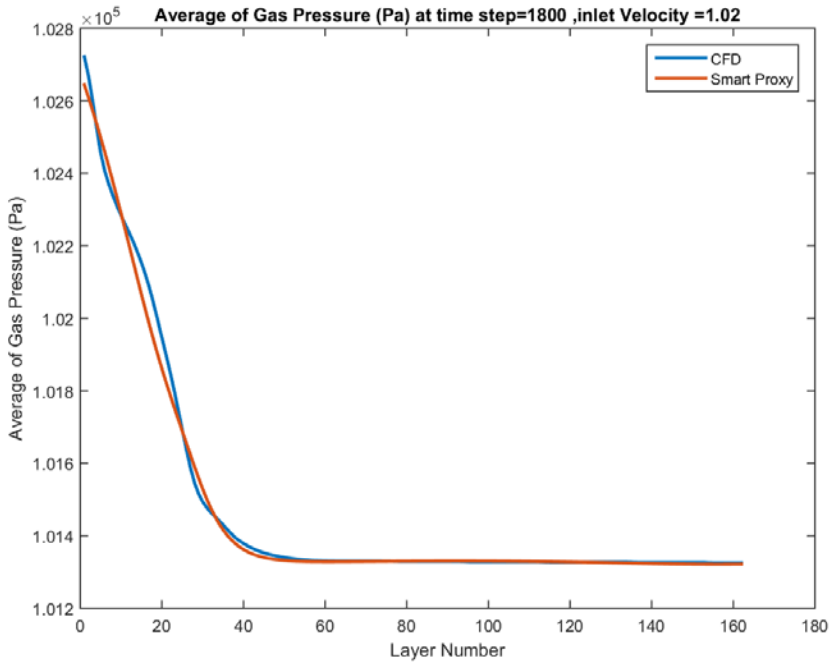

Figure 9-16 Spatially averaged CFD and smart proxy results for gas pressure at time step = 1800 for blind test condition of V_{in}=1.02 m/s

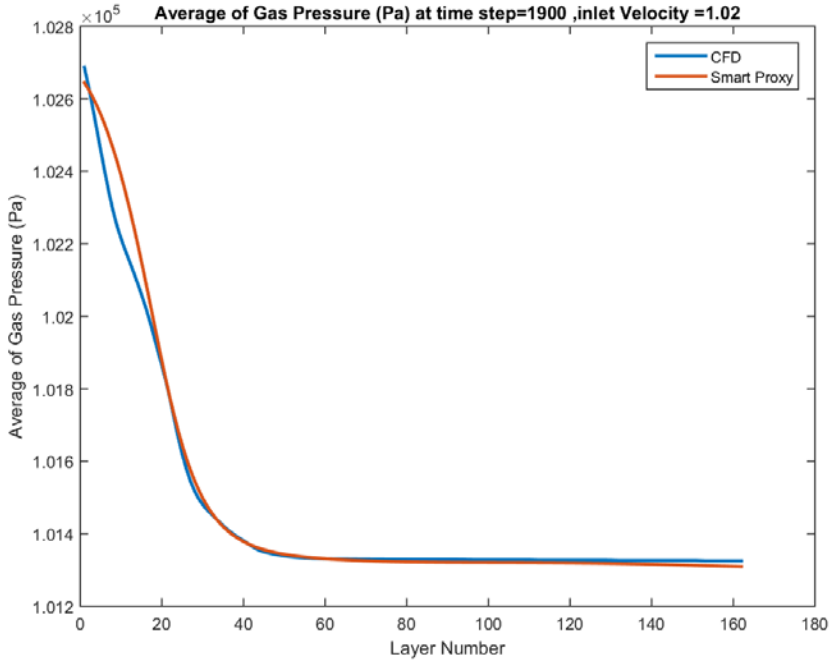

Figure 9-17 Spatially averaged CFD and smart proxy results for gas pressure at time step = 1900 for blind test condition of V_{in}=1.02 m/s

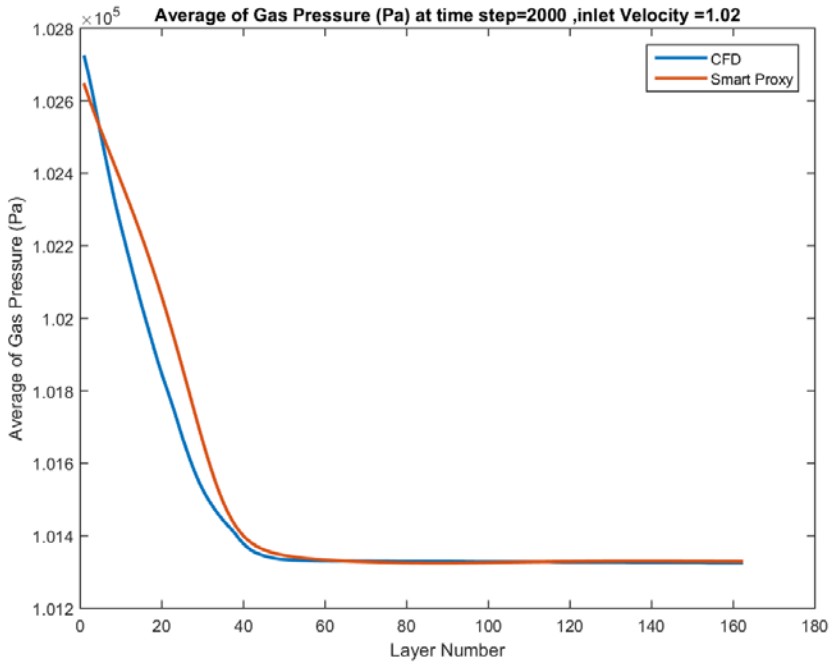

Figure 9-18 Spatially averaged CFD and smart proxy results for gas pressure at time step = 2000 for blind test condition of V_{in}=1.02 m/s

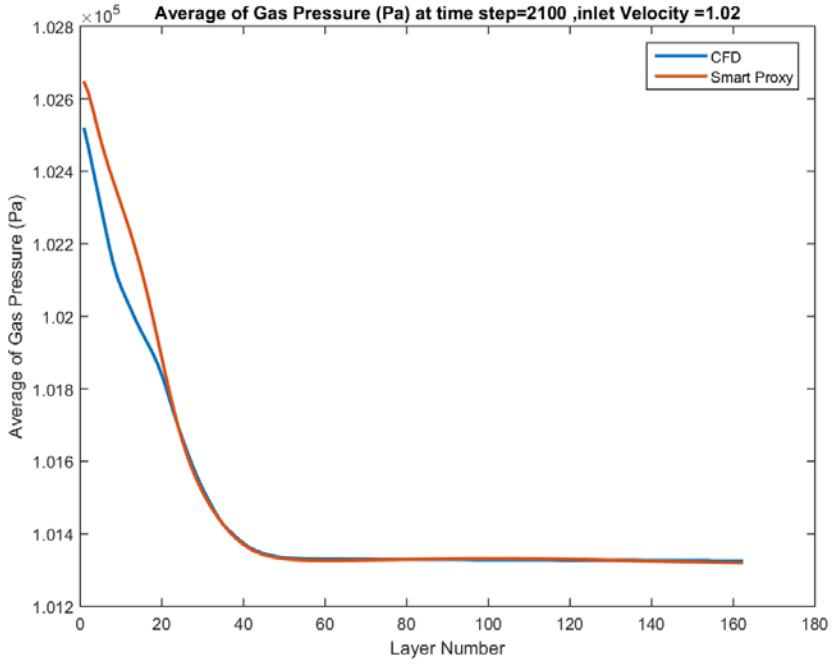

Figure 9-19 Spatially averaged CFD and smart proxy results for gas pressure at time step = 2100 for blind test condition of V_{in}=1.02 m/s

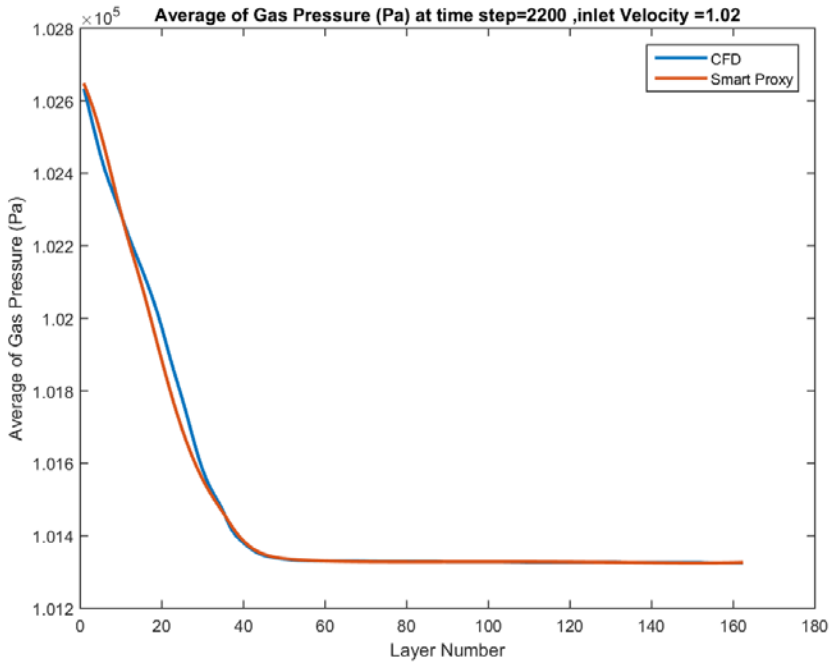

Figure 9-20 Spatially averaged CFD and smart proxy results for gas pressure at time step = 2200 for blind test condition of V_{in}=1.02 m/s

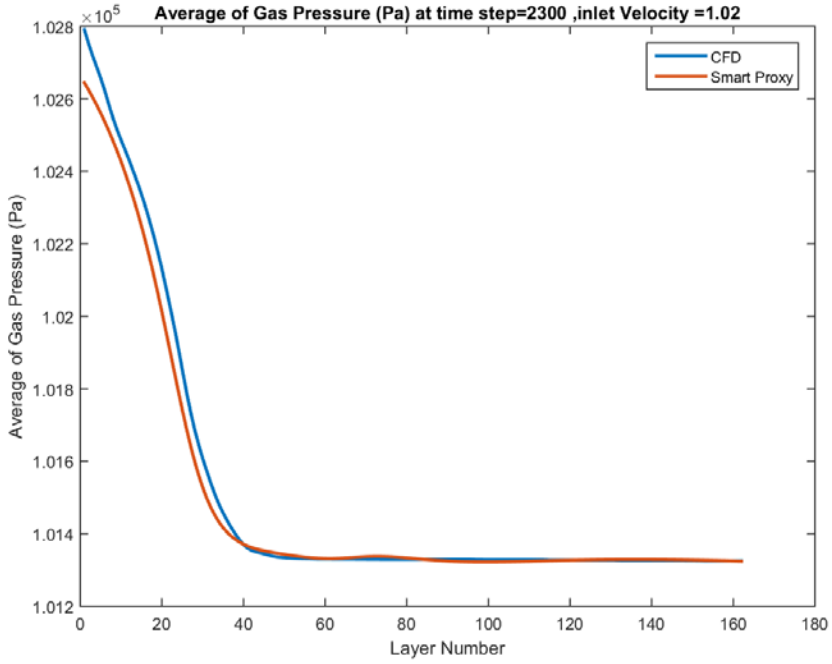

Figure 9-21 Spatially averaged CFD and smart proxy results for gas pressure at time step = 2300 for blind test condition of V_{in}=1.02 m/s

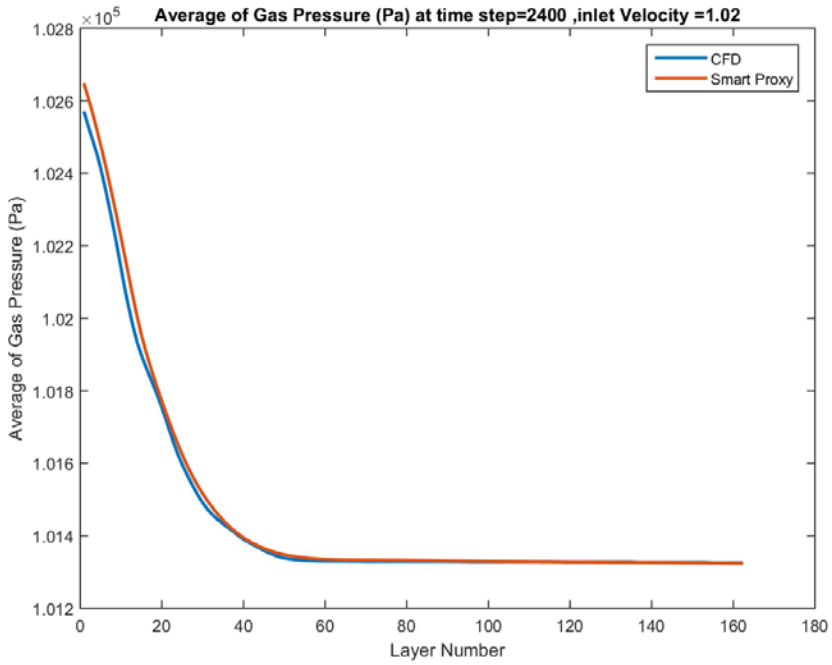

Figure 9-22 Spatially averaged CFD and smart proxy results for gas pressure at time step = 2400 for blind test condition of V_{in}=1.02 m/s

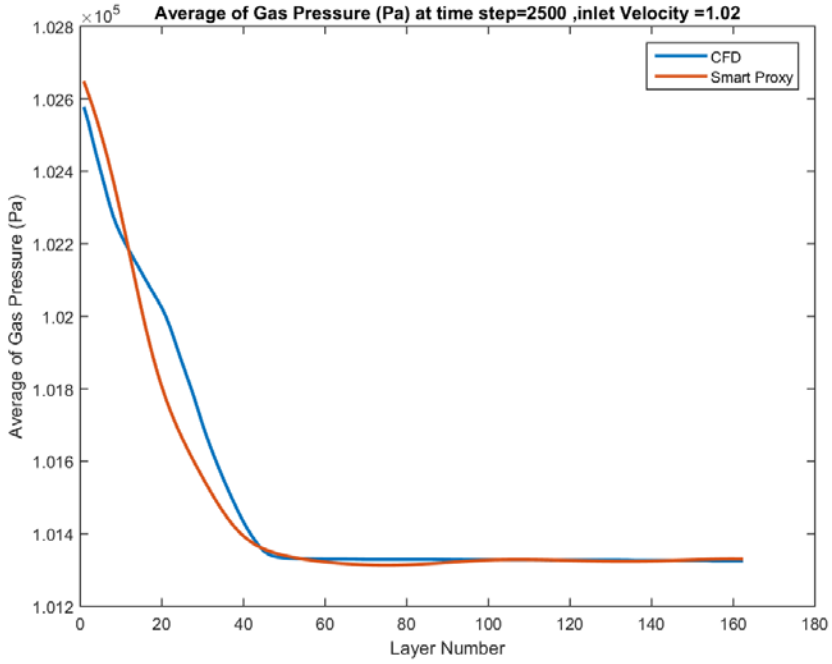

Figure 9-23 Spatially averaged CFD and smart proxy results for gas pressure at time step = 2500 for blind test condition of V_{in}=1.02 m/s

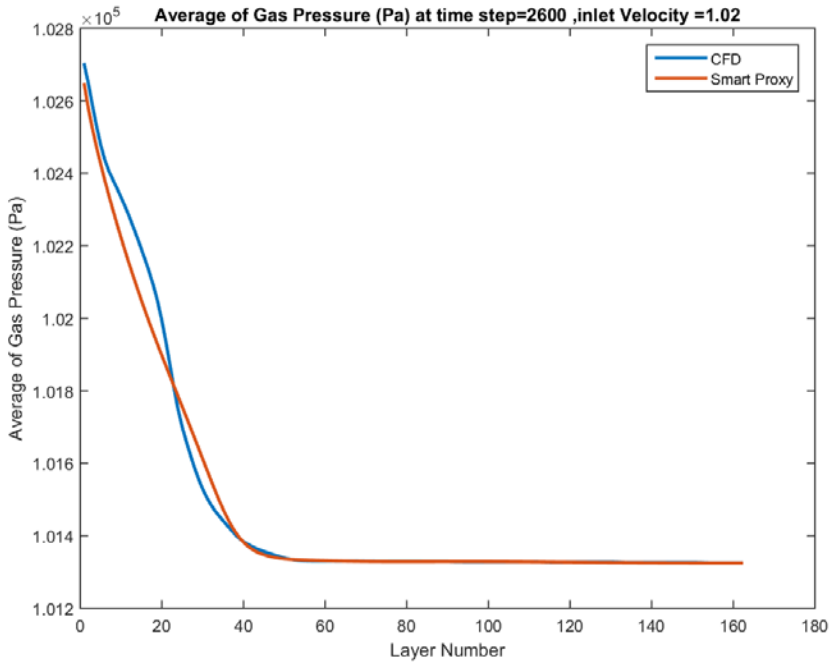

Figure 9-24 Spatially averaged CFD and smart proxy results for gas pressure at time step = 2600 for blind test condition of V_{in}=1.02 m/s

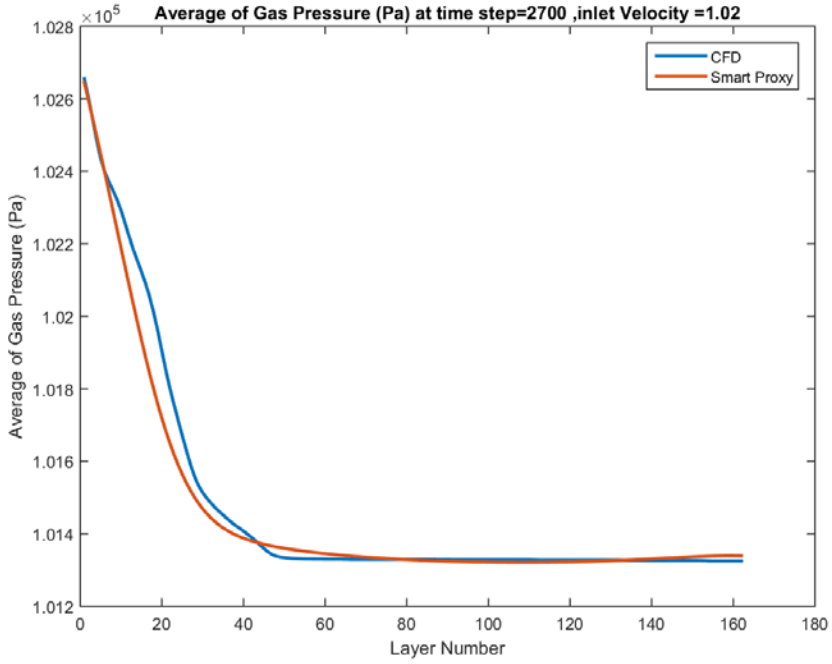

Figure 9-25 Spatially averaged CFD and smart proxy results for gas pressure at time step = 2700 for blind test condition of V_{in}=1.02 m/s

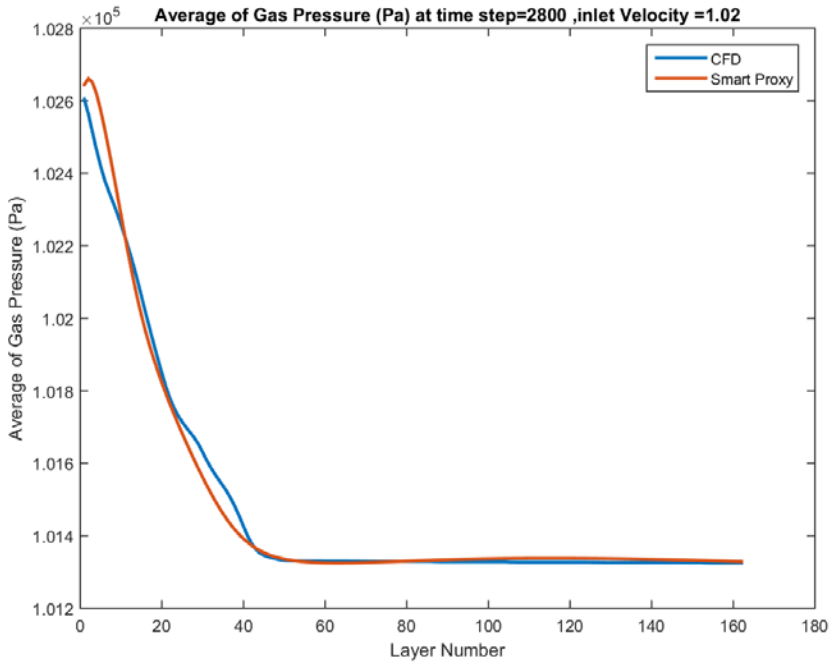

Figure 9-26 Spatially averaged CFD and smart proxy results for gas pressure at time step = 2800 for blind test condition of V_{in}=1.02 m/s

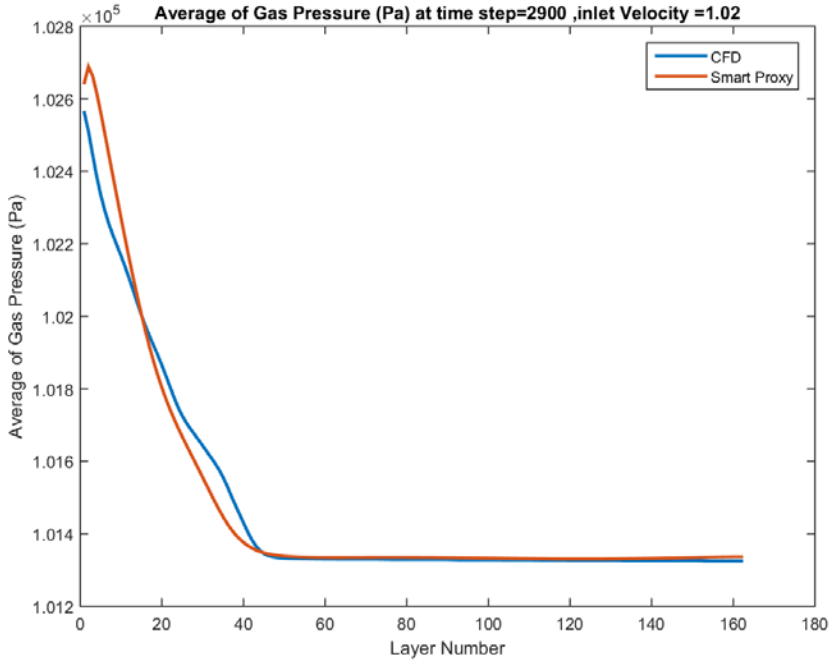

Figure 9-27 Spatially averaged CFD and smart proxy results for gas pressure at time step = 2900 for blind test condition of V_{in}=1.02 m/s

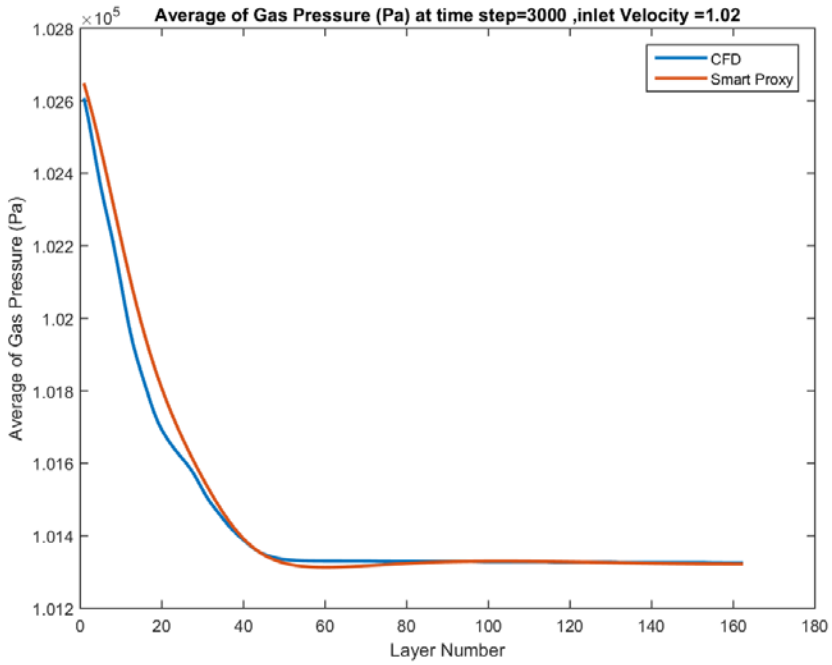

Figure 9-28 Spatially averaged CFD and smart proxy results for gas pressure at time step = 3000 for blind test condition of V_{in}=1.02 m/s

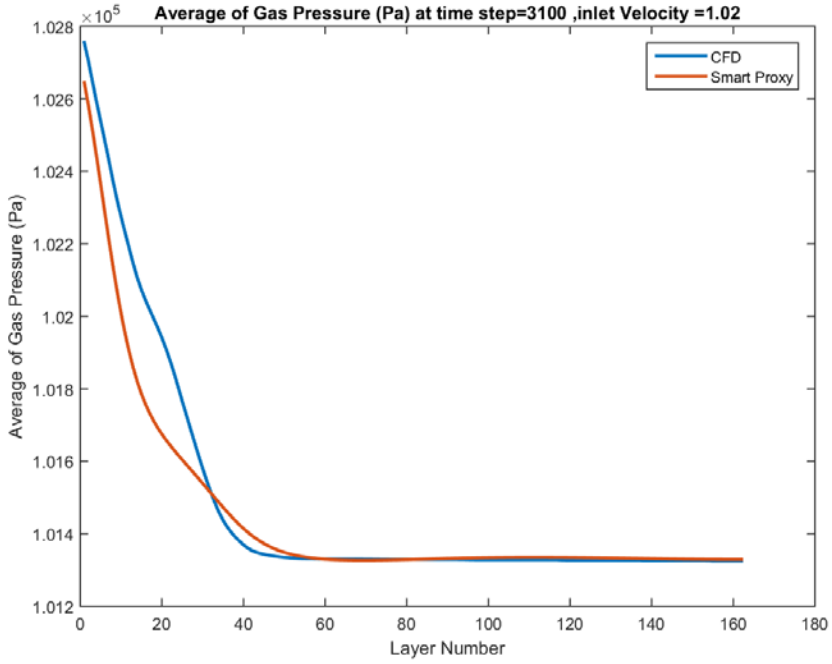

Figure 9-29 Spatially averaged CFD and smart proxy results for gas pressure at time step = 3100 for blind test condition of V_{in}=1.02 m/s

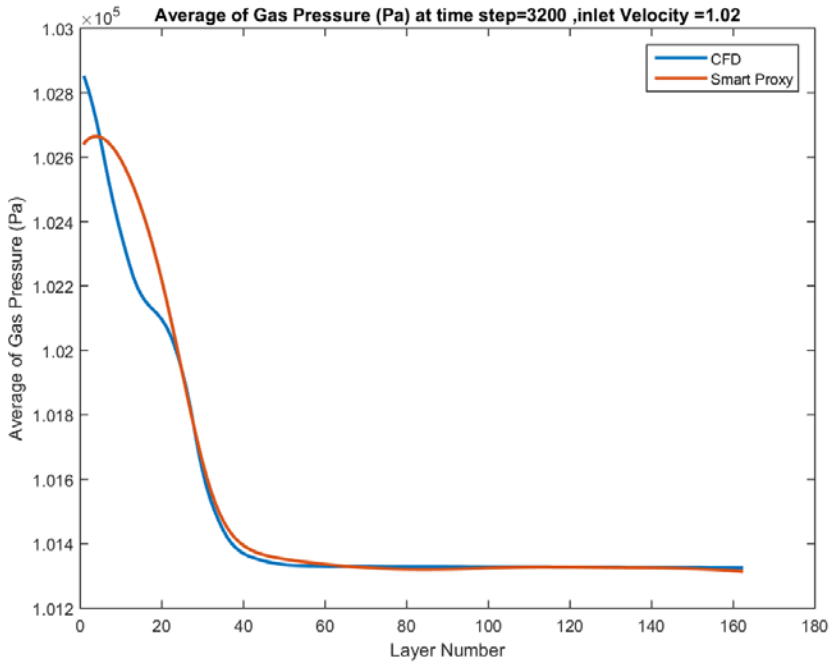

Figure 9-30 Spatially averaged CFD and smart proxy results for gas pressure at time step = 3200 for blind test condition of V_{in}=1.02 m/s

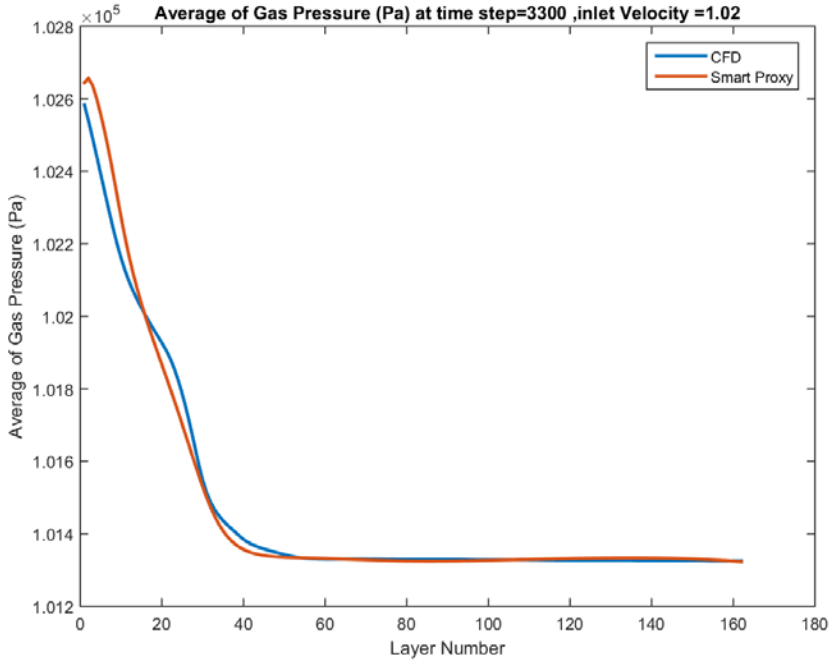

Figure 9-31 Spatially averaged CFD and smart proxy results for gas pressure at time step = 3300 for blind test condition of V_{in}=1.02 m/s

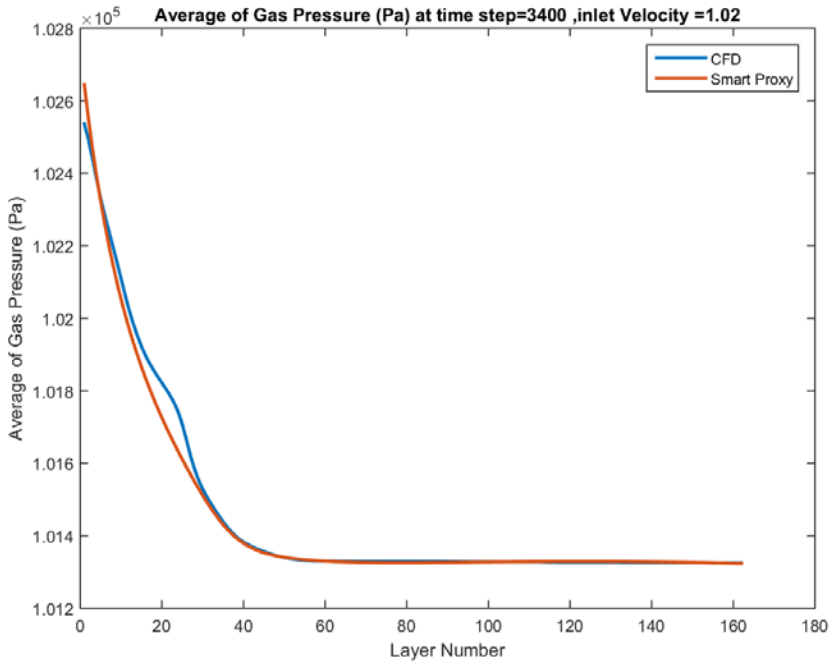

Figure 9-32 Spatially averaged CFD and smart proxy results for gas pressure at time step = 3400 for blind test condition of V_{in}=1.02 m/s

10. APPENDIX IV: GAS PRESSURE PROFILE AT BLIND TEST CONDITION OF V_{IN}=1.1 M/S, WITH INFORMATION CASCADING FROM UPSTREAM TO DOWNSTREAM FOR TIME STEPS 500 THROUGH 3400

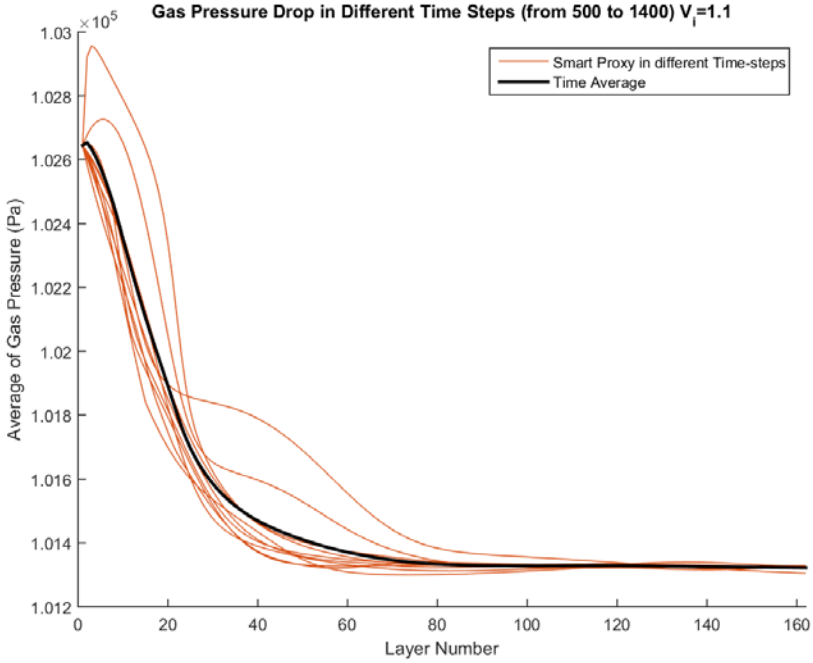

Figure 10-1 Spatial average profile of smart proxy results for gas pressure, all time steps (500 to 1400) at inlet velocity of 1.1 m/s

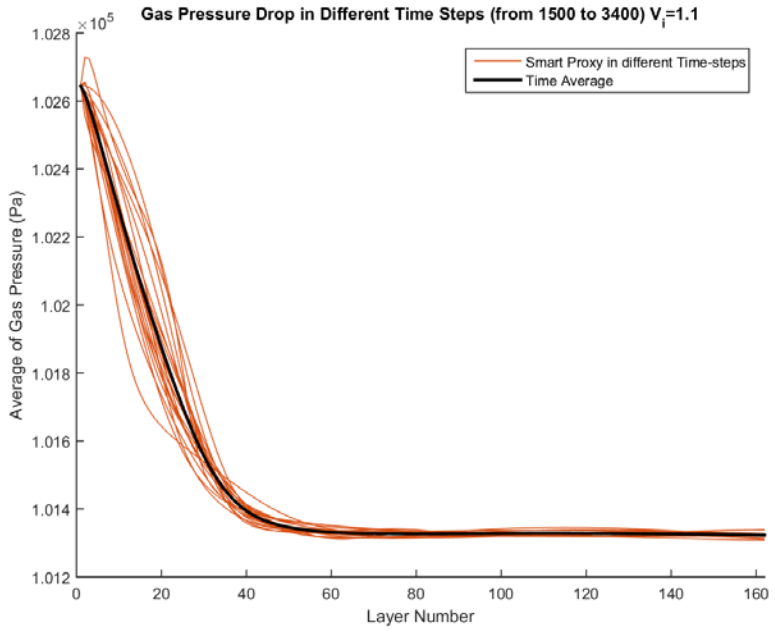

Figure 10-2 Spatial average profile of smart proxy results for gas pressure, all time steps (1500 to 3400) at inlet velocity of 1.1 m/s

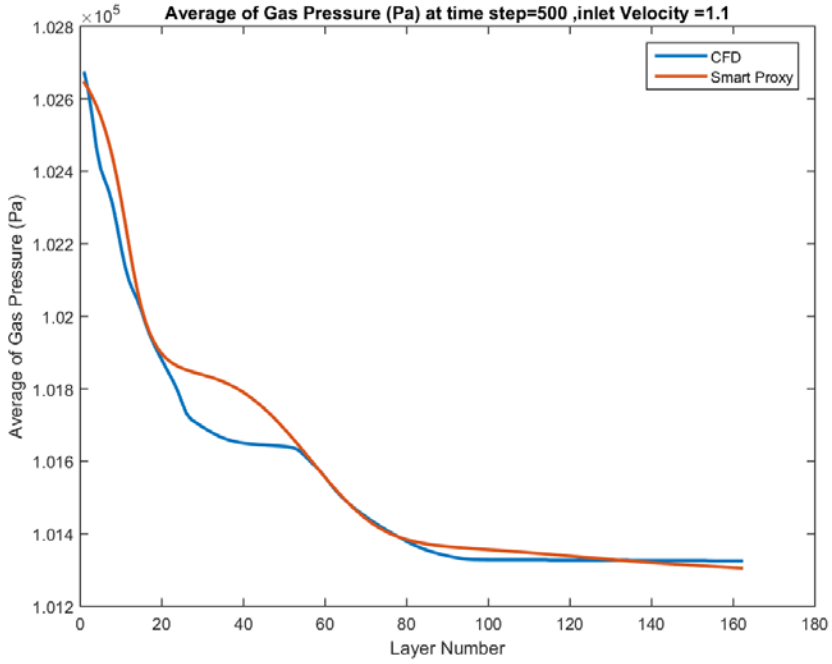

Figure 10-3 Spatially averaged CFD and smart proxy results for gas pressure at time step = 500 for blind test condition of V_{in}=1.1 m/s

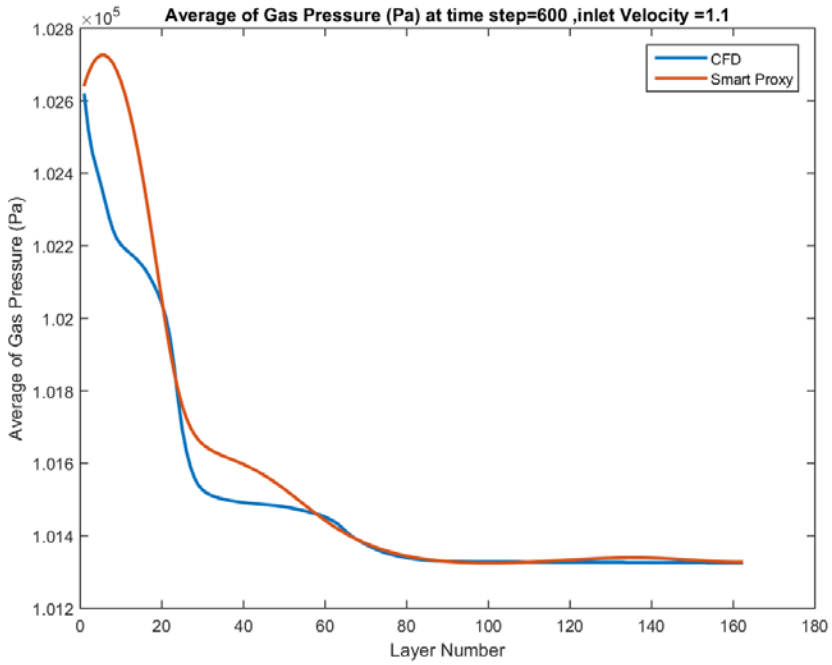

Figure 10-4 Spatially averaged CFD and smart proxy results for gas pressure at time step = 600 for blind test condition of V_{in}=1.1 m/s

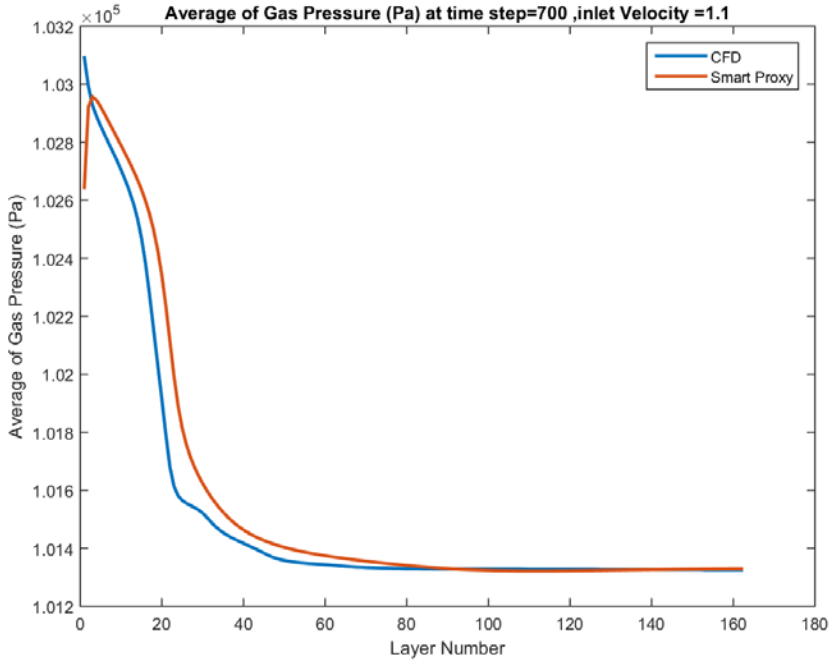

Figure 10-5 Spatially averaged CFD and smart proxy results for gas pressure at time step = 700 for blind test condition of V_{in}=1.1 m/s

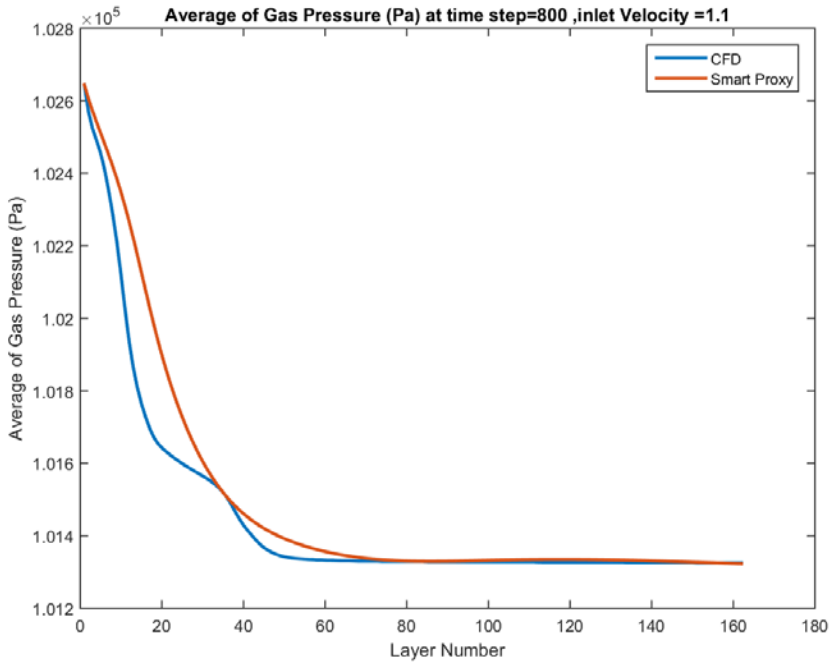

Figure 10-6 Spatially averaged CFD and smart proxy results for gas pressure at time step = 800 for blind test condition of V_{in}=1.1 m/s

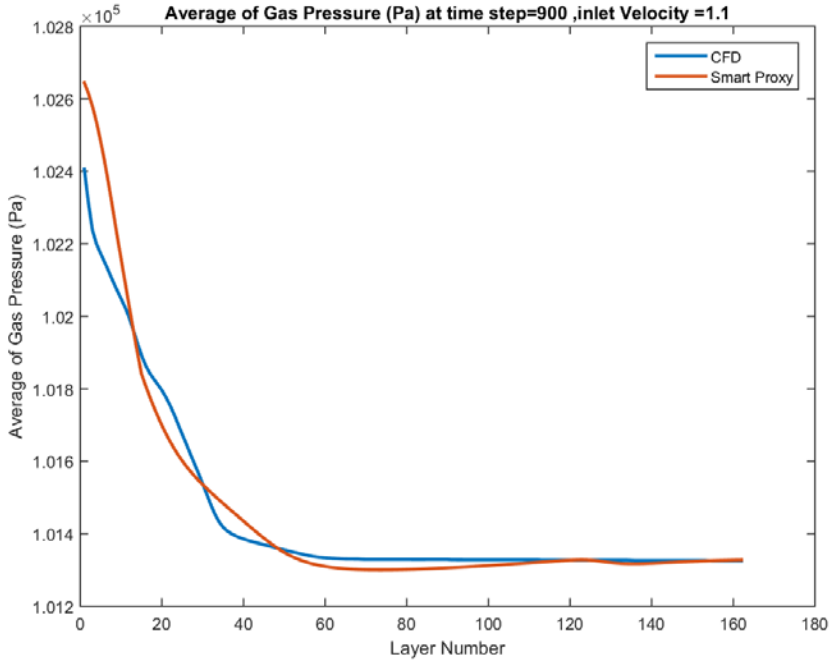

Figure 10-7 Spatially averaged CFD and smart proxy results for gas pressure at time step = 900 for blind test condition of V_{in}=1.1 m/s

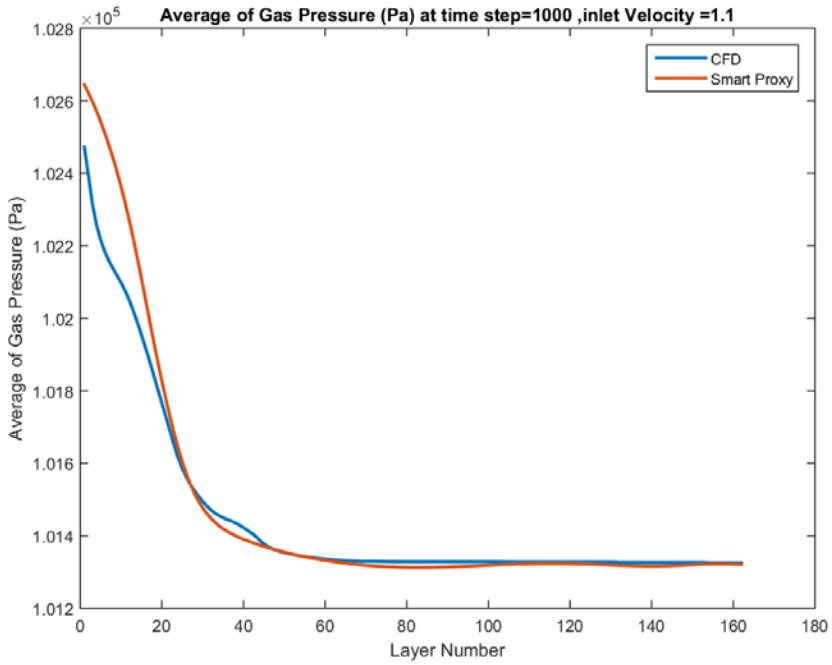

Figure 10-8 Spatially averaged CFD and smart proxy results for gas pressure at time step = 1000 for blind test condition of V_{in}=1.1 m/s

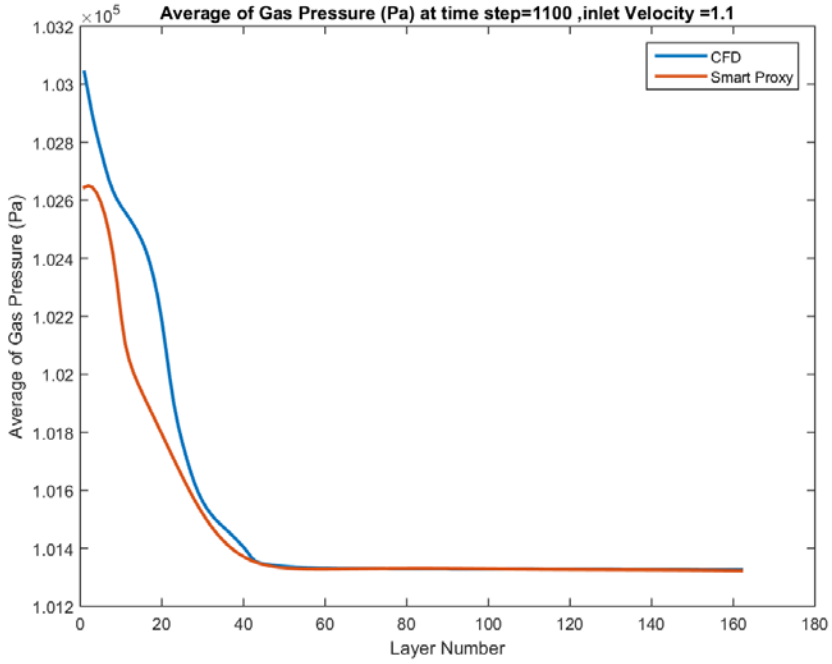

Figure 10-9 Spatially averaged CFD and smart proxy results for gas pressure at time step = 1100 for blind test condition of V_{in}=1.1 m/s

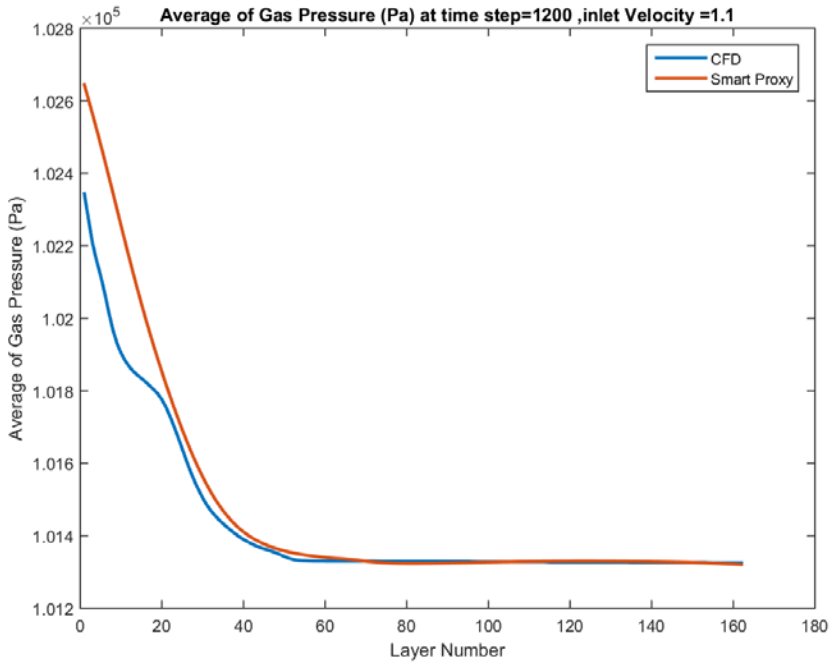

Figure 10-10 Spatially averaged CFD and smart proxy results for gas pressure at time step = 1200 for blind test condition of V_{in}=1.1 m/s

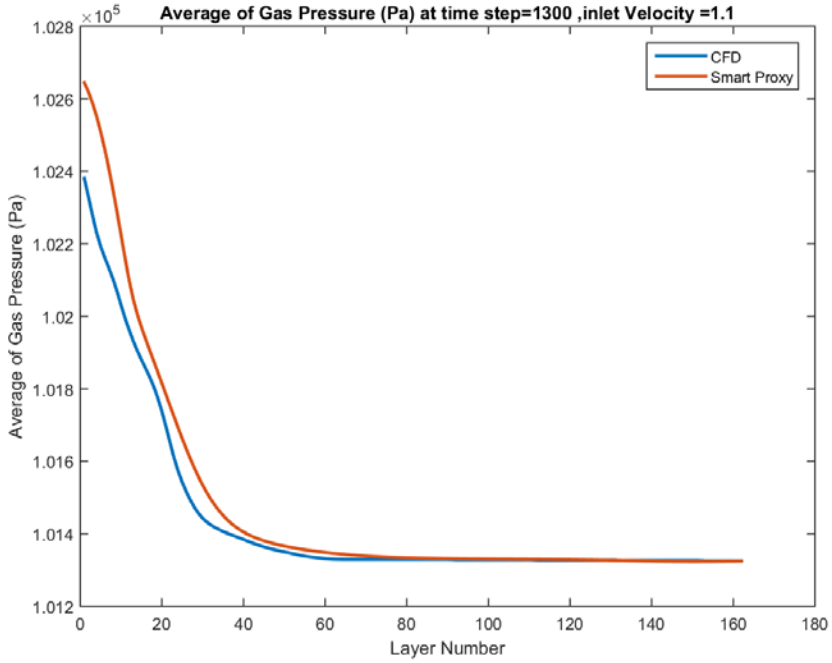

Figure 10-11 Spatially averaged CFD and smart proxy results for gas pressure at time step = 1300 for blind test condition of V_{in}=1.1 m/s

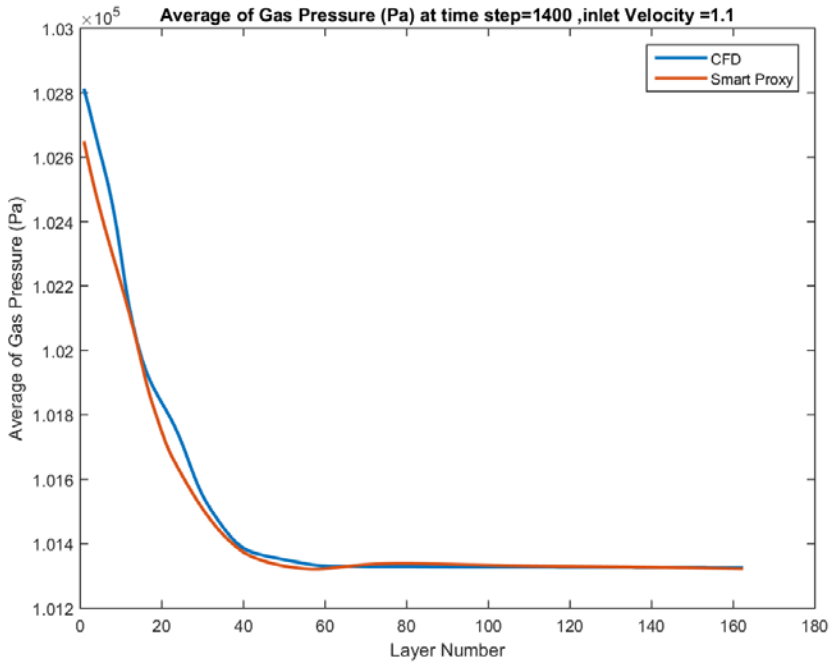

Figure 10-12 Spatially averaged CFD and smart proxy results for gas pressure at time step = 1400 for blind test condition of V_{in}=1.1 m/s

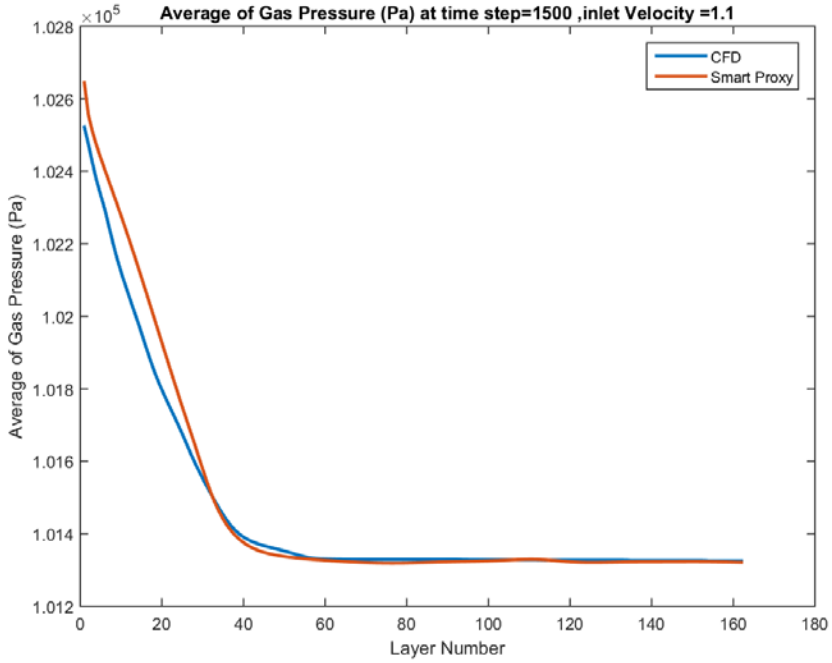

Figure 10-13 Spatially averaged CFD and smart proxy results for gas pressure at time step = 1500 for blind test condition of V_{in}=1.1 m/s

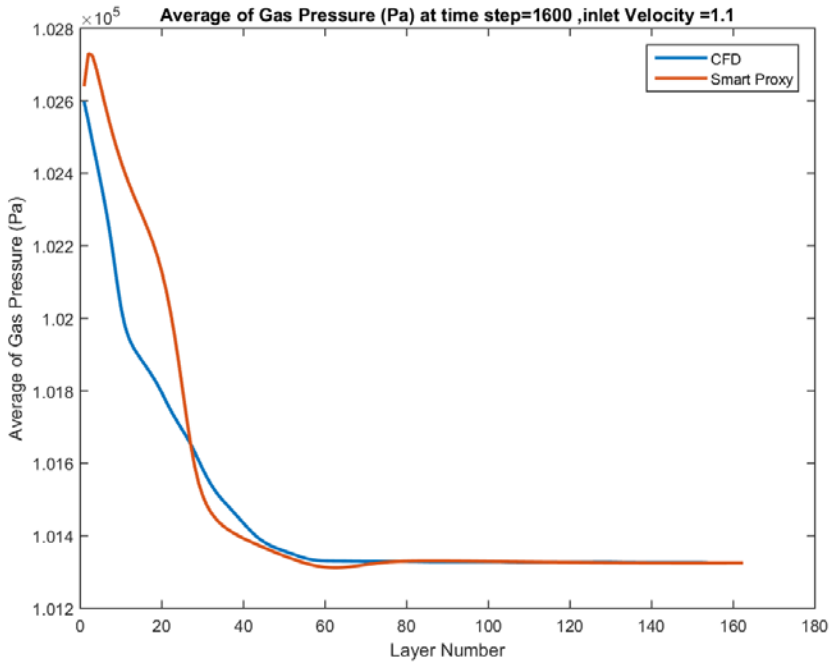

Figure 10-14 Spatially averaged CFD and smart proxy results for gas pressure at time step = 1600 for blind test condition of V_{in}=1.1 m/s

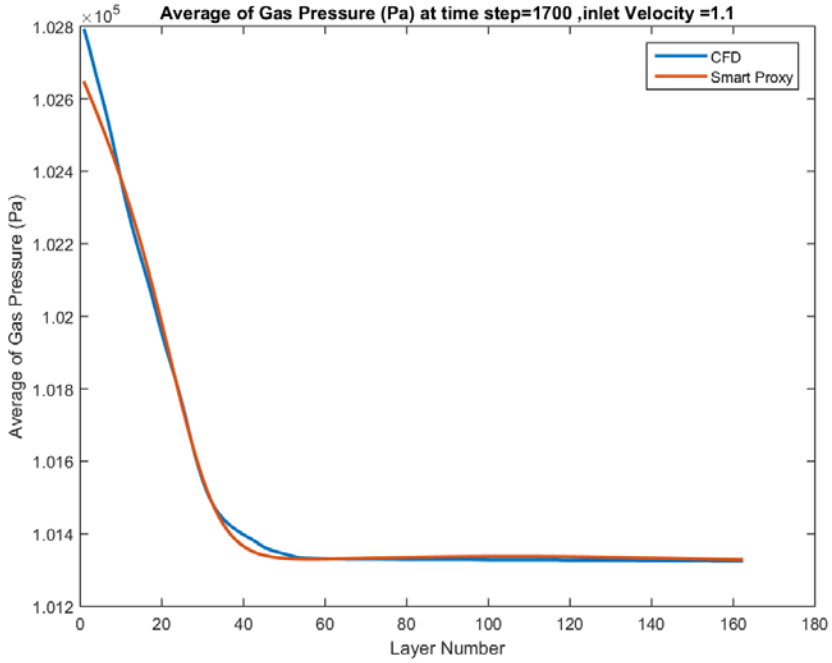

Figure 10-15 Spatially averaged CFD and smart proxy results for gas pressure at time step = 1700 for blind test condition of V_{in}=1.1 m/s

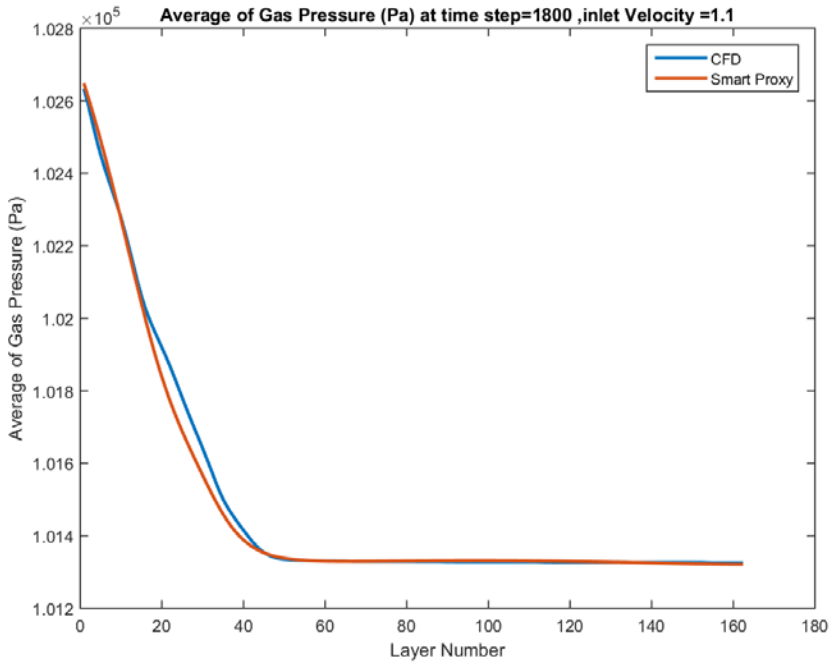

Figure 10-16 Spatially averaged CFD and smart proxy results for gas pressure at time step = 1800 for blind test condition of V_{in}=1.1 m/s

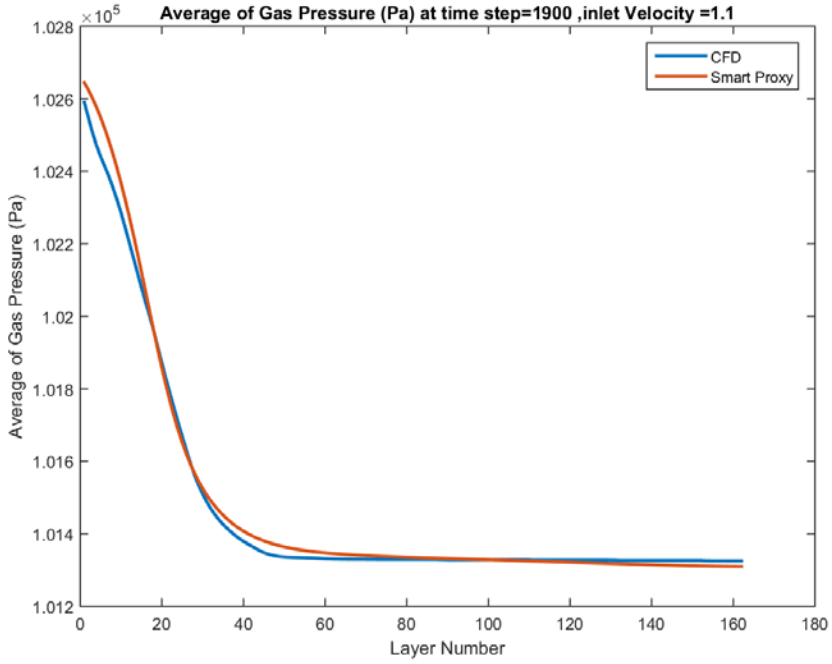

Figure 10-17 Spatially averaged CFD and smart proxy results for gas pressure at time step = 1900 for blind test condition of V_{in}=1.1 m/s

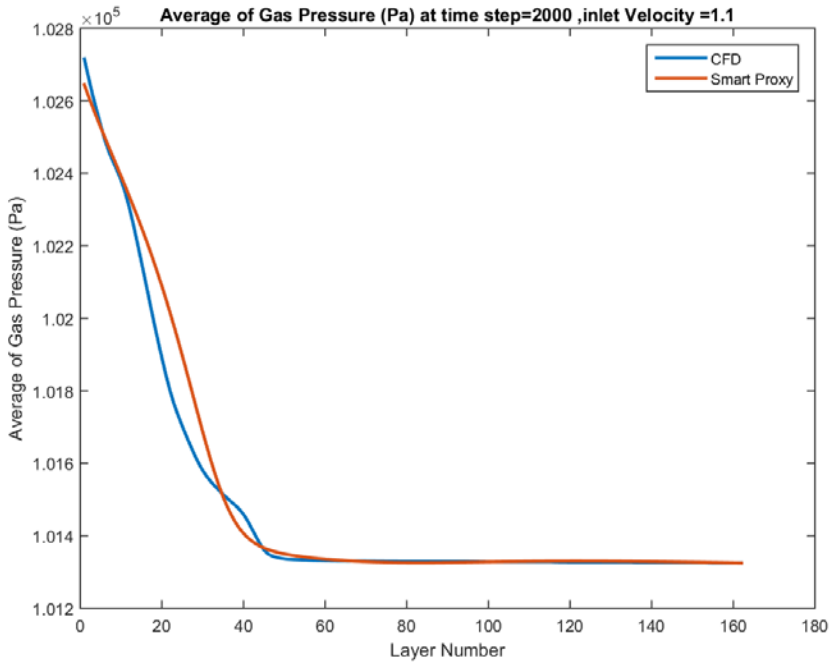

Figure 10-18 Spatially averaged CFD and smart proxy results for gas pressure at time step = 2000 for blind test condition of V_{in}=1.1 m/s

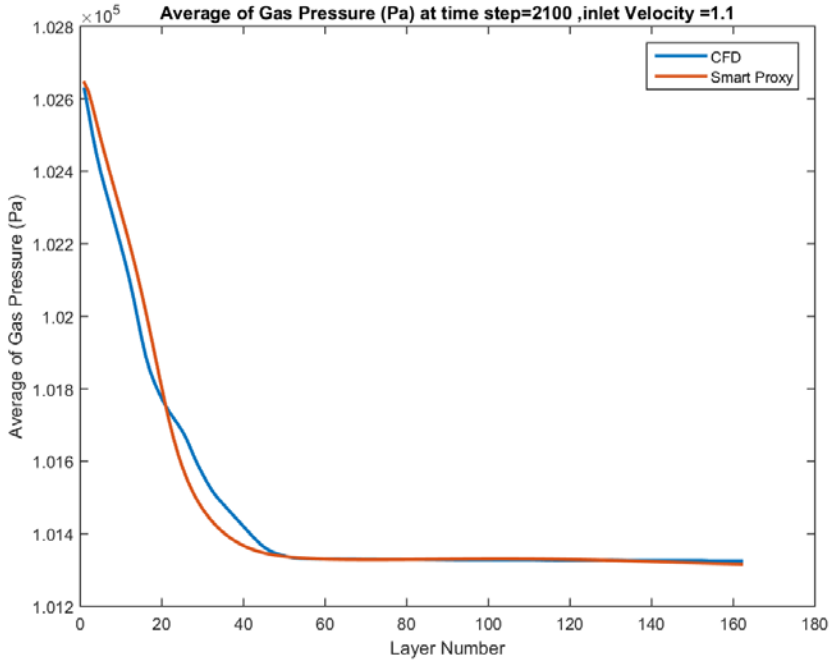

Figure 10-19 Spatially averaged CFD and smart proxy results for gas pressure at time step = 2100 for blind test condition of V_{in}=1.1 m/s

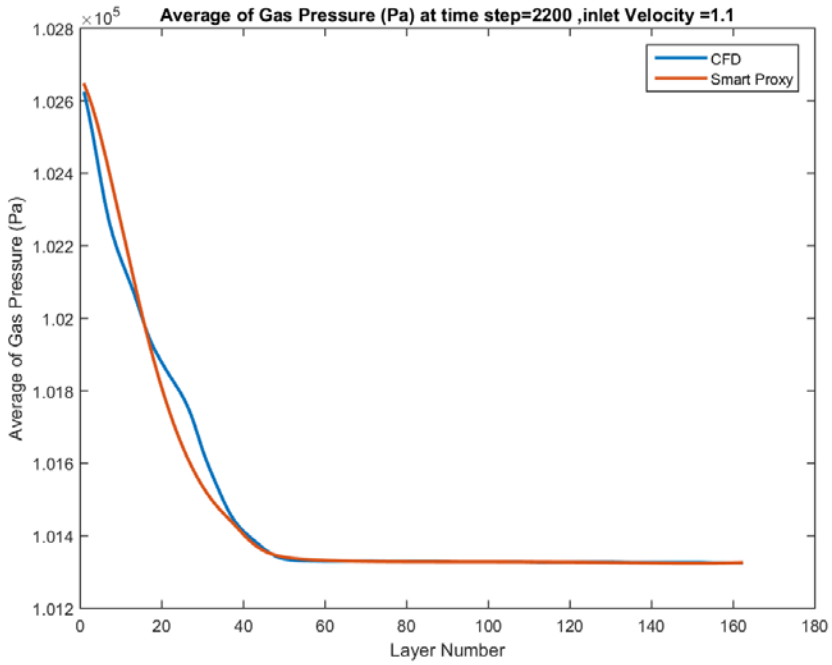

Figure 10-20 Spatially averaged CFD and smart proxy results for gas pressure at time step = 2200 for blind test condition of V_{in}=1.1 m/s

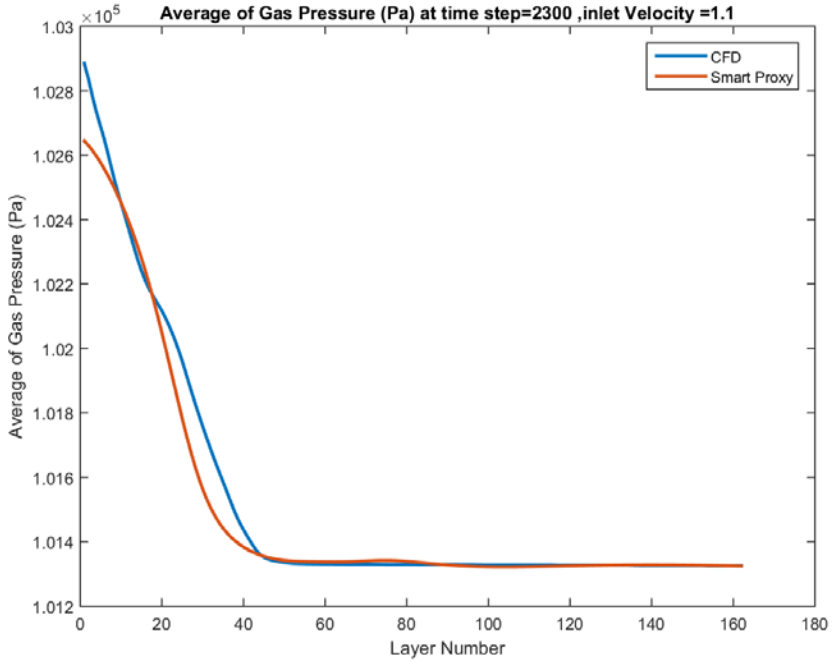

Figure 10-21 Spatially averaged CFD and smart proxy results for gas pressure at time step = 2300 for blind test condition of V_{in}=1.1 m/s

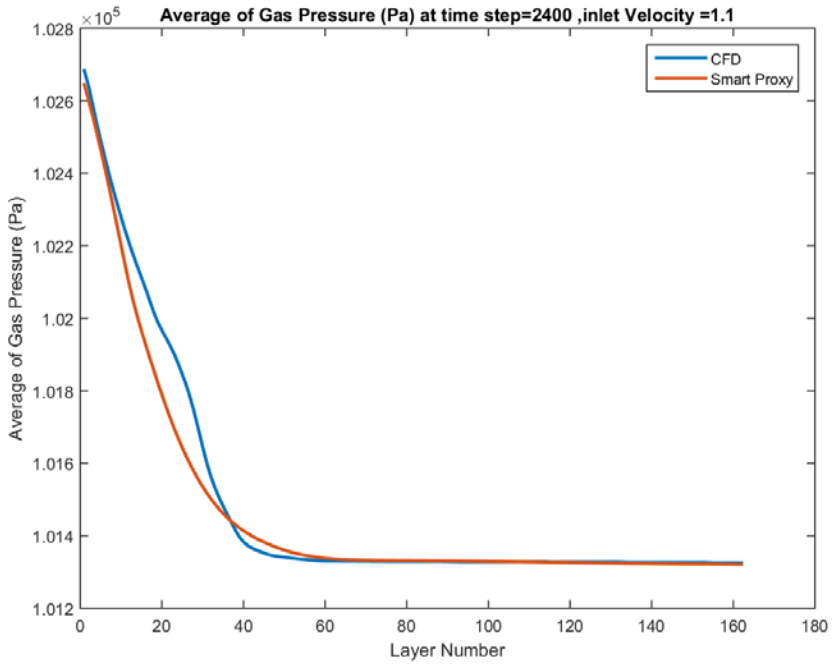

Figure 10-22 Spatially averaged CFD and smart proxy results for gas pressure at time step = 2400 for blind test condition of V_{in}=1.1 m/s

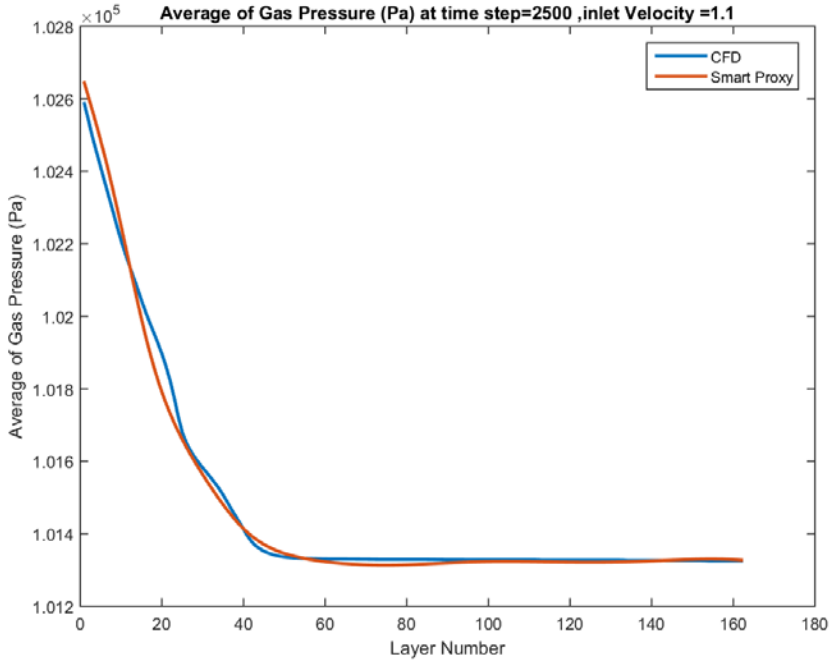

Figure 10-23 Spatially averaged CFD and smart proxy results for gas pressure at time step = 2500 for blind test condition of V_{in}=1.1 m/s

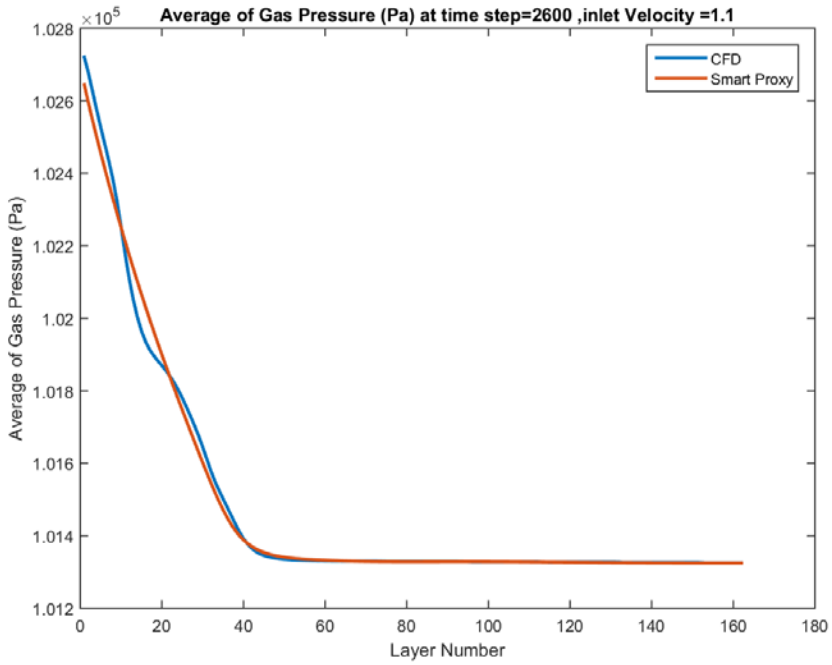

Figure 10-24 Spatially averaged CFD and smart proxy results for gas pressure at time step = 2600 for blind test condition of V_{in}=1.1 m/s

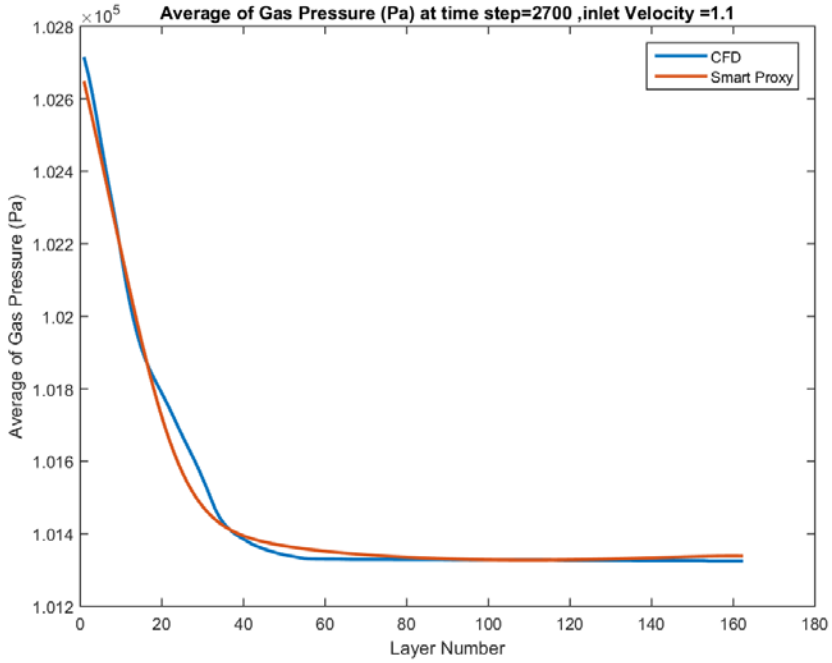

Figure 10-25 Spatially averaged CFD and smart proxy results for gas pressure at time step = 2700 for blind test condition of V_{in}=1.1 m/s

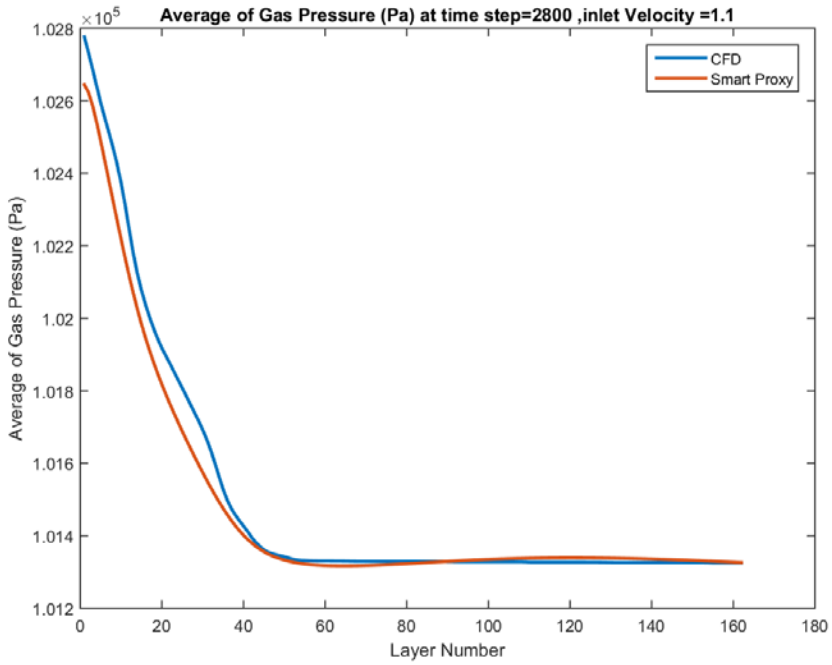

Figure 10-26 Spatially averaged CFD and smart proxy results for gas pressure at time step = 2800 for blind test condition of V_{in}=1.1 m/s

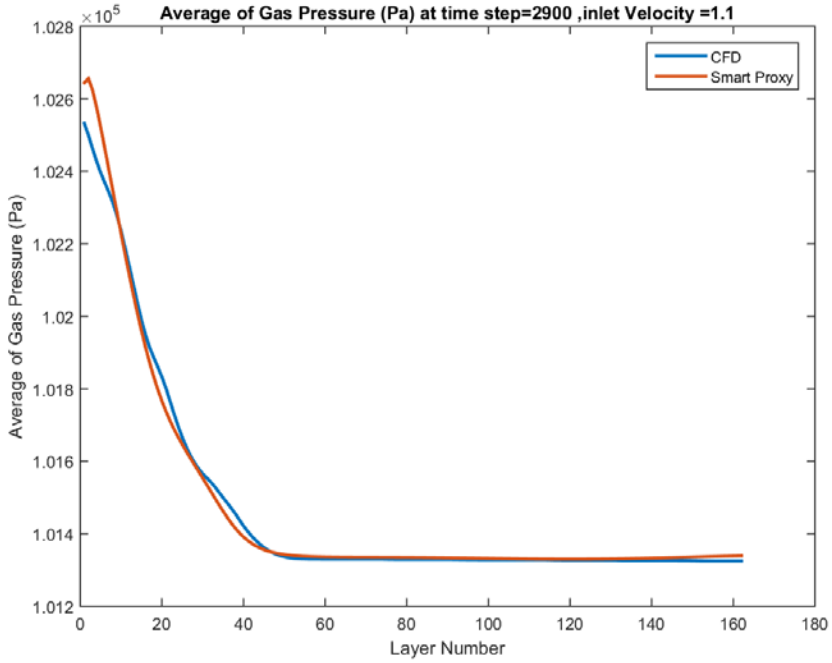

Figure 10-27 Spatially averaged CFD and smart proxy results for gas pressure at time step = 2900 for blind test condition of V_{in}=1.1 m/s

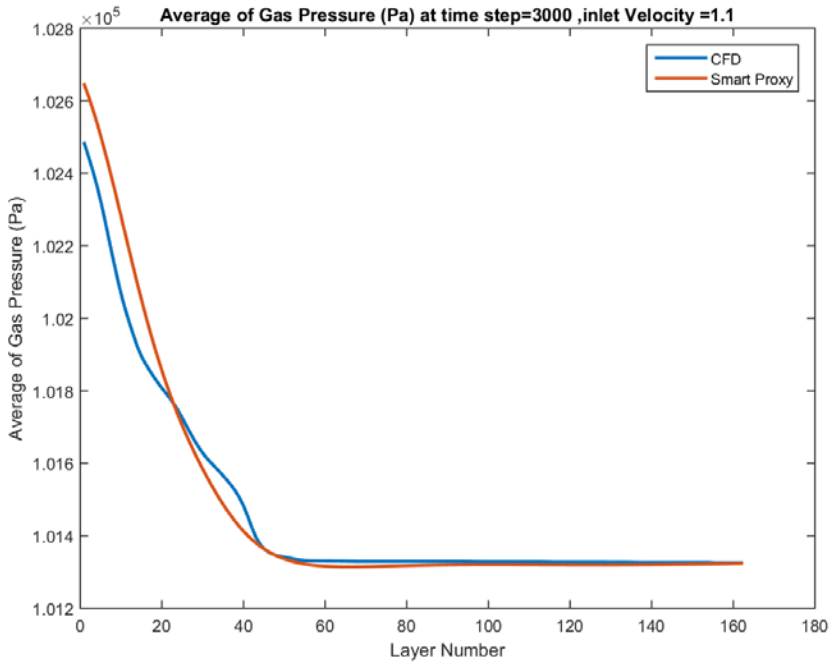

Figure 10-28 Spatially averaged CFD and smart proxy results for gas pressure at time step = 3000 for blind test condition of V_{in}=1.1 m/s

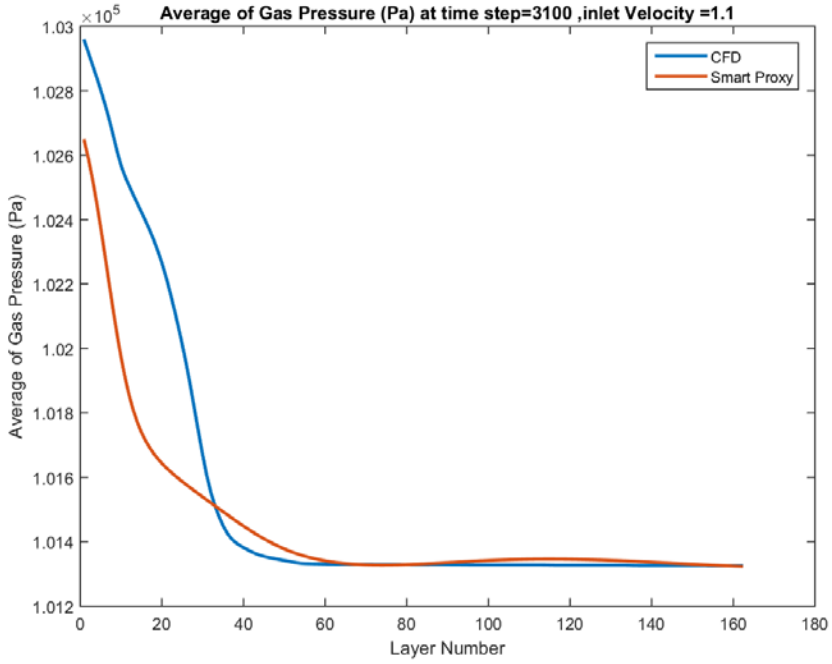

Figure 10-29 Spatially averaged CFD and smart proxy results for gas pressure at time step = 3100 for blind test condition of V_{in}=1.1 m/s

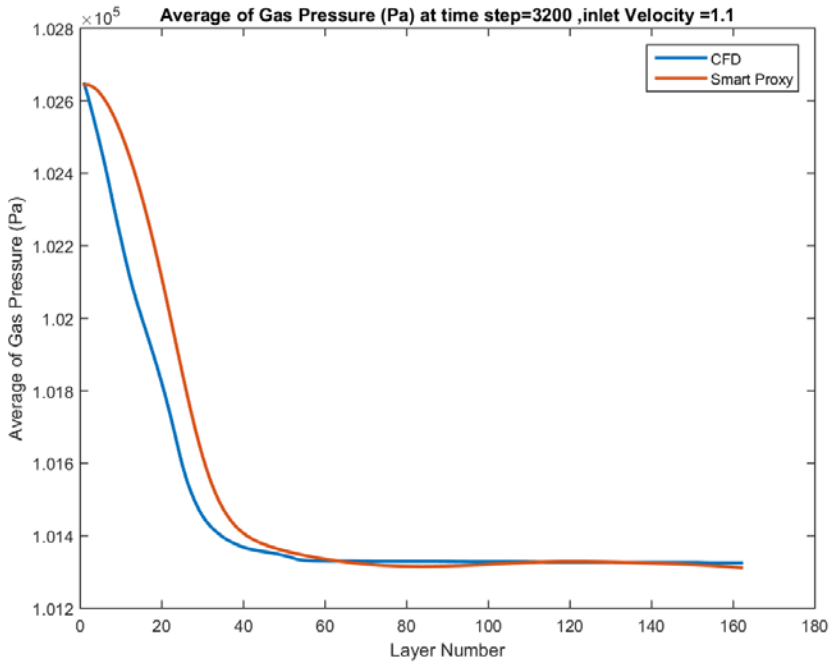

Figure 10-30 Spatially averaged CFD and smart proxy results for gas pressure at time step = 3200 for blind test condition of V_{in}=1.1 m/s

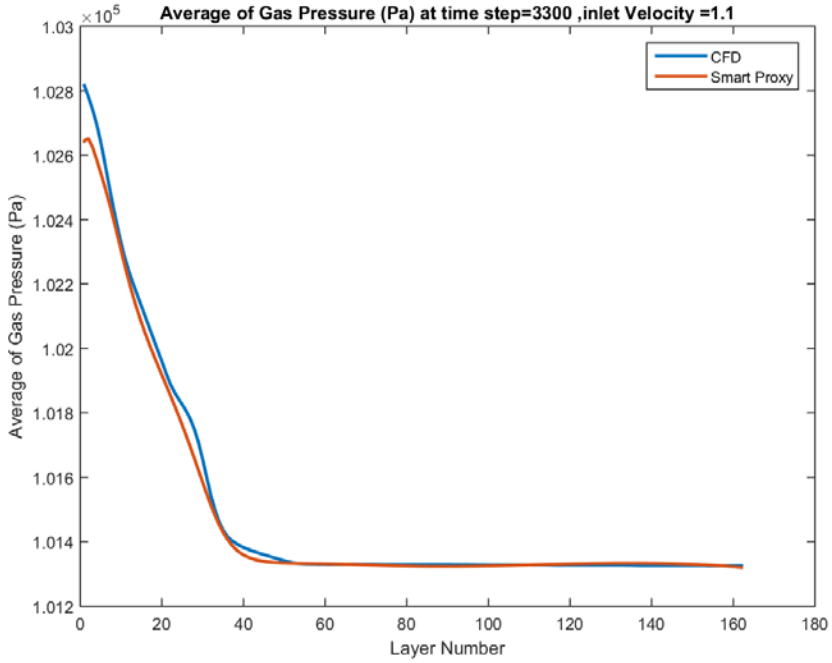

Figure 10-31 Spatially averaged CFD and smart proxy results for gas pressure at time step = 3300 for blind test condition of V_{in}=1.1 m/s

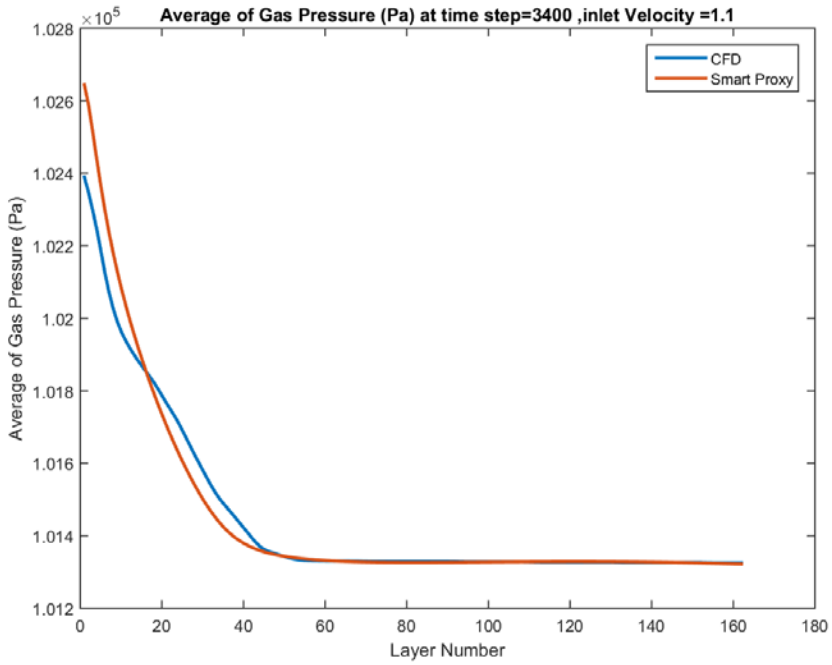

Figure 10-32 Spatially averaged CFD and smart proxy results for gas pressure at time step = 3400 for blind test condition of V_{in}=1.1 m/s

Sean Plasynski

Executive Director

Technology Development & Integration Center

National Energy Technology Laboratory

U.S. Department of Energy

John Wimer

Associate Director

Strategic Planning

Science & Technology Strategic Plans & Programs

National Energy Technology Laboratory

U.S. Department of Energy

David Alman

Executive Director

Research & Innovation Center

National Energy Technology Laboratory

U.S. Department of Energy

U.S. DEPARTMENT OF ENERGY

NATIONAL ENERGY TECHNOLOGY LABORATORY